Magnetophoretic Cell Clarification

by

Sonja Ann Sharpe

B.S. Chem. Eng., University of Maryland at College Park, College Park, MD (1997)

M.S.C.E.P. Chem. Eng., Massachusetts Institute of Technology, Cambridge, MA (1999)

Submitted to the Department of Chemical Engineering in partial fulfillment of the requirements for the degree of

Doctor of Philosophy

at the
Massachusetts Institute of Technology
September 2004

Signature of Author.....
Department of Chemical Engineering
August 5, 2004

Certified by.....
T. Alan Hatton
Ralph Landau Professor of Chemical Engineering Practice
Thesis Supervisor

Accepted by.....
Daniel Blankschtein
Professor of Chemical Engineering
Chairman, Committee for Graduate Students

Magnetophoretic Cell Clarification

by

Sonja Ann Sharpe

Submitted to the Department of Chemical Engineering on August 5, 2004,
in partial fulfillment of the requirements for the degree of
Doctor of Philosophy in Chemical Engineering

ABSTRACT

A new approach for the removal of micron-sized particles from aqueous suspensions was developed and applied to the problem of cell clarification from raw fermentation broth. The concepts of magnetophoretic separation were exploited to take advantage of the force that acts on a non-magnetic particle when it is immersed in a magnetic fluid (ferrofluid) that is subjected to a non-uniform magnetic field. The magnetic "pressure" difference across the non-magnetic particle owing to the magnetization of the surrounding magnetic fluid forces the particles away from areas of high magnetic field strength and into areas of low magnetic field strength. This force is proportional to the volume of the non-magnetic particles, and is therefore stronger for larger particles. In this way, non-magnetic particles can be focused and moved out of the bulk fluid by applying a non-uniform magnetic field to the system, leading to magnetophoretic clarification.

The magnetic fluid used in this work was composed of magnetite nanoparticles coated with a poly(acrylic acid)-poly(ethylene oxide)-poly(propylene oxide) graft copolymer layer that stabilized the nanoparticles in water and prevented their aggregation. The magnetic nanoparticles were approximately 32 nm in diameter, with the magnetite core itself being approximately 8 nm in diameter.

Magnetophoretic clarification was investigated using two different flow configurations. In the first case, the particle-laden magnetic fluid was pumped through a flow tube while a series of magnets around the tube moved counter to the direction of the feed flow; the non-magnetic particles in the feed were captured and effectively removed from the bulk fluid by the moving magnets. A removal efficiency of 95% of *E. coli* cells from the feed fluid was achieved after one pass through the counter current system. In the second case, four permanent magnets were arranged in a quadrupole around a central column to create areas of high magnetic field at the column walls and areas of low magnetic field at the centerline, inducing non-magnetic particles to concentrate at the centerline, where they were removed through a coaxial central outlet tube at the top of the column. Depending on the flow rate, up to 99% of polystyrene beads of different sizes could be removed from the feed after one pass through the quadrupole system. The recovery efficiency decreased with increasing flow rate, i.e. with decreasing residence time in the device. *E. coli* cells were able to be removed with separation efficiencies as high as 95% at much higher flow rates due to the formation of ~12 micron aggregates in the presence of the magnetic nanoparticles; these large aggregates experienced enhanced magnetic forces

over individually-dispersed cells and could be recovered more effectively. The governing equations for magnetophoretic clarification were applied to the quadrupole configuration to predict particle trajectories through the column and to predict the separation efficiency under different flow conditions, which showed a good match to the experimental results. It was also shown that axial magnetic field gradients near the entrance region acted effectively as a barrier to entry of particles in the slow moving regions near the walls; this retardation of their axial movement provided a longer residence time for the particles that allowed them to be moved more efficiently to the centerline by the radial magnetic field gradients, hence enhancing the separation capability of the process. These results indicate that magnetophoretic cell clarification is a viable approach for micron-sized particle removal and concentration from aqueous suspensions, with potential applications in the biotechnological and pharmaceutical industries for the clarification of cells from raw fermentation broth.

Thesis Supervisor: T. Alan Hatton
Title: Ralph Landau Professor of Chemical Engineering Practice

Acknowledgements

First and foremost, I need to sincerely thank Prof. Alan Hatton for his constant support and guidance during the tortuous path that my research has taken here at MIT. I would never have been able to complete this project without his sage advice and boundless patience. In addition, his willingness to indulge my love for travel has not only resulted in a broadening of my horizons, but it also introduced me to my husband, and for that opportunity, I am forever grateful. I would also like to thank my thesis committee members, Professors Cooney, Smith, and Wang, for their many helpful suggestions that without a doubt contributed to the successful completion of this research project. I am very pleased with the work that I have been able to do with the support of the brilliant faculty and staff at MIT, and I feel it provides an excellent framework for those who will follow after me.

I would also like to thank all of the people who contributed their time and effort in helping me complete this project. My undergraduate assistants Iman Kandil and Rose Lee were instrumental in completing many of the experiments, and their tireless enthusiasm when performing even the most mundane experimental tasks will be greatly missed. In addition, I need to thank many Hatton group members, both past and present, for their assistance. In particular, my heartfelt thanks go to Lino Gonzalez for patiently helping me to work through the theories I needed to model my system. The quality of this work would certainly have suffered without his assistance. I would also like to thank Tim Finegan for his many insightful discussions about my research and just about everything else, and also for keeping my computer running smoothly. Thanks as well to Geoff Moeser for his many helpful discussions about magnetic fluid when I was first starting on this project, and for the many, completely random conversations we had as cubicle neighbors. My time here at MIT would have been much less pleasant without his presence in the lab. Thanks also to Sanjoy Sircar for keeping me supplied with candy in the afternoons, and to the remaining members of the Hatton Lab for all of their help and support. In addition, this department would cease to operate without the constant support of people like Carol Phillips (we miss you, Carol), Suzanne Easterly, and Beth Tuths, who among her other duties, kept me constantly supplied with tissues during my stay here. Thanks also to Peter Morley and Andrew Gallant in the MIT Machine Shop, John Jordan of BOC gases, and the whole VWR team for putting up with my many requests and constant stream of questions.

I also need to thank my parents, Baerbel and Lee Sharpe, for their untiring love and support throughout my many years as a student, and for instilling in me the belief that I could succeed at anything. I literally would not be here without them. My thanks go out as well to my three sisters, Stephanie, Susan, and Stacey, for helping to keep me sane and for our many conversations about life, love, and occupational pursuits.

Most importantly of all, I need to thank my husband, Jeb Keiper, for his unconditional love and support throughout the last three years. Jeb, you are the source of my inspiration and motivation, and the true meaning of my life. Without your love and support, I never would have finished. This is for you.

Table of Contents

Chapter 1 17
1.1 Motivation 17
1.2 Approach 18
1.3 Current Cell Clarification Technologies 20
1.3.1 Centrifugation 21
1.3.2 Membrane Filtration 22
1.4 Magnetic Fluids 23
1.4.1 Structure 23
1.4.2 Magnetic Fluid Synthesis 26
1.4.2.1 General Concept 26
1.4.2.2 Chemical Coprecipitation 26
1.4.3 Current Uses of Magnetic Fluids and Magnetic Particles 27
1.4.3.1 Industrial Applications of Magnetic Fluids 27
1.4.3.2 Biomedical Applications of Magnetic Fluids 28
1.5 Separation using Magnetic Fluids 29
1.5.1 Industrial Separation using Magnetic Fluids 29
1.5.2 Cell Separation using Magnetic Particles 30
1.5.3 Magnetophoretic Separation Devices 31
1.5.4 Magnetophoretic Separation using Magnetic Fluids 32
1.6 Research Overview 34
1.7 References 35
Chapter 2 43
2.1 Introduction 43
2.2 Magnetic Fluid Synthesis 43
2.2.1 The Graft Copolymer 43
2.2.1.1 Materials 44
2.2.1.2 Graft Copolymer Synthesis 44
2.2.2 Magnetite Nanoparticles 46
2.2.2.1 Materials 46
2.2.2.2 Magnetite Nanoparticle Synthesis 46
2.3 Iron Analysis Test 48
2.4 Physical Characterization of Magnetic Fluid 50
2.4.1 Magnetic Nanoparticle Stability 50
2.4.2 Magnetic Nanoparticle Size 51
2.4.3 Physical Properties 53
2.4.4 Magnetic Properties 54
2.4.5 Electrostatic Properties 55
2.5 Summary 58
2.6 References 59
Chapter 3 61
3.1 Introduction 61
3.2 *E. coli* Production 61
3.2.1 Safety and Sterilization Procedures 61

3.2.2 Shaker Flask Growth 62
3.2.2.1 Materials 62
3.2.2.2 Shaker Flask Procedure 64
3.2.3 Processing of Cells and Fermentation Broth 65
3.3 Optical Density Measurements 65
3.4 Physical Characterization of *E. coli* Cells 66
3.4.1 Cell Size and Density 67
3.4.2 Electrostatic Properties 68
3.5 Analysis of Cell and Magnetic Fluid Mixtures 68
3.5.1 Optical Density in the Presence of Magnetic Fluid 69
3.5.2 Iron Analysis Test in the Presence of Cells 70
3.5.3 Physical Properties of Cell and Magnetic Fluid Mixtures 71
3.6 Polystyrene Beads as a Model Particle 72
3.6.1 Materials 72
3.6.2 Optical Density Measurements 73
3.6.3 Physical Characterization of Polystyrene Beads 73
3.6.3.1 Bead Size and Density 73
3.6.3.2 Electrostatic Properties 74
3.6.4 Analysis of Polystyrene and Magnetic Fluid Mixtures 74
3.6.4.1 Optical Density in the Presence of Magnetic Fluid 74
3.6.4.2 Iron Analysis Test in the Presence of Polystyrene Beads 75
3.6.4.3 Physical Properties of Polystyrene and Magnetic Fluid Mixtures. 76
3.7 Summary 77
3.8 References 78
Chapter 4 79
4.1 Introduction 79
4.2 Counter Current Device Specifications 79
4.2.1 Magnet Pairs 79
4.2.2 Magnetic Field Profile 80
4.3 Counter Current Experiments 83
4.3.1 Experimental Procedure 83
4.3.2 Experiments with Polystyrene Beads 84
4.3.2.1 Analytical Measurements 84
4.3.2.2 Control Experiments 85
4.3.2.3 Magnetic Fluid Experiments 85
4.3.3 Experiments with *E. coli* Cells 86
4.3.3.1 Analytical Measurements 87
4.3.3.2 Magnetic Fluid Experiments 87
4.4 Importance of the Operating Parameters 88
4.5 Summary 95
4.6 References 96
Chapter 5 97
5.1 Introduction 97
5.2 Theory of Magnetophoresis 97
5.2.1 Assumptions for the Separation of Micron Sized Particles 97
5.2.2 Magnetic Force on Non-magnetic Particles 98

5.2.3 The Flux Relationship Defining Magnetophoresis 99
5.3 Model for Quadrupole Magnetophoresis 101
5.3.1 Geometry of the Quadrupole Design 102
5.3.2 Quadrupole Model for Magnetophoresis 102
5.4 Matlab Model for the Quadrupole Design 104
5.4.1 Quadrupole Model Parameters 104
5.4.1.1 Velocity Profile and Particle Diffusivity 105
5.4.1.2 Magnetization of Magnetic Fluid 105
5.4.1.3 Quadrupole Magnetic Field Profile 106
5.4.2 Non-dimensional Quadrupole Model for Matlab 110
5.5 Model Results for the Quadrupole Design 112
5.6 Summary 114
5.7 References 115
Chapter 6 117
6.1 Introduction 117
6.2 Quadrupole System 117
6.2.1 Magnet Assembly 117
6.2.2 Magnetic Field Profile 120
6.2.3 Cylindrical Column 121
6.2.4 Completed Quadrupole System 125
6.3 Quadrupole Experiments 126
6.3.1 Experimental Procedure 126
6.3.2 Experiments with Polystyrene Beads 128
6.3.2.1 Analytical Measurements 128
6.3.2.2 Control Experiments 129
6.3.2.2.1 Polystyrene in Water 129
6.3.2.2.2 Magnetic Fluid Alone 131
6.3.2.3 Polystyrene and Magnetic Fluid Experiments 134
6.3.2.4 Effects of Operating Parameters on Polystyrene Particle Separation and Concentration 145
6.3.3 Experiments with *E. coli* Cells 151
6.3.3.1 Analytical Measurements 151
6.3.3.2 Control Experiments 152
6.3.3.3 Cells and Magnetic Fluid Experiments 153
6.4 Summary 157
6.5 References 159
Chapter 7 161
7.1 Summary of Research 161
7.2 Process Considerations 163
7.3 Future Research Directions 165
Appendix 169
Appendix A: Calculation of Error 169
Appendix B: Matlab Code for the Counter Current Device 170
Appendix C: Matlab Code for the Quadrupole Device 173

List of Figures

Figure 1-1. Schematic of the motion of a non-magnetic particle due to the force exerted on the particle from the magnetization of the surrounding fluid in the presence of a non-uniform magnetic field.....19

Figure 1-2. General structure of the magnetic nanoparticles that make up magnetic fluid, which consist of a magnetite core that is stabilized in water by a copolymer shell surrounding the core.....24

Figure 2-1. Amino-terminated polyethylene oxide (PEO)/polypropylene oxide (PPO) random block copolymer (Jeffamine M-2070), where R = H (for EO) or CH_3 (for PO) and the overall EO/PO ratio is 70/30. With an average molecular weight of 2000, *n* is approximately 34.....44

Figure 2-2. Synthesis of the graft copolymer via amidation by reacting the carboxylic acid groups on the PAA chains with the amino-terminated PEO/PPO random block copolymer, yielding a comb polymer with PEO/PPO grafted onto a PAA backbone. Approximately 84% of the carboxylic acid groups are left unreacted for subsequent attachment to the magnetite cores.....45

Figure 2-3. Chemical coprecipitation of iron(III) and iron(II) to magnetite with the addition of base, with stabilization of the magnetite provided by the PAA-PEO/PPO graft copolymer.....47

Figure 2-4. Size distribution of magnetic nanoparticles in magnetic fluid using dynamic light scattering, with (a) number average distribution and (b) volume average distribution.....52

Figure 2-5. Magnetization response of 1 wt% magnetic fluid (1 wt% magnetite) under changing applied magnetic field. Negative values of the magnetic field indicate that the field was applied in the opposite direction. The SQUID measurements show zero residual magnetization at zero applied field, indicative of superparamagnetic behavior.....55

Figure 2-6. Zeta potential of dilute magnetic nanoparticles in the working pH range of the magnetic fluid for magnetophoretic clarification. The dashed line is present to indicate trends in the data.....58

Figure 3-1. Photograph of *E. coli* cells using an optical microscope at 1000x resolution.....67

Figure 3-2. The absorption at 600 nm as a function of cell concentration for samples containing only cells (squares) and samples containing both cells and magnetic fluid (circles). The optical density measurements at 600 nm are either the pure measurements,

for cells alone, or the corrected measurements, with the magnetic fluid contribution subtracted, for mixtures of cells and magnetic fluid.....70

Figure 3-3. The absorption at 600 nm as a function of polystyrene concentration for samples containing 2 micron polystyrene beads in water (squares) and samples containing 2 micron polystyrene beads in magnetic fluid (circles). The optical density measurements at 600 nm are either the pure measurements, for polystyrene in water, or the corrected measurements, with the magnetic fluid contribution subtracted, for polystyrene in magnetic fluid.....75

Figure 4-1. Schematic of the counter current device showing general geometry and direction of magnet movement and fluid flow.....81

Figure 4-2. Complete counter current system, including tubing and syringe pump for pumping the feed fluid through the device.....81

Figure 4-3. Measured magnetic field profile along the axis of the rotating chain in the counter current device. The boxes at the bottom of the graph represent the position of the magnet pairs. The peaks of strongest magnetic field occur in the center of the magnet pairs, while the troughs of weakest magnetic field occur in the middle of the space separating the magnet pairs.....82

Figure 4-4. Results of the experiment using 5 mL of 1 wt% polystyrene and 1 wt% magnetic fluid as the feed. Clarified Feed represents the amount of the polystyrene collected in the fluid that exited the counter current device, and PS in Collection Tube represents the amount of polystyrene removed from the feed and collected in the collection tube.....86

Figure 4-5. Results of the experiment using 5 mL of 1 wt% cells on a dry cell basis and 1 wt% magnetic fluid as the feed. Clarified Feed represents the amount of cells collected in the fluid that exited the counter current device, and Cells in Collection Tube represents the amount of cells removed from the feed and collected in the collection tube.....88

Figure 4-6. Surface plots showing the effects of magnetic fluid concentration and flow rate on the separation capability of the counter current device, with each plot representing a different cell concentration in the feed fluid.....90

Figure 4-7. Force balance on a non-magnetic particle in the counter current device.....91

Figure 4-8. Dependence of the separation capability of the counter current device, in terms of the percent of cells removed from the feed fluid, on the dimensionless parameter (D_{md}). The dashed line is present to indicate trends in the data.....93

Figure 4-9. Percent of cells removed from the feed in the counter current device

as a function of feed flow rate. The dashed line is present to indicate trends in the data.....94

Figure 4-10. Percent of cells removed from the feed in the counter current device as a function of magnetic fluid concentration. The dashed line is present to indicate trends in the data.....95

Figure 5-1. Schematic of the quadrupole design, showing an overall cylindrical geometry that is radially symmetric.....102

Figure 5-2. Magnetization response of 1 wt% magnetic fluid (1 wt% magnetite) under changing applied magnetic field, including the fit of the experimental data to the empirical model. Negative values of the magnetic field indicate that the field was applied in the opposite direction.....107

Figure 5-3. Contour plot of the magnetic flux density produced by the quadrupole orientation of the four permanent magnets. Lighter colors represent a stronger magnetic flux density. The units are in Tesla.....108

Figure 5-4. Cross sectional profiles of the magnetic flux density shown centered through the faces of the magnets and tangent to the edges of the magnets, with the polynomial fit to the magnetic flux density included in the positive *r* direction.....109

Figure 5-5. The predicted concentration profiles of 2 micron polystyrene beads at different points along the length of the quadrupole column for an initial feed concentration of 1 wt% polystyrene in 1 wt% magnetic fluid with a maximum linear velocity along the centerline of 31.8 cm/hr (50 mL/hr).....113

Figure 6-1. Technical schematic of the four permanent magnets and their stainless steel housing box, top view, where 1 indicates the magnets, 2 and 3 indicate the stainless steel plates needed to construct the housing box for the magnets, and N/S indicates the polarity of the magnetic field for each magnet in the finished magnet assembly.....118

Figure 6-2. Technical schematic of the four permanent magnets and their stainless steel housing box, side view.....119

Figure 6-3. A photo of the completed magnet assembly manufactured by Dura Magnetics.....119

Figure 6-4. Contour plot of the magnetic flux density produced by the quadrupole orientation of the four permanent magnets. Lighter colors represent a stronger magnetic flux density. The units are in Tesla.....121

Figure 6-5. Technical schematic of the aluminum column used with the magnet assembly, shown at two different side views, each at 90 degrees to one another. The units are in millimeters.....123

Figure 6-6. Completed aluminum column with tubing shown attached. The body of the column is uniform in diameter, not tapered as the reflected light on the column body makes it appear in the photograph.....124

Figure 6-7. Aluminum column sitting in the magnet assembly in the orientation used for all experiments, with the feed flow directed against gravity.....124

Figure 6-8. The complete quadrupole system, including the magnet assembly, the aluminum column, the peristaltic pump, the tubing, and the valves. A beaker used to hold the feed and glass vials used to collect the samples from the outlets are also shown.....126

Figure 6-9. Flow pattern in the quadrupole column associated with a 20% flow rate for the central outlet.....127

Figure 6-10. Concentration profile of the polystyrene content in the quadrupole outlets for a control experiment using 160 mL of 1 wt% polystyrene as the feed with no magnetic fluid present in the system. Clarified Feed represents the average concentration of the polystyrene collected at specific time intervals from the two side outlet streams, and Collection Outlet represents the polystyrene concentration collected at specific time intervals from the central outlet stream.....130

Figure 6-11. Results for the control experiment using 150 mL of 1 wt% magnetic fluid as the feed, with 1 wt% magnetic fluid present in the device at the start of the experiment. Clarified Feed represents the average magnetite concentration and nanoparticle size collected from the two side outlet streams, Collection Outlet represents the magnetite concentration and nanoparticle size collected from the central outlet stream, Feed represents the magnetite concentration and nanoparticle size of the feed fluid, and Retained represents the magnetite concentration and nanoparticle size of the fluid retained in the column at the end of the experiment.....132

Figure 6-12. The volume-average distribution of the hydrodynamic diameter of magnetic particles in the feed, the outlets, and the fluid retained in the column at the end of the control experiment. Feed represents the feed fluid, Clarified Feed represents the fluid collected from the two side outlet streams, Collection Outlet represents the fluid collected from the central outlet stream, and Retained in Column represents the fluid retained in the device at the end of the experiment, with (a) depicting the full curves and (b) showing a close up of the front half of the curves to show detail.....133

Figure 6-13. Concentration profile of the polystyrene content in the quadrupole outlets for 2 micron polystyrene beads using 160 mL of 1 wt% polystyrene and

1 wt% magnetic fluid as the feed with 1 wt% magnetic fluid present in the system. Clarified Feed represents the average concentration of the polystyrene collected at specific time intervals from the two side outlet streams, and Collection Outlet represents the polystyrene concentration collected at specific time intervals from the central outlet stream.....135

Figure 6-14. Close up of the inlet section of the aluminum column in the magnet assembly.....137

Figure 6-15. Contour plot showing the magnetic flux density (B) along an axial cross section of the quadrupole column and magnets. The axial magnetic flux density gradient extends approximately a quarter centimeter on either side of the magnet edges through the column. The units are in Tesla.....138

Figure 6-16. Axial field lines for the magnetic flux density at different points along the radius of the column, with r = 1 corresponding to the column walls and r = 0 corresponding to the column centerline. The dashed line at an axial distance of 1 cm corresponds to the edges of the magnets, or the entrance into the magnet assembly.....139

Figure 6-17. Velocity field profile for 2 micron particles at different flow rates, (a) 2 mL/hr, (b) 10 mL/hr, and (c) 30 mL/hr. The thick dashed line at an axial distance of 1 cm corresponds to the edges of the magnets, or the entrance into the magnet assembly. The velocity field profile is unchanged from approximately 2 cm (1 cm after entry into the magnet assembly) to the top of the column, shown here up to 3 cm. The arrows representing the fluid velocity have been normalized as v/v_{max}, where v_{max} is the maximum linear velocity of the fluid through the column...140

Figure 6-18. Particle trajectories at different flow rates, (a) 2 mL/hr (axial scale changed to enhance detail), (b) 30 mL/hr, (c) 120 mL/hr, (d) 240 mL/hr. The thick dashed lines represent position in the column at constant time. The dashed line at an axial distance of 1 cm corresponds to the edges of the magnets, or the entrance into the magnet assembly. The dashed line at a radial position of 0.25 cm corresponds to the position of the coaxial inner cylinder at the top of the column.....142

Figure 6-19. Particle trajectories at 2 mL/hr, (a) calculated with the presence of the axial and radial magnetic field gradients at the entrance to the magnet assembly, (b) calculated in the absence of the axial gradients but in the presence of the radial gradients at the entrance, and (c) calculated in the absence of both the axial and radial gradients at the entrance to the magnet assembly. The thick dashed lines represent position in the column at constant time. The dashed line at an axial distance of 1 cm corresponds to the edges of the magnets, or the entrance into the magnet assembly. The dashed line at a radial position of 0.25 cm corresponds to the position of the coaxial inner cylinder at the top of the column.....144

Figure 6-20. Concentration profile of the polystyrene content in the quadrupole outlets for 1.17 micron polystyrene beads using 160 mL of 1 wt% polystyrene and

1 wt% magnetic fluid as the feed with 1 wt% magnetic fluid present in the system. Clarified Feed represents the average concentration of the polystyrene collected at specific time intervals from the two side outlet streams, and Collection Outlet represents the polystyrene concentration collected at specific time intervals from the central outlet stream.....146

Figure 6-21. Percent of polystyrene beads removed from the feed fluid versus feed flow rate for 1 and 2 micron polystyrene beads, using 1 wt% polystyrene and 1 wt% magnetic fluid for the feed.....148

Figure 6-22. Concentration of 2 micron non-magnetic particles as a function of radial distance in the column for different $\tilde{\Psi}^2$ and $\tilde{\beta}$ values, shown at a constant axial distance of 16 cm up the column, just before reaching the central outlet.....150

Figure 6-23. Percent of polystyrene beads in the central outlet versus feed flow rate for 1 and 2 micron polystyrene beads using 1 wt% polystyrene and 1 wt% magnetic fluid, with the model predictions present as the dark solid lines. Circles represent 1 micron experimental results, while squares represent the results using 2 micron polystyrene beads.....150

Figure 6-24. Concentration profile of the cell content in the quadrupole outlets for *E. coli* cells using 160 mL of 0.4 wt% cells and 1 wt% magnetic fluid as the feed with 1 wt% magnetic fluid present in the system. Clarified Feed represents the average concentration of the cells collected at specific time intervals from the two side outlet streams, and Collection Outlet represents the cell concentration collected at specific time intervals from the central outlet stream.....155

Figure 6-25. Trajectories for 12 micron cell aggregates at different radial locations in the quadrupole column at a flow rate of 500 mL/hr. The thick dashed lines represent position in the column at constant time. The dashed line at an axial distance of 1 cm corresponds to the edges of the magnets, or the entrance into the magnet assembly. The dashed line at a radial position of 0.25 cm corresponds to the position of the coaxial inner cylinder at the top of the column.....157

Figure 7-1. Parallel process design for scale up of the quadrupole device.....165

Figure 7-2. Alternate quadrupole system designs for minimizing the barrier-to-entry force, where (a) shows a different design for the permanent magnets and (b) shows a different method of entry into the column for the feed fluid.....166

List of Tables

Table 3-1. Stock solutions used to create the semi-defined growth medium for the cells, listed with chemical concentrations for both the stock itself and for the final semi-defined growth medium.....63

Table 3-2. Preparation of 100 mL the semi-defined growth medium from the chemical stock solutions for a 500 mL sterile baffled shaker flask.....64

Table 4-1. Values of the operational parameters tested using a Box Behnken design for the counter current device.....89

Table 4-2. Results from all experiments performed with the counter current device used to evaluate the importance of the feed flow rate, the concentration of magnetic fluid, and the concentration of cells in the feed on the separation capability of the device.....92

Table 5-1. Assumptions for the molar diffusive flux equation relative to mass average velocity for micron sized non-magnetic particles surrounded by magnetic fluid.....101

Table 5-2. Values for the constant parameters used for solving the overall equation for magnetophoresis for the quadrupole system.....111

Chapter 1

Introduction

1.1 Motivation

Fermentation processes have become increasingly commonplace as recombinant DNA technology has become sophisticated enough to allow a variety of cell types to be custom designed for the manufacture of an astonishing assortment of biological products. According to Business Communications Company (Norwalk, CT), the global market for bioengineered protein drugs is expected to grow from $40 billion in 2003 to almost $71 billion in 2008, with the bulk of the growth expected to occur for monoclonal antibodies and fusion proteins.[1] These products are high value biologicals, but up to 90% of the cost of manufacturing them occurs in downstream purification processes after the products have already be produced by the cells in the fermentation tank.[2] Novel technologies for the recovery and purification of biological products are therefore in demand to reduce processing costs and increase product yield.

Following production in a fermentation tank, the first step in downstream recovery and purification of a biological product typically involves removing the cells from the bulk fermentation fluid, a process called cell clarification. The most common cell clarification techniques currently used in industry are centrifugation and membrane filtration, and both technologies are fairly well developed.

Centrifugation takes advantage of the density difference between the cells and the raw liquid to force the heavier cells to sediment out of the fluid. Centrifugation can clarify feed flows up to 20,000 L/hr, but has the principle disadvantages of large capital and maintenance costs, high shear stress on the cells, and the inherent danger of high speed moving parts. Membrane filtration takes advantage of the size difference between cells and the product of interest by excluding the cells while allowing smaller molecules or particles to pass through a membrane barrier. Membrane filtration can clarify feeds with a flux through the membrane of up to 250 μm/s (900 L/hr/m^2) for microfiltration, which is the filtration type most often used for cell clarification.[3]. Membrane filtration has the advantage of being easy to scale up, but depending on the extent of filtration

needed for the process, large capital costs, clogging and fouling, low flux through the membrane, and the need for multiple membrane stages could result.[4]

The primary goal of this project was to explore a new method for cell clarification that addressed some of the disadvantages associated with the traditional cell clarification techniques used in industry. Magnetophoretic separation processes have the potential advantages of consisting of open systems with no high-speed moving parts that are not prone to clogging or fouling. Magnetophoretic clarification was also shown to be gentle enough on cells during the separation process that the technology could be used to recover cells when the cells themselves were the product of interest, as opposed to a biologic produced by the cells. The results using the magnetophoretic devices were quite successful, and future designs at larger scales have applications in the biotechnological and pharmaceutical industries wherever cells or other non-magnetic particles need to be removed from a bulk liquid.

1.2 Approach

Magnetophoretic cell clarification takes advantage of the force that a non-magnetic particle feels when surrounded by a magnetized fluid in the presence of a non-uniform magnetic field:

$$F_m = \mu_o V_p M \nabla H \tag{1-1}$$

where μ_o is the permeability of free space, V_p is the volume of the non-magnetic particle, M is the magnetization of the fluid surrounding the particle, and ∇H is the magnetic field gradient.[5] Equation 1-1 shows that the force on the non-magnetic particle is proportional to the volume of the particle, the magnetization of the surrounding fluid, and the gradient of the magnetic field. Thus, the non-magnetic particle experiences a force that pushes it away from areas of high magnetic field and into areas of low magnetic field, and this force is stronger for larger non-magnetic particles and for stronger magnetic field gradients, as shown schematically in Figure 1-1.

The non-magnetic particle will continue to migrate along the path of decreasing magnetic field until it encounters a region where either the magnetic field or the magnetic field gradient becomes zero.[6] Thus, by carefully designing the overall geometry and magnetic field gradient of a device, the magnetic force given by Equation 1-1 can be used

to focus and concentrate non-magnetic particles in a liquid mixture and move them out of the bulk fluid. This is the essence of successful magnetophoretic cell clarification.

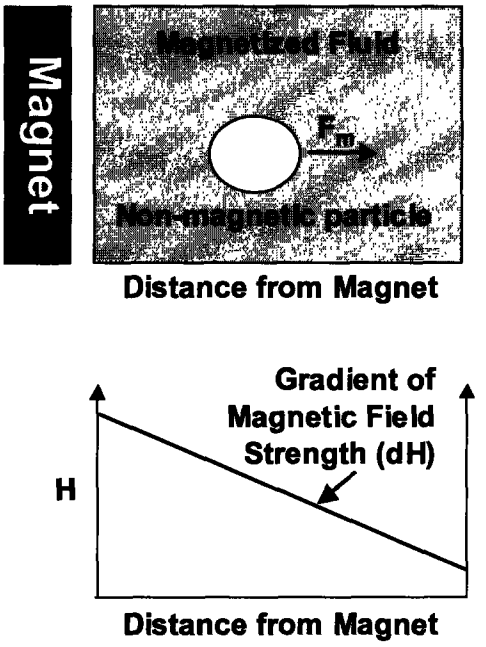

Figure 1-1. Schematic of the motion of a non-magnetic particle due to the force exerted on the particle from the magnetization of the surrounding fluid in the presence of a non-uniform magnetic field.

To achieve separation of non-magnetic particles using a magnetic field, the particles must be mixed with a magnetizable fluid. These fluids, called magnetic fluids in this work, must offer strong magnetization in the presence of a magnetic field while also remaining essentially inert when mixed with complex fluids such as cells in fermentation broth. The magnetic fluids synthesized for use in this work (discussed in more detail in Chapter 2) are aqueous colloidal dispersions of polymer stabilized magnetic cores. Each magnetic core consists of a magnetite crystal approximately 8 nm in diameter that is surrounded by a graft copolymer shell, which acts as a stabilizing agent for the magnetite core in water. These magnetic particles have an average diameter of 32 nm, including the core and polymer shell. The colloidal suspension of these magnetic nanoparticles in water is referred to as magnetic fluid, and the small size of the magnetic particles allows the magnetic fluid to be treated as a continuum when mixed with the non-magnetic particles used in this work, which all possessed diameters on the order of microns.

Using magnetic fluids as a separation additive offers several advantages for cell clarification from fermentation broth. Magnetophoretic clarification is size dependent, as is membrane filtration, but unlike membrane filtration, which requires the use of a physical barrier to separate different sized particles, magnetophoretic clarification relies on an applied magnetic field to exert the magnetic force used to push the non-magnetic particles out of the bulk fluid. Since the magnetic field can be applied externally, the magnetic separation force can be applied to open, bulk fluid mixtures of cells and magnetic fluid passing through the magnetic field. Thus, magnetophoretic clarification can be designed as an open system that would not be prone to fouling or clogging, as is often the case in membrane filtration. Additionally, an applied magnetic field does not disrupt the motion of charged particles and molecules in the fluid, as is the case with electrophoretic separation. Magnetophoretic clarification also requires no high speed moving parts and is very gentle on cells, unlike centrifugation. Thus, this novel cell clarification technique addresses several of the disadvantages of the cell clarification technologies currently used in industry. Additionally, the magnetic particles can be recovered from the clarified fluid after magnetophoretic clarification by using high gradient magnetic separation (HGMS), which is discussed in more detail in subsequent sections of this chapter, allowing the production of completely clarified fluid streams.

1.3 Current Cell Clarification Technologies

The most common methods currently used to separate cells from fermentation broth on an industrial scale are centrifugation and membrane filtration. The choice between the two techniques depends on what cell type needs to be removed (yeast, bacteria, fungi, etc.), whether the final product was intracellularly or extracellularly produced, the concentration of the cells in the broth, the cost sensitivity of the product, the molecular size of the product, the volume of liquid that must be processed, and the regulatory environment, which is particularly important when the final product is for pharmaceuticals or for food.[4,7] This section discusses each of these separation techniques and their general mode of operation.

1.3.1 Centrifugation

Centrifugation takes advantage of the density difference between cells and the surrounding liquid broth to force the heavier cells to sediment out of the fluid, accelerating and enhancing the cell sedimentation that would occur naturally if the cell suspension was left to settle undisturbed in a tank. Centrifugation is able to continuously separate micron sized particles from fluids with a solids content up to 60 vol%, depending on the type of centrifuge selected.[8]

Different centrifuge configurations exist for fluids containing various solid loads and particle sizes, and each is optimal for a specific type of fluid separation. Disc-stack centrifuges are the most versatile, able to handle a solids content of up to 25 vol% and particle sizes from 0.1-800 μm at processing rates of up to 20,000 L/hr, with self-cleaning and continuous discharge models available that eject the solid cell cake without the need for shutting down the machine.[8-10] Disc-stack centrifuges have been used to process 6-7 vol% *E. coli* cell suspensions at process flow rates of 3000 L/hr, achieving a clarified effluent containing only 0.02 vol% solids.[10] Decanter centrifuges are also available for separating slurries containing up to 60 vol% solids with particle sizes from a few microns up to 20 mm and have the advantage of fully continuous operation.[8,9] However, decanter centrifuges are not as effective for recovering cells as disc-stack centrifuges unless a flocculating agent is added to the broth or the cells are very concentrated.[10]

In general, centrifugation is optimal for processing large volumes of fluid with a solids content ranging from 1-60 vol% and particle sizes between 1-800 μm.[8] Centrifugation has the advantage of being able to process large volumes of fluid continuously while maintaining a relatively small footprint, requiring little space for mechanical operation.[8] The disadvantages of centrifugation include high shear stress on the cells and safety issues concerning high speed moving parts and off-balance machines, as well as large upfront capital costs, high maintenance requirements, and high energy costs.[8,11]

1.3.2 Membrane Filtration

Membrane filtration takes advantage of the size difference between cells and the product of interest by excluding cells and cellular material while allowing smaller molecules or particles to pass through a membrane barrier. Two major types of membrane filtration are microfiltration and ultrafiltration. Ultrafiltration typically retains macromolecules, such as proteins, and everything larger while passing only solvents, ions, and small molecules through the membrane.[9] Microfiltration typically retains materials ranging from 0.2-10 μm in size, such that very large macromolecules and microorganisms are retained but most proteins pass through.[9-11] Microfiltration is the most common membrane filtration system used for cell clarification.[9]

Both dead-end membrane filtration and cross-flow or tangential flow membrane filtration are common for microfiltration.[9] In dead-end filtration, the fluid contacts the membrane perpendicularly and is pushed through statically under pressure, whereas for cross-flow filtration, the liquid to be filtered flows parallel to the membrane at high velocity and pressure, leading to much less clogging and fouling of the filter than is found with the dead-end design but also requiring recycling of the retentate to recover product that did not flow through the membrane after the first pass through the system.[3,9,11] Cross-flow membrane filters can typically handle a high solids content while dead-end filtration is normally only used for fluids with a low solids content, usually less than 0.5%, due to the tendency of the membrane filters to readily plug and clog when used in this manner.[9] However, dead-end membrane filters are typically much less expensive than cross-flow membrane filters and are easier to clean through back flushing.[9]

Several types of cross-flow membrane filters are available for both microfiltration and ultrafiltration, including hollow fiber and flat sheet, where the flat sheet membrane is typically designed in either a plate and frame or spiral wound configuration.[3,7,9,10] Flat sheet membranes are used most often, and are capable of processing viscous liquids and those with a high solids content, since they can be operated at higher transmembrane pressures than hollow fiber cartridges.[3,7,9]

The principle advantage of membrane filtration over centrifugation is more efficient separation for smaller particle sizes and the ability to produce completely sterile filtrates, leading to a high quality end product.[3,7,9] One example of this is the use of

microfiltration in the dairy industry as a non-thermal means of sterilizing milk.[9] Membrane filtration also tends to be more cost effective than centrifugation, even at low flux rates, for the separation of smaller particles, where centrifugation is much less efficient.[7] For example, to obtain efficient separation of *E. coli* cells, which are typically around 2 μm in size, the centrifuge throughput must usually be adjusted to 5-10% of the total capacity of the machine.[2] Membrane filtration is also able to operate at conditions that are less than ideal for centrifugation, such as the clarification of high-viscosity fluids, and is relatively easy to scale up.[3] However, several membrane stages may be required to completely remove all unwanted particles.[4]

The primary disadvantage of membrane filtration is the tendency of the filters to clog or foul due to the presence of fouling compounds, such as polyglucans, nucleic acids, lipids, proteins and cell debris, leading to decreased flux through the membrane and less efficient separation. For this reason, membrane filtration is commonly used for the separation of whole cells from fermentation fluid where the biological product of interest was produced extracellularly, whereas centrifugation is preferred for the separation of cell debris after lysing the cells to release intracellularly produced inclusion bodies.[10,12] Capital costs for membrane filtration are also high; however, membrane filtration offers lower maintenance costs than centrifugation along with lower operating costs.[3,9,11]

1.4 Magnetic Fluids

The driving force of magnetophoretic clarification is provided by the magnetization of the magnetic fluid in the system. Without the presence of the magnetic fluid, the separation of cells from fermentation broth could not be achieved. Thus, it is important to understand the nature of the magnetic nanoparticles that comprise magnetic fluid. The following sections discuss magnetic fluid structure and synthesis, as well as the most common uses of magnetic fluid in industry.

1.4.1 Structure

Magnetic fluids, or ferrofluids, are defined as colloidal dispersions of magnetic nanoparticles that are suspended in a carrier liquid and, due to their small size, do not

settle under the influence of either gravity or moderate magnetic fields.[5] The magnetic fluids synthesized for this work were composed of magnetite cores stabilized in aqueous solution by a graft copolymer coating, and were shown to be extremely stable not only under gravitational and magnetic fields, but also at elevated temperatures and various pH and ionic strength conditions (see Chapter 2 for more details). The general structure of the magnetic nanoparticles that make up magnetic fluid is shown schematically in Figure 1-2 below.

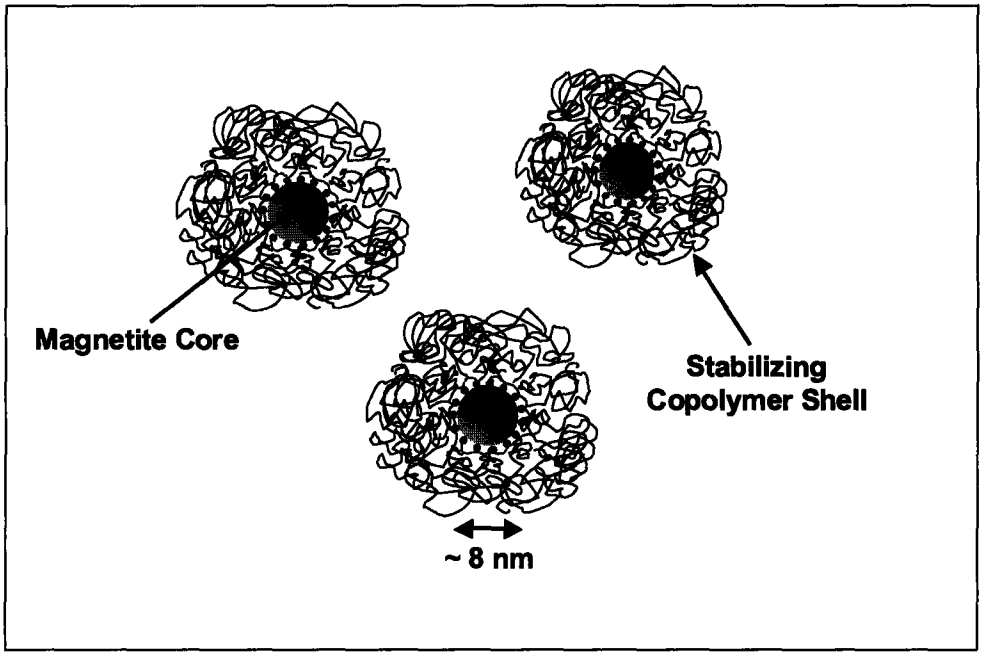

Figure 1-2. General structure of the magnetic nanoparticles that make up magnetic fluid, which consist of a magnetite core that is stabilized in water by a copolymer shell surrounding the core.

The magnetic nanoparticles created for this research were composed of magnetite, which is a ferrimagnetic, spinel iron oxide species composed of Fe^{3+} and Fe^{2+} in a 2:1 molar ratio, with a molecular formula of $Fe_2O_3 \cdot FeO$.[13] The magnetite crystals form with an average core size of ~8 nm,[14,15] which is sufficiently small for Brownian motion to dominate the movement of the nanoparticles in solution and prevent their sedimentation due to gravity and applied magnetic fields.[5]

The magnetite cores of the magnetic nanoparticles were stabilized in water with a polymer coating that prevented the cores from aggregating and settling out of solution

due to the presence of attractive van der Waals forces between the cores, which for magnetite are stronger at short distances than attractive interparticle magnetic forces.[15,16] The polymer coating prevented aggregation of the magnetic nanoparticles by exerting a repulsive force between the particles at short range. In this research, both steric and electrostatic stabilization were provided by the polymer coating, which consisted of a polyacrylic acid (PAA) backbone onto which a random copolymer of polyethylene oxide (PEO) and polypropylene oxide (PPO) was grafted. The hydrated PEO and PPO moieties provided steric stabilization for the magnetite core while the acid groups on the PAA deprotonated in aqueous solution and provided electrostatic stabilization. Although stable magnetic fluids have been produced without the use of a stabilizing layer on the magnetic core, the ionic strength and pH of the solution must be strictly controlled to ensure sufficient charge on the surface of the bare particles in order to maintain electrostatic stabilization in aqueous solution.[17] Since the magnetic fluids used in this work were intended for use in fermentation broth, which has a relatively high ionic strength, stable bare magnetite nanoparticles were not a viable option, and the stabilizing polymer layer was required.

The PAA-PEO/PPO graft copolymer was attached to the magnetite core through the carboxylic acid groups on the PAA backbone. Carboxylic acid forms a strong *d*-orbital chelate bidentate structure with the Fe^{3+} atoms on the magnetite surface.[18] This method of attachment dates back to the earliest magnetic fluids, which used fatty acids as the stabilizing moiety, where the carboxylic acid head group attached to the magnetite core while the alkyl tail provided steric stabilization in an organic medium.[19]

Magnetite as a bulk metal possesses a magnetic domain size of ~25 nm.[20] This indicates that the ~8 nm magnetite core in the magnetic nanoparticles is composed of a single crystal of magnetite possessing a single magnetic domain with a permanent magnetic dipole.[14] Since these magnetic dipoles are randomly oriented in the bulk solution due to Brownian motion, which dominates the movement of the nano-sized magnetic particles,[5] the magnetic fluid as a whole exhibits no net magnetism outside of an applied field. Magnetic fluid is therefore superparamagnetic,[5] since the magnetic nanoparticles exhibit no net magnetization in the absence of a magnetic field, due to the random orientation of the particles with respect to each other, but exhibit significant

magnetization while in the presence of an applied magnetic field, as the magnetic dipoles in the nanoparticles become aligned with the field.

1.4.2 Magnetic Fluid Synthesis

1.4.2.1 General Concepts

The synthesis of the magnetic fluid used in this research involved two steps that were performed almost simultaneously: the formation of the magnetite nanoparticles and the coating of the nanoparticles with the stabilizing graft copolymer layer. The synthesis of the magnetite nanoparticles was conducted in the presence of the graft copolymer to prevent aggregation of the magnetite particles as they nucleated, in addition to providing long-term stability of the particles. The exact technique used to create the magnetic fluid for this research, called chemical coprecipitation, is discussed in detail in the next section. Chemical coprecipitation lends itself well to producing aqueous magnetic fluids; however it should be noted that both size reduction and organometallic decomposition are also common techniques for preparing magnetic fluid, although these techniques lend themselves more easily to producing magnetic fluids suspended in organic solutions.[14,21]

1.4.2.2 Chemical Coprecipitation

Chemical coprecipitation is a synthesis technique that uses inexpensive bulk metal salts to produce magnetic fluids in aqueous solution, and is one of the most common methods for synthesizing magnetic fluid due to its low cost and relative simplicity.[14] Chemical coprecipitation can produce several ferrite particles, including magnetite (Fe_3O_4),[19] maghemite (γ-Fe_2O_3),[17] and cobalt ferrite ($CoFe_2O_4$).[22,23] Magnetite formation will be the only synthesis procedure discussed in this section, as it was the only magnetic material synthesized in this work and is the most commonly cited component of magnetic fluid in the literature.

The synthesis of magnetite ($Fe_2O_3 \cdot FeO$, or Fe_3O_4) as a bulk metal is sufficiently straightforward and results from the coprecipitation of iron (III) chloride and iron (II) chloride in aqueous solution upon the addition of base. Magnetite forms with a 2:1 molar ratio of Fe^{3+} to Fe^{2+}, and the magnetic properties of magnetite result from the spinel

structure of the Fe^{3+} and Fe^{2+} ions.[13] With the use of ammonium hydroxide as the precipitating base, the overall stoichiometry of the reaction is given by Equation 1-2[14]:

$$2\,FeCl_3 + FeCl_2 + 8\,NH_4OH \rightarrow Fe_3O_4 + 8\,NH_4Cl + 4\,H_2O \qquad (1\text{-}2)$$

The ammonium hydroxide is added in excess so that the pH of the aqueous solution remains strongly basic (pH of 12-14) to facilitate the formation of the magnetite. The creation of magnetite nanoparticles, instead of bulk magnetite, results when the coprecipitation reaction is conducted in the presence of a dissolved graft copolymer. The dissolved polymer binds to the nascent magnetite crystals and limits their growth to ~8 nm. Differences in the metal salt concentrations, the graft copolymer concentration, and the reaction temperature all affect the size, composition, and inherent magnetic properties of the synthesized nanoparticles.[14,24] For the formation of the magnetic nanoparticles used in this work, a reaction temperature of approximately 80°C was found to be optimal and was the only temperature used for magnetic fluid synthesis.[14,25]

1.4.3 Current Uses of Magnetic Fluids and Magnetic Particles

1.4.3.1 Industrial Applications of Magnetic Fluids

Colloidally stabilized magnetic fluids of the general type synthesized for this work have been used in various commercial industries for decades, and are most commonly found in the computing, semiconducting, audio speaker, and petrochemical industries, where they are used primarily for sealing, damping, sensing, and heat transfer.[26] In permanent magnet stepper motors, magnetic fluid is used to fill the gap between the stator and the rotor teeth to damp the system from acceleration, shock and vibration, and since the magnetic fluid is held in place by the field generated by the permanent magnet, no external seals are needed for the device.[26] Magnetic fluid is also used to provide environmentally friendly seals for rotary pump shafts and to create frictionless bearings, which are produced when a permanent magnet or a similar magnetic structure is induced to float and slide upon a layer of magnetic fluid.[5,26]

In the presence of an applied magnetic field, magnetic fluid can also develop convection cells,[5] which, coupled with their inherently high thermal conductively, can be used as a coolant, an application currently utilized in the production of loudspeakers.[27] Each of these applications typically uses organically-suspended magnetic fluids, with synthetic oils being a common choice, to reduce or eliminate evaporation of the fluid,[26] and all utilize the magnetic fluid primarily for its magnetic properties, as opposed to the chemical properties present on the magnetic nanoparticle surfaces. Other non-traditional applications of magnetic fluids are also being developed, such as the use of cobalt-based magnetic fluids to enhance microwave heating of nonpolar liquids,[28] and the use of magnetite and maghemite magnetic fluids in combination with ink-jet technology to produce micron sized magnetic layers and structures by deposition of the magnetic nanoparticles.[29]

1.4.3.2 Biomedical Applications of Magnetic Fluids

Industrial uses of magnetic fluids typically require the fluids to be suspended in organic media both to prevent losses by evaporation and to allow for easy control over fluid viscosity. For biomedical applications of magnetic fluids, aqueous suspensions are required, and the magnetic nanoparticles themselves must be further tailored to provide stability and biocompatibility in the body, an issue which has been the focus of much research in recent years. Biocompatible magnetic fluids use primarily ferrite-based magnetic cores, such as magnetite, maghemite, and cobalt-ferrite, with stabilizing layers including dextran, albumin, dodecanoic acid and ethoxylated polyalcohol, starch, and citrate.[30-35]

The primary applications of magnetic fluids for biomedical use are in magnetic resonance imaging (MRI) and drug delivery.[30,36] When used with MRI, magnetic fluids result in improved imaging of organs and tumors in the body when compared to the use of conventional paramagnetic ions such as gadolinium and manganese, with a typical magnetic fluid composition consisting of magnetite stabilized by a biocompatible coating such as dextran or poly(D,L lactide-co-glycolide).[37-39] Magnetic drug delivery utilizes magnetic fluids by absorbing or attaching the desired drug to the magnetic nanoparticle

surface and then directing the doped magnetic nanoparticles to the target tissue with the use of externally applied magnetic fields.[32,36]

The most studied application of magnetic drug delivery involves cancer therapy, where the magnetic nanoparticles are doped with an anti-cancer drug that is then directed by an applied magnetic field to a tumor in the body.[36] Cancer therapies using magnetohyperthermia have also been studied, and involve the use of an externally applied alternating magnetic field, which causes significant heating of the magnetic fluid that has been localized at the tumor site, resulting in the death of the tumor cells.[21,34,40] Other applications of magnetic fluids for cancer therapy are also being developed, such as the use of cobalt-ferrite fluids, where radioactive cobalt, ^{60}Co, is used for the magnetic nanoparticle core and provides the means for the destruction of the cancerous cells.[34,41]

1.5 Separation using Magnetic Fluids

1.5.1 Industrial Separation using Magnetic Fluids

Magnetic fluids are used in industry to separate a variety of substances. Most commonly, magnetic fluids are used in magnetic levitation to separate mineral grains or coal particles, which are typically around 1 mm in size.[42] This levitation technique, called magnetoflotation, is similar to magnetophoresis as studied in this work. When magnetic fluid is placed in a non-uniform magnetic field, non-magnetic particles, in this case minerals or coal particles, are forced by the magnetization of the magnetic fluid away from areas of high magnetic field and into areas of low magnetic field according to Equation 1-1. When both the fluid and the degrading magnetic field are oriented vertically, the force on the non-magnetic particles from the magnetized fluid is balanced by the gravitational force that, without the presence of the magnetic fluid, would cause the particles to settle. Thus, the particles will levitate in the magnetized magnetic fluid at the point where the gravitational force equals the magnetic force. This technique is used commercially to separate mineral grains and coal particles of different densities, since particles with different densities will float at different levels above the magnetic field under equilibrium conditions.[5,42,43] Alternatively, the magnetic field gradient can be adjusted so that the magnetic force balances the gravitational force for one type of

particle but not for another heavier particle, obtaining effective separation by causing one particle to float on the magnetic fluid and the more dense particles to sink.[44]

1.5.2 Cell Separation using Magnetic Particles

Magnetic fluids and magnetic particles have been used to separate a variety of biological products, including cells, DNA, and proteins. This section reviews the magnetic separation techniques employed for the capture of cells, although the same techniques typically apply for the capture of proteins and other cell products, as well.

The most common technique for the commercial separation of cells utilizes functionalized magnetic particles with affinity ligands attached to their surfaces that bind to the cells directly.[45] Immunomagnetic separation is the most popular of these, and employs the use of antibodies on the magnetic particle surfaces, which bind to specific cell surface epitopes.[46,47] Once the magnetic particles are attached, a magnetic field is used to separate the magnetic particles and attached cells from the bulk suspension fluid. If the collected cells are the desired product, a third step involving the detachment of the magnetic particles is usually, but not always, required.[48]

Typically, cell separation of this type involves the use of functionalized micron sized polymer beads with magnetic nanoparticles embedded in them to provide the appropriate magnetic properties.[46] Commercially available beads of this type include Dynabeads from Dynal Biotech (Oslo, Norway), SPHERO Magnetic Particles from Spherotech, Inc. (Libertyville, IL), Iobeads from Immunotech (Marseille, France), and MagaBeads from Cortex Biochem, Inc. (San Leandro, CA), to name a few.[30,46] Specific applications of immunomagnetic separation include the use of functionalized magnetic beads to detect *Escherichia coli*, particularly strain O157, in the food supply.[49-52] The magnetic beads used for these separations are not true magnetic fluids, however, since they are much larger than the magnetic nanoparticles synthesized for this research, and are approximately the same size as the cells being separated, and so can not be considered as a continuum when compared to the cells.

Some research has been performed using true magnetic fluids for cell separation; however, the method of separation remains the same, with the magnetic nanoparticles containing functionalized surface groups for direct attachment to the cells, such as the use

of functionalized maghemite nanoparticles for separating erythrocyte cells,[21,30] or chitosan-conjugated magnetite for separating recombinant *E. coli*.[53] When magnetic nanoparticles are used, the cells become covered with many attached particles and often internalize them,[54] in contrast to the use of micron sized magnetic beads, where typically only a few magnetic beads attach to the cellular surface, depending on cell size. Separation is still achieved in the same manner as with the larger magnetic particles, with the magnetically tagged cells directed out of the cell suspension fluid through the use of an applied magnetic field.

All of these magnetic cell separation techniques rely on a specific functional moiety that is present on the magnetic particles. These techniques are therefore specific to the separation of one particular cell type, and are not intended for the bulk removal of cells from fermentation broth. The functionalization of the magnetic particles for immunomagnetic separation also involves the use of antigen/antibody combinations, which is expensive and limits the types of cells that can be separated to those for which known antigen/antibody combinations exist.[55] The use of immunomagnetic separation of cells is therefore highly successful for separating specific cells from a mixture of different cell types, but it is not well suited for the bulk separation of cells from fermentation broth. More generalized functionalities such as ion-exchange moieties on magnetic particle surfaces are possible and offer lower costs, but such functionalities also increase the probability of particle binding to undesired cells, cell products, and ions in solution when used with raw fermentation broth.[55]

1.5.3 Magnetophoretic Separation Devices

Cells and other biological entities that have been tagged with magnetic particles are separated using either batch or flow-through magnetic devices.[46] Batch devices typically use a strong permanent magnet located at a specific location in the device that attracts the magnetic particles to it and concentrates them in that location, often at the bottom of a tube or vial.[46] These techniques work well for micron sized magnetic particles.

Flow-through magnetic devices make use of a specific arrangement of permanent or electromagnets. A commonly used flow-through device is a high gradient magnetic

separator (HGMS). In these devices, a column packed with fine magnetizable wires, such as steel wool, is placed between two strong magnets. The magnetic field produced by the magnets magnetizes the metal fibers in the column and creates areas of high magnetic field gradient around the fibers. When the cell suspension is passed through the column in an HGMS device, the magnetically tagged cells are retained on the metal fibers, while the rest of the suspension passes through. The magnetically tagged cells are then recovered by removing the magnetic field and eluting the captured particles.[46] HGMS works well for capturing magnetic particles smaller than one micron, down to about 30 nm.[14]

Another commonly used flow-through device is the quadrupole magnetic separator. In this separator, four magnets are used to surround a cylindrical column and create a focused magnetic field that is constant axially along the length of the column but that degrades in the radial direction, with the weakest fields located at the center line in the column and the strongest fields located at the outer column wall.[56] As the cell suspension is introduced to the quadrupole device, the magnets attract the magnetically labeled cells, which deviate from the flow of the bulk fluid towards the areas of higher magnetic field at the outer walls. In this way, the quadrupole device splits the inlet cell stream into two fractions, one which contains the magnetically tagged cells, and the other which contains the depleted suspension fluid.[46,47,56] This design has been successfully used for the immunomagnetic separation of lymphocytes[47,56,57] and breast carcinoma (epithelial tumor) cells,[58] to name a few examples. One of the principle drawbacks of this design as it is used for immunomagnetic separation is that the feed containing the labeled cells is typically added to the device along with a carrier fluid, which prevents the non-labeled cells from drifting to the outer fraction where the labeled cell congregate.[47,56] The addition of the carrier fluid significantly increases the total amount of liquid processed by the quadrupole system.

1.5.4 Magnetophoretic Separation using Magnetic Fluids

Magnetophoretic separation of the type described previously for magnetic levitation of mineral grains and coal particles is currently the only known commercial use of magnetophoresis using magnetic fluids for the separation of non-magnetic particles

from a bulk fluid. This approach is different from the biological separations discussed in the previous section, as it utilizes the magnetic fluid for its magnetic properties only, not for any functionalized surface properties. A few studies using magnetic fluids for magnetophoretic separation of non-magnetic particles have been reported in the literature. All of these studies looked at the separation of non-magnetic polystyrene beads in magnetic fluid under a non-uniform magnetic field.[6,59-61]

Gonzalez, et al. tested the migration of 840 nm and 510 nm sized polystyrene beads in a colloidal magnetic fluid of a type similar to that produced in this work by using a flow tube with a permanent magnet placed at one end, thus creating a system with an axially degrading magnetic field, similar in design to the simplified schematic given in Figure 1-1. The results showed that both particle sizes migrated under the magnetic force and became concentrated at the point where the gradient of the magnetic field vanished, with the larger particles migrating faster than the smaller particles, as predicted by Equation 1-1.[6] These results showed that magnetophoretic separation is possible for particle sizes less than one micron in size.

Similar experiments were independently performed by Watarai and Namba using micron sized polystyrene beads in capillary tubes. The experimental setup was similar to that used by Gonzalez, et al., with a non-uniform magnetic field applied to the capillary tubes; however, the magnetizable fluid used was a paramagnetic solution of manganese (II) chloride, not a colloidal magnetic fluid of the type used in this work. The results were similar, however, with the polystyrene beads moving away from the areas of high magnetic field and concentrating in the areas of low magnetic field, as predicted by Equation 1-1.[60-62] Although this study showed that magnetophoretic separation of micron sized non-magnetic particles is possible, only dilute concentrations of the beads were used in small volumes of fluid that experienced no bulk fluid flow. Additionally, the use of paramagnetic salt solutions is not optimal, since colloidal magnetic fluids are more environmentally and biologically friendly than paramagnetic salts, and stronger fluid magnetizations can be achieved with their use.[6]

1.6 Research Overview

No magnetophoretic technique for the separation of non-magnetic micron sized particles is known for fluids experiencing bulk fluid flow through a system, nor is a separation technique known that involves the use of unfunctionalized, bulk magnetic nanoparticles to separate cells from fermentation broth. Such a technique could bring with it advantages of low cost, biological and environmental compatibility, and the flexibility to remove cells from any fermentation broth, regardless of cell type. Such a technique, deemed magnetophoretic cell clarification, is the focus of this work.

The overall goals of this research were: i) to synthesize magnetic fluid for use as a medium for cell clarification, ii) to explore the feasibility of two different flow devices as potential technologies for magnetophoretic cell clarification using magnetic fluid, and iii) to devise a model of the magnetophoretic cell clarification process, both generally and as applied to the specific devices studied in this work. Chapter 2 describes in detail the synthesis of the aqueous solutions of magnetic fluid, including the method used to create the graft copolymer that served as the steric stabilizing layer for the magnetic nanoparticles. In addition, this chapter also describes the basic physical properties of magnetic fluid, such as particle size, surface charge, and magnetic properties. The analytical techniques used to measure the amount of magnetite in the magnetic fluid solutions are also discussed here. Chapter 3 describes the method employed to grow the *E. coli* cells that were used in this research, as well as the characterization of cell properties, including size and surface charge. The analytical techniques used to measure cell concentration in aqueous solution, both in the presence and absence of magnetic fluid, are also discussed in this chapter, as well as the characterization and use of polystyrene beads as model non-magnetic particles for magnetophoretic clarification. Chapter 4 contains the results of the feasibility study of magnetophoretic cell clarification using a counter-current flow device. Chapter 5 discusses the model that was constructed to theoretically describe the magnetophoretic clarification process. The application of the model to the design and construction of the second device for magnetophoretic clarification, the quadrupole flow device, is also discussed in this chapter. Chapter 6 discusses the results of the experiments using the quadrupole flow device and how the separation capability of the device compared to the model predictions. Chapter 7

summarizes the results of this work and presents ideas and suggestions for further applications using magnetophoretic cell clarification, including its potential industrial applications.

1.7 References

1. Chemical-Processing, "In the News: Separations Adapt to Bioprocessing Needs". 2003, http://www.chemicalprocessing.com/.

2. Sanchez-Ruiz, S.A., "Studies on Cell Disruption and Cell Debris Removal in Downstream Bioprocessing", Ph.D. Thesis, Department of Applied Biological Sciences; Massachusetts Institute of Technology: Cambridge, MA, 1989.

3. Alfa Laval, "Membrane Filtration: Product Catalog". 2003: Sweden.

4. Norton, T., "Industrial Cell Clarification Technologies". 2003, DuPont, personal communication.

5. Rosensweig, R.E., *Ferrohydrodynamics*. 1997, Mineola, NY: Dover Publications, Inc.

6. Gonzalez, L., S.E.K. Fateen, K. Smith and T.A. Hatton. "Magnetophoresis of Nonmagnetic, Submicrometer Particles in Magnetic Fluids". in *Singapore-MIT Alliance (SMA) Symposium*. 2004. Singapore.

7. Ogez, J.R., J.C. Hodgdon, M.P. Beal and S.E. Builder, "Downstream Processing of Proteins: Recent Advances". *Biotech. Adv.*, 1989. **7**: p. 467-488.

8. Cooney, C.L., "Downstream Processing", Massachusetts Institute of Technology, Summer Session. 2001: Cambridge, MA.

9. Perry, R.H., D.W. Green and J.O. Maloney, eds. *Perry's Chemical Engineers' Handbook*. 7 ed. 1997, McGraw-Hill: New York.

10. Ladisch, M.R., *Bioseparations Engineering: Principles, Practice, and Economics*. 2001, New York: John Wiley & Sons, Inc.

11. Bhave, R.R., "Cross-Flow Filtration", in *Fermentation and Biochemical Engineering Handbook: Principles, Process Design, and Equipment, Second*

Edition, H.C. Vogel and C.L. Todaro, Editors. 1997, Noyes Publications: Westwood, NJ.

12. Hamel, J.-F.P. and J.B. Hunter, "Modeling and Applications of Downstream Processing: A Survey of Innovative Strategies", in *Downstream Processing and Bioseparation: Recovery and Purification of Biological Products*, J.-F.P. Hamel, J.B. Hunter, and S.K. Sikdar, Editors. 1990, American Chemical Society: Washington, DC.

13. Gokon, N., A. Shimada, H. Kaneko, Y. Tamaura, K. Ito and T. Ohara, "Magnetic coagulation and reaction rate for the aqueous ferrite formation reaction". *Journal of Magnetism and Magnetic Materials*, 2002. **238**(1): p. 47-55.

14. Moeser, G.D., "Colloidal Magnetic Fluids as Extractants for Chemical Processing Applications", Ph.D. Thesis, Department of Chemical Engineering; Massachusetts Institute of Technology: Cambridge, MA, 2003.

15. Shen, L.F., A. Stachowiak, S.E.K. Fateen, P.E. Laibinis and T.A. Hatton, "Structure of Alkanoic Acid Stabilized Magnetic Fluids. A Small-Angle Neutron and Light Scattering Analysis". *Langmuir*, 2001. **17**(2): p. 288-299.

16. Harris, L.A., J.D. Goff, A.Y. Carmichael, J.S. Riffle, J.J. Harburn, T.G. St. Pierre and M. Saunders, "Magnetite Nanoparticle Dispersions Stabilized with Triblock Copolymers". *Chemistry of Materials*, 2003. **15**(6): p. 1367-1377.

17. Massart, R., R. Dubois, V. Cabuil and E. Hasmonay, "Preparation and Properties of Monodisperse Magnetic Fluids". *Journal of Magnetism and Magnetic Materials*, 1995. **149**: p. 1-5.

18. Mikhailik, O.M., V.I. Povstugar, S.S. Mikhailova, A.M. Lyakhovich, O.M. Fedorenko, G.T. Kurbatova, N.I. Shklovskaya and A.A. Chuiko, "Surface Structure of Finely Dispersed Iron Powders. I. Formation of Stabilizing Coating". *Colloids and Surfaces*, 1991. **52**: p. 315-324.

19. Reimers, G.W. and S.E. Khalafalla, "Preparing Magnetic Fluids by a Peptizing Method". 1972, Twin Cities Metallurgy Research Center, U.S. Department of the Interior: Minneapolis.

20. Lee, J., T. Isobe and M. Senna, "Preparation of Ultrafine Fe3O4 Particles by Precipitation in the Presence of PVA at High pH". *Journal of Colloid and Interface Science*, 1996. **177**: p. 490-494.

21. Halbreich, A., J. Roger, J.N. Pons, D. Geldwerth, M.F. Da Silva, M. Roudier and J.C. Bacri, "Biomedical applications of maghemite ferrofluid". *Biochimie*, 1998. **80**(5-6): p. 379-390.

22. Giri, A.K., K. Pellerin, W. Pongsaksawad, M. Sorescu and S.A. Majetich, "Effect of Light on the Magnetic Properties of Cobalt Ferrite Nanoparticles". *Ieee Transactions on Magnetics*, 2000. **36**(5): p. 3029-3031.

23. Morais, P.C., V.K. Garg, A.C. Oliveira, L.P. Silva, R.B. Azevedo, A.M.L. Silva and E.C.D. Lima, "Synthesis and characterization of size-controlled cobalt-ferrite-based ionic ferrofluids". *Journal of Magnetism and Magnetic Materials*, 2001. **225**: p. 37-40.

24. Feltin, N. and M.P. Pileni, "New Technique for Synthesizing Iron Ferrite Magnetic Nanosized Particles". *Langmuir*, 1997. **13**(15): p. 3927-3933.

25. Shen, L.F., P.E. Laibinis and T.A. Hatton, "Bilayer Surfactant Stabilized Magnetic Fluids: Synthesis and Interactions at Interfaces". *Langmuir*, 1999. **15**(2): p. 447-453.

26. Raj, K., B. Moskowitz and R. Casciari, "Advances in Ferrofluid Technology". *Journal of Magnetism and Magnetic Materials*, 1995. **149**: p. 174-180.

27. Raj, K. and R. Moskowitz, "Commercial Applications of Ferrofluids". *Journal of Magnetism and Magnetic Materials*, 1990. **85**: p. 233-245.

28. Holzwarth, A., J.F. Lou, T.A. Hatton and P.E. Laibinis, "Enhanced Microwave Heating of Nonpolar Solvents by Dispersed Magnetic Nanoparticles". *Industrial & Engineering Chemistry Research*, 1998. **37**(7): p. 2701-2706.

29. Voit, W., W. Zapka, L. Belova and K.V. Rao. "Application of inkjet technology for the deposition of magnetic nanoparticles to form micron-scale structures". in *IEE Proceedings: Science, Measurement, and Technology*. 2003. Stockholm, Sweden.

30. Roger, J., J.N. Pons, R. Massart, A. Halbreich and J.C. Bacri, "Some biomedical applications of ferrofluids". *European Physical Journal: Applied Physics*, 1999. **5**: p. 321-325.

31. Freitas, M.L.L., L.P. Silva, J.L. Freitas, R.B. Azevedo, Z.G.M. Lacava, P.I. Homem de Bittencourt Jr., R. Curi, N. Buske and P.C. Morais, "Investigation of lipid peroxidation and catalase activity in magnetic fluid treated mice". *Journal of Applied Physics*, 2003. **93**(10, Parts 2 & 3): p. 6709-6711.

32. Sincai, M., L. Deleanu, D. Argherie and D. Bica, "The effects of magnetic fluids on blood parameters in dogs". *Journal of Magnetism and Magnetic Materials*, 2002. **252**: p. 406-408.

33. Kuckelhaus, S., S.C. Reis, M.F. Carneiro, A.C. Tedesco, D.M. Oliveira, E.C.D. Lima, P.C. Morais, R.B. Azevedo and Z.G.M. Lacava, "In vivo investigation of cobalt ferrite-based magnetic fluid and magnetoliposomes using morphological tests". *Journal of Magnetism and Magnetic Materials*, 2004. **272-276**: p. 2402-2403.

34. Kuckelhaus, S., V.A.P. Garcia, L.M. Lacava, R.B. Azevedo, Z.G.M. Lacava, E.C.D. Lima, F. Figueiredo, A.C. Tedesco and P.C. Morais, "Biological investigation of a citrate-coated cobalt-ferrite-based magnetic fluid". *Journal of Applied Physics*, 2003. **93**(10, Parts 2 & 3): p. 6707-6708.

35. Kim, D.K., M. Mikhaylova, Y. Zhang and M. Muhammed, "Protective Coating of Superparamagnetic Iron Oxide Nanaparticles". *Chemistry of Materials*, 2003. **15**: p. 1617-1627.

36. Lubbe, A.S., C. Bergemann, J. Brock and D.G. McClure, "Physiological aspects in magnetic drug-targeting". *Journal of Magnetism and Magnetic Materials*, 1999. **194**(1-3): p. 149-155.

37. Kawaguchi, T., A. Yoshino, M. Hasegawa, T. Hanaichi, S. Maruno and N. Adachi, "Dextran-magnetite complex: temperature dependence of its NMR relaxivity". *Journal of Materials Science: Materials in Medicine*, 2002. **13**(1): p. 113-117.

38. Lee, S.-J., J.-R. Jeong, S.-C. Shin, J.-C. Kim, Y.-H. Chang, Y.-H. Chang and J.-D. Kim, "Nanoparticles of magnetic ferric oxides encapsulated with poly(D,L latide-co-glycolide) and their applications to magnetic resonance imagning contrast agent". *Journal of Magnetism and Magnetic Materials*, 2004. **272-276**: p. 2432-2433.

39. Morales, M.P., O. Bomati-Miguel, R. Perez de Alejo, J. Ruiz-Cabello, S. Veintemillas-Verdaguer and K. O'Grady, "Contrast agents for MRI based on iron oxide nanoparticles prepared by laser pyrolysis". *Journal of Magnetism and Magnetic Materials*, 2003. **266**: p. 102-109.

40. Suzuki, M., M. Shinkai, M. Kamihira and T. Kobayashi, "Preparation and characteristics of magnetite-labeled antibody with the use of poly(ethylene glycol) derivatives". *Biotechnology and Applied Biochemistry*, 1995. **21**: p. 335-345.

41. Sincai, M., D. Ganga, D. Bica and L. Vekas, "The antitumor effect of locoregional magnetic cobalt ferrite in dog mammary adenocarcinoma". *Journal of Magnetism and Magnetic Materials*, 2001. **225**: p. 235-240.

42. Jakabsky, S., M. Lovas, A. Mockovciakova and S. Hredzak, "Utilization of ferromagnetic fluids in mineral processing and water treatment". *Journal of Radioanalytical and Nuclear Chemistry*, 2000. **246**(3): p. 543-547.

43. Moffat, G., R.A. Williams, C. Webb and R. Stirling, "Selective Separations in Environmental and Industrial-Processes Using Magnetic Carrier Technology". *Minerals Engineering*, 1994. **7**(8): p. 1039-1056.

44. Fofana, M. and M.S. Klima, "Use of a magnetic fluid based process for coal separations". *Minerals and Metallurgical Processing*, 1997. **14**(1): p. 35-40.

45. Safarikova, M. and I. Safarik, "The application of magnetic techniques in biosciences". *Magnetic and Electrical Separation*, 2001. **10**(4): p. 223-252.

46. Safarik, I. and M. Safarikova, "Use of magnetic techniques for the isolation of cells". *Journal of Chromatography B*, 1999. **722**(1-2): p. 33-53.

47. Sun, L., M. Zborowski, L.R. Moore and J.J. Chalmers, "Continuous, Flow-Through Immunomagnetic Cell Sorting in a Quadrupole Field". *Cytometry*, 1998. **33**: p. 469-475.

48. Partington, K.M., E.J. Jenkinson and G. Anderson, "A novel method of cell separation based on dual parameter immunomagnetic cell selection". *Journal of Immunological Methods*, 1999. **223**: p. 195-205.

49. Reinders, R.D., A. Barna, L.J.A. Lipman and P.G.H. Bijker, "Comparison of the sensitivity of manual and automated immunomagnetic separation methods for detection of Shiga toxin-producing *Escherichia coli* O157:H7 in milk". *Journal of Applied Microbiology*, 2002. **92**: p. 1015-1020.

50. Jenkins, C., M.C. Pearce, A.W. Smith, H.I. Knight, D.J. Shaw, T. Cheasty, G. Foster, G.J. Gunn, G. Dougan, H.R. Smith, and G. Frankel, "Detection of *Escherichia coli* serogroups O26, O103, O111 and O145 from bovine faeces using immunomagnetic separation and PCR/DNA probe techniques". *Letters in Applied Microbiology*, 2003. **37**: p. 207-212.

51. Hepburn, N.F., M. MacRae, M. Johnston, J. Mooney and I.D. Ogden, "Optimizing enrichment conditions for the isolation of *Escherichia coli* O157 in

soils by immunomagnetic separation". *Letters in Applied Microbiology*, 2002. **34**: p. 365-369.

52. Guan, J. and R.E. Levin, "Quantitative detection of *Escherichia coli* O157:H7 in ground beef by immunomagnetic separation and polymerase chain reaction". *Food Biotechnology*, 2002. **16**(2): p. 135-144.

53. Honda, H., A. Kawabe, M. Shinkai and T. Kobayashi, "Recovery of recombinant *Escherichia coli* by chitosan-conjugated magnetite". *Biochemical Engineering Journal*, 1999. **3**: p. 157-160.

54. Wilhelm, C., C. Billotey, J. Roger, J.N. Pons, J.C. Bacri and F. Gazeau, "Intracellular uptake of anionic superparamagnetic nanoparticles as a function of their surface coating". *Biomaterials*, 2003. **24**: p. 1001-1011.

55. Deponte, S., J. Steingroewer, C. Loser, E. Boschke and T. Bley, "Biomagnetic separation of *Escherichia coli* by use of anion-exchange beads: measurement and modeling of the kinetics of cell-bead interactions". *Analytical and Bioanalytical Chemistry*, 2004. **379**(3): p. 419-426.

56. Chalmers, J.J., M. Zborowski, L. Sun and L.R. Moore, "Flow Through, Immunomagnetic Cell Separation". *Biotechnology Progress*, 1998. **14**(1): p. 141-148.

57. Zborowski, M., L. Sun, L.R. Moore, P.S. Williams and J.J. Chalmers, "Continuous cell separation using novel magnetic quadrupole flow sorter". *Journal of Magnetism and Magnetic Materials*, 1999. **194**: p. 224-230.

58. Nakamura, M., K. Decker, J. Chosy, K. Comella, K. Melnik, L.R. Moore, L.C. Lasky, M. Zborowski and J.J. Chalmers, "Separation of a Breast Cancer Cell Line from Human Blood Using a Quadrupole Magnetic Flow Sorter". *Biotechnology Progress*, 2001. **17**(6): p. 1145-1155.

59. Fateen, S.E.K., "Magnetophoretic Focusing of Submicron Particles Dispersed in a Polymer-Stabilized Magnetic Fluid", Ph.D. Thesis, Department of Chemical Engineering; Massachusetts Institute of Technology: Cambridge, MA, 2002.

60. Watarai, H. and M. Namba, "Magnetophoretic Behavior of Single Polystyrene Particles in Aqueous Manganese(II) Chloride". *Analytical Sciences*, 2001. **17**: p. 1233-1236.

61. Watarai, H., M. Suwa and Y. Iiguni, "Magnetophoresis and electromagnetophoresis of microparticles in liquids". *Analytical and Bioanalytical Chemistry*, 2004. **378**: p. 1693-1699.

62. Watarai, H., H. Monjushiro, S. Tsukahara, M. Suwa and Y. Iiguni, "Migration Analysis of Micro-Particles in Liquids Using Microscopically Designed External Fields". *Analytical Sciences*, 2004. **20**: p. 423-434.

Chapter 2

Magnetic Fluid Synthesis and Characterization

2.1 Introduction

The concept of magnetophoretic clarification relies on the force that a non-magnetic particle feels when it is surrounded by a magnetized fluid, which pushes the particle away from areas of high magnetic field and into areas of low magnetic field. Since this magnetic force on the non-magnetic particle does not occur in the absence of a magnetically susceptible fluid, the magnetic fluid is a crucial component of the process, and thus its synthesis and physical properties must be well understood in order to be effectively utilized.

The magnetic fluid used in this research consists of an aqueous suspension of magnetite nanoparticles coated with a graft copolymer shell that provides steric colloidal stability in water. This chapter discusses in detail the synthesis and characterization of the graft copolymer, the synthesis of the polymer coated magnetite nanoparticles, and a complete characterization of the physical properties of the magnetic fluid, which is composed of these coated magnetite nanoparticles suspended in aqueous solution.

2.2 Magnetic Fluid Synthesis

2.2.1 The Graft Copolymer

The graft copolymer used to coat the magnetite core of each magnetic nanoparticle is essential to the stability of the magnetic fluid. Without the polymer coating, the magnetite in solution would aggregate and precipitate, leading to unstable and thus unusable magnetic fluid. The graft copolymer used to stabilize the magnetite was a comb graft copolymer consisting of a polyacrylic acid (PAA) backbone onto which a random block copolymer composed of polyethylene oxide (PEO) and polypropylene oxide (PPO) was grafted using an amidation reaction. The materials used to synthesize

the graft copolymer, the synthesis procedure, and the physical characterization of the final graft copolymer are described in detail in the next two sections.

2.2.1.1 Materials

The synthesis procedure used to produce the graft copolymer required two components, polyacrylic acid (PAA) and an amino-terminated polyethylene oxide (PEO)/polypropylene oxide (PPO) random block copolymer. Polyacrylic acid (50 wt% in water, M_w = 5000) was obtained from Aldrich Chemical Company (Milwaukee, WI). The amino-terminated PEO/PPO block copolymer (99.8%, M_w = 2000) was obtained as a gift from the Huntsman Corporation (Houston, TX), where it is sold under the trade name Jeffamine M-2070. All chemicals were used as received.

The amino-terminated PEO/PPO random block copolymer (Jeffamine M-2070) used for this research consisted of a polymer chain of ethylene oxide (EO) and propylene oxide (PO) monomer units repeated at random down the length of the chain, with an overall ratio of 70% EO units to 30% PO units, or 2.3 EO: 1 PO, as shown in Figure 2-1.

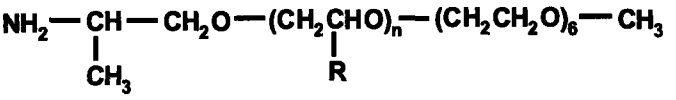

Figure 2-1. Amino-terminated polyethylene oxide (PEO)/polypropylene oxide (PPO) random block copolymer (Jeffamine M-2070), where R = H (for EO) or CH_3 (for PO) and the overall EO/PO ratio is 70/30. With an average molecular weight of 2000, *n* is approximately 34.

2.2.1.2 Graft Copolymer Synthesis

The graft copolymer was prepared by amidation, where the carboxylic acid groups on the PAA chains were reacted with the amino groups on the amino-terminated PEO/PPO chains, as shown in Figure 2-2. PAA and amino-terminated PEO/PPO were mixed in a flask, sparged with nitrogen, and heated to 180°C. Once at 180°C, the mixture was allowed to react for two hours under constant nitrogen flow, which provided mixing, prevented oxidation of the polymer, and expelled the water produced by the reaction. At

the completion of the reaction, the resultant graft copolymer was cooled to ambient temperature, and dissolved in water to create a 33 wt% graft copolymer solution.

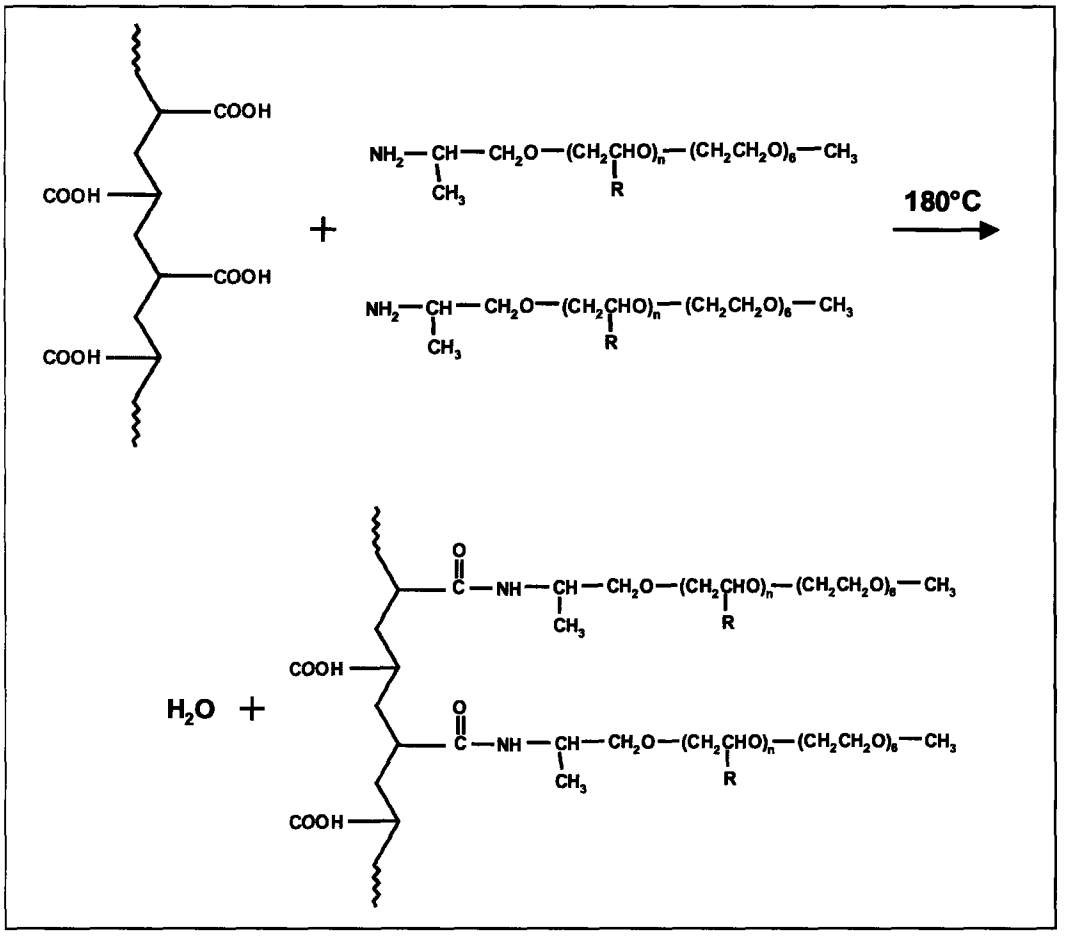

Figure 2-2. Synthesis of the graft copolymer via amidation by reacting the carboxylic acid groups on the PAA chains with the amino-terminated PEO/PPO random block copolymer, yielding a comb polymer with PEO/PPO grafted onto a PAA backbone. Approximately 84% of the carboxylic acid groups are left unreacted for subsequent attachment to the magnetite cores.

The polymers were added in a stoichiometric ratio such that there were approximately 6.3 carboxylic acid groups available for every amino-terminated copolymer chain. Previous work showed that the amidation reaction proceeds to approximately 95% completion,[1] resulting in an average of 10 PEO/PPO side chains grafted onto every PAA backbone chain for an approximate total molecular weight of 26,000 g/mol, with the PEO/PPO side chains comprising 80% of the total weight of the comb copolymer. The stoichimetric ratio for the reaction also kept 85% of the carboxylic

acid groups unreacted on the final synthesized graft copolymer. These free acid groups are important, as they provide the means of attachment of the graft copolymer to the magnetite core, as discussed in the next section.

2.2.2 Magnetite Nanoparticles

The polymer stabilized magnetite nanoparticles that comprise magnetic fluid were synthesized by chemical coprecipitation in a single batch reaction using the PAA-PEO/PPO graft copolymer, iron(III) chloride, iron(II) chloride, and base. The materials used to synthesize the particles, the synthesis procedure, and the physical characterization of the final, stabilized magnetite particles are described in detail in the next few sections.

2.2.2.1 Materials

The PAA-PEO/PPO graft copolymer needed to stabilize the magnetite core was used exactly as produced in the synthesis procedure described in the previous section, with no further purification or alteration. Iron(III) chloride hexahydrate (98%), iron(II) chloride tetrahydrate (99%), and ammonium hydroxide (28 wt% in water) were all obtained from Aldrich Chemical Company (Milwaukee, WI), and were used as received.

2.2.2.2 Magnetite Nanoparticle Synthesis

The synthesis of the stabilized magnetite nanoparticles involved two distinct steps performed almost simultaneously, precipitating the magnetite nanoparticles in aqueous solution, and coating them with the stabilizing graft copolymer. Both of these steps were performed in a one-step batch process involving the chemical coprecipitation of iron(III) and iron(II) chlorides in an aqueous solution containing dissolved graft copolymer with the addition of base, as shown in Figure 2-3.

The coated particles were prepared by first dissolving the 33 wt% solution of PAA-PEO/PPO graft copolymer in deionized water. The solution was then sparged with nitrogen under vigorous stirring for approximately 20 minutes to remove the dissolved oxygen in the mixture. Iron(III) chloride hexahydrate and iron(II) chloride tetrahydrate were then added to the mixture in a 2:1 molar ratio of iron(III) to iron(II), corresponding to the 2:1 molar ratio of Fe^{3+} and Fe^{2+} in magnetite, which has the chemical formula $Fe_2O_3 \cdot FeO$. The mixture of polymer and iron chlorides was then heated to 80°C under

continuous sparging with nitrogen. At approximately 70°C during the heating process, the flow of nitrogen was stopped and concentrated ammonium hydroxide was added to the mixture to initiate the precipitation of iron oxide, in the form of magnetite, from the dissolved iron in the solution. The mixing of the base with the water in the solution is exothermic, which is why the base was added before the mixture reached its final temperature of 80°C. Once at 80°C, the solution was stirred for 30 minutes before cooling to room temperature, where it was then sonicated for approximately 2 minutes using a tip sonicator (Branson Sonifier Model 450) to encourage the break up of any aggregates that may have formed during the synthesis procedure.

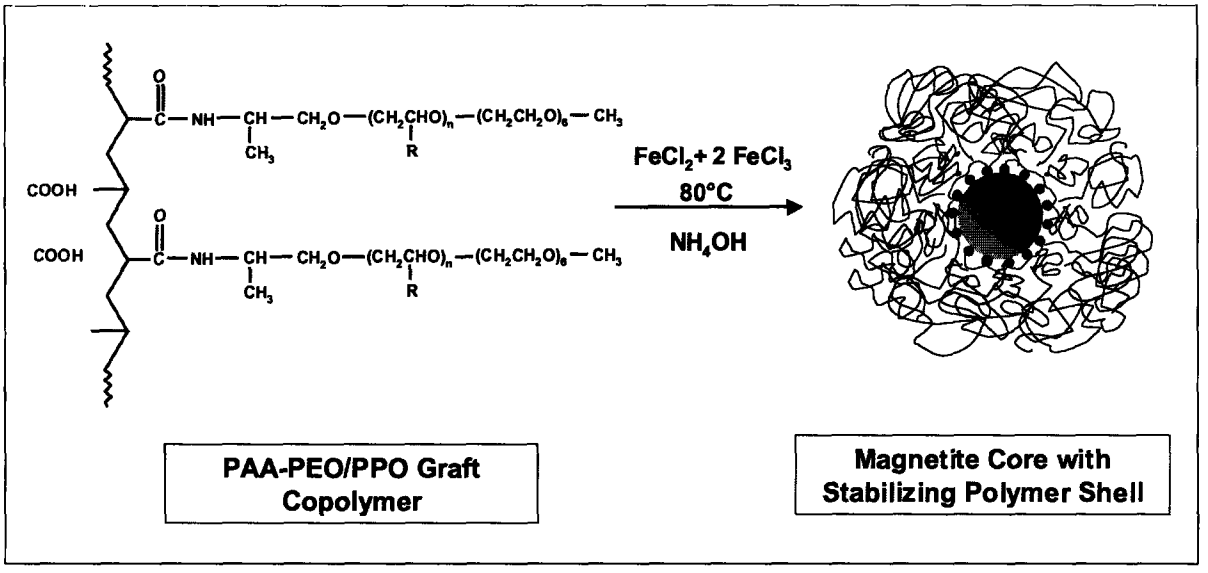

Figure 2-3. Chemical coprecipitation of iron(III) and iron(II) to magnetite with the addition of base, with stabilization of the magnetite provided by the PAA-PEO/PPO graft copolymer.

The stability of the magnetite particles that form with the addition of the base is the result of the interaction of the dissolved graft copolymer with the emerging crystals of magnetite. As the magnetite crystals nucleate and begin to grow, the carboxylic acid groups on the backbone of the copolymer chelate to the iron on the developing magnetite particles. Sufficient polymer eventually covers the surface of the nascent crystals that their growth is effectively stopped at a size of approximately 8-10 nm.[1] The PEO/PPO side chains attached to the PAA backbone of the graft copolymer then form a shell around the particle, stabilizing it in water.

The total weight of the graft polymer used in the synthesis of magnetic fluid was adjusted so that the mass of the dissolved polymer was approximately 1.25 times the mass of the magnetite that formed in the solution after the addition of the base. This ratio provided sufficient polymer to coat the magnetite cores and create colloidally stable particles while minimizing the amount of excess free polymer in the final solution. Still, previous studies showed that only two-thirds of the polymer present during synthesis actually binds chemically to the magnetite, leading to a bound-polymer to magnetite mass ratio of approximately 0.8:1.[1] In addition, the total mass of iron used in the synthesis was adjusted so that the mass of magnetite in the final solution represented approximately 2 wt% of the total mass.

After sonication, the raw magnetic fluid was then washed to remove the excess free polymer and the ions in solution using a Centricon Plus-80 Biomax-100 centrifugal ultrafiltration cell with a 100,000 molecular weight cutoff, purchased from the Millipore Corporation (Bedford, MA). The ultrafiltration cells were first rinsed with deionized water before using them to wash the raw magnetic fluid. The magnetic fluid was diluted to approximately 1.0 wt% magnetite with deionized water and then concentrated to greater than 8 wt% in the filter. The polymer-coated magnetite nanoparticles were retained by the membrane while the unattached polymer and remaining ions in solution were washed through under the force of centrifugation. The retained, concentrated magnetic fluid was then diluted again with deionized water to approximately 1 wt% magnetite, and the process was repeated. A total of four washes were used for each synthesized batch of magnetic fluid to remove the free polymer and ions. After the last wash, the concentrated magnetic fluid in the filter was diluted to a final concentration of 3-4 wt% magnetite, and following this, the purified magnetic fluid was sonicated again for approximately 2 minutes using the tip sonicator.

2.3 Iron Analysis Test

Since magnetic fluid derives its magnetic properties from the magnetite core at the center of each nanoparticle, it was important to develop an analysis technique that could easily and accurately quantify the amount of magnetite in a given batch of magnetic fluid. A colorimetric iron analysis technique was developed to determine Fe^{3+}

and Fe^{2+} concentrations in solution, from which the total amount of magnetite in the fluid could be calculated.

The colorimetric determination technique stems from the ability of certain organic compounds to chelate with free iron ions in solution, and the iron complex that forms strongly absorbs light of a certain wavelength. The amount of light absorbed by the iron complex can be measured precisely using UV-Vis spectrophotometry, with the strength of this absorption being directly proportional to the amount of iron in solution.

The organic compound chosen for this colorimetric technique was 4,5-dihydroxy-1,3-benzenedisulfonic acid, disodium salt, a compound more commonly known as Tiron. This organic compound chelates with Fe^{3+} and Fe^{2+} ions in a ratio of three Tiron molecules to every one iron molecule, and shows a consistent, extremely strong absorbance at 480 nm for iron solutions with a pH greater than 9.5.[2] This strong absorbance at 480 nm is easily quantified using UV-Vis spectrophotometry and can be directly correlated to the amount of magnetite in the original solution.

To use the Tiron with magnetic fluid, a method was developed to liberate the magnetite core of its iron content so the iron would be free to chelate to the Tiron in solution. This was achieved by adding concentrated HCl to a small sample of magnetic fluid, which dissolved the magnetite core and released the iron into solution as both Fe^{3+} and Fe^{2+}. The Tiron was then added to the acidic solution, followed by the addition of base to neutralize the acid and bring the pH of the solution above 9.5. Upon the addition of the base, the solution turned deep red, due to the strong absorbance of light at 480 nm following the chelation of the Tiron to the iron in solution. The solution was then diluted until the concentration of the iron in the magnetic fluid was 1000 times the original concentration. The pH of this diluted solution was typically greater than 12, which was necessary since the maximum absorption at 480 nm occurs only at pH values of 9.5 and greater.[2] The absorbance of the 1000x diluted solution at 480 nm was then measured using a Hewlett Packard UV-Visible Spectrophotometer (Model 8463).

Calibration curves were prepared by performing the colorimetric iron analysis test described above on solutions containing known concentrations of $FeCl_3$ and $FeCl_2$. Tiron was confirmed to bind to both Fe^{3+} and Fe^{2+} equally well, and the absorbance at 480 nm was plotted against the known concentration of iron in the solutions to obtain a linear

correlation relating absorbance at 480 nm to iron concentration. Once the iron concentration was known, the wt% of magnetite in the solution could be calculated. The iron analysis test was shown to accurately determine magnetite concentration with a precision of ± 4-5%, so a 2.00 wt% magnetic fluid solution would have an error associated with it of ± 0.09 wt%.

The colorimetric iron analysis test as described above was shown to be valid for magnetic fluids with a concentration of 3 wt% or less. At 3 wt% magnetite, the molar ratio of Tiron to iron in the iron analysis solution is 3.9:1. Tiron chelates to iron in a 3:1 molar ratio, so for magnetic fluid concentrations much higher than 3 wt%, the amount of Tiron becomes limiting. For magnetic fluid with an expected concentration higher than 3 wt%, such as freshly washed batches of magnetic fluid, the original concentration was diluted by ¼ before performing the iron analysis test, ensuring that the amount of Tiron added would be sufficient to chelate all the iron in solution. The results of the iron analysis test were shown to scale linearly with dilutions of the magnetic fluid.

2.4 Physical Characterization of Magnetic Fluid

2.4.1 Magnetic Nanoparticle Stability

Magnetic fluid prepared as described in the previous sections is a black, opaque liquid that is extremely stable. Although magnetic fluid will follow the path traced by a small magnet that is held up against the vial containing it, no sedimentation of magnetic fluid at room temperature was ever observed as a result of an applied magnetic field. Even over a period of six months, magnetic fluid remained stable on the shelf with less than 3% of particles settling out of solution, and the stability was not affected even when mixed with cells in raw fermentation broth, despite the broth's relatively high ionic strength (0.27 mol/L). Magnetic fluid has been shown in previous studies to remain stable up to approximately 80°C at an ionic strength of 0.27 mol/L.[1] In addition, magnetic fluid is extremely stable throughout the full pH range, from 2 to greater than 14, although it is easily destroyed on contact with concentrated acids, which dissolve the magnetite core.

2.4.2 Magnetic Nanoparticle Size

Previous studies using transmission electron microscopy (TEM) showed that the magnetite cores were fairly polydisperse in size and ranged from 5-10 nm in diameter, with an average core size around 8 nm.[1,3] The size of the entire particle, including the polymer shell, was determined using dynamic light scattering.

Dynamic light scattering (DLS) measures the hydrodynamic diameter of particles in a fluid by measuring the intensity of light from a laser beam that has scattered after hitting the particles, and then tracking changes in the intensity of the scattered light over a period of time. The changes in the scattered light intensity correspond to changes in the relative positions of the particles owing to their natural diffusion through the solution. A correlation function with an exponential fitting software program was used to fit the scattered light intensity in order to determine the diffusion coefficient of the particles in the fluid. The Stokes-Einstein equation was used by the software to convert the diffusion coefficient to the hydrodynamic diameter of the particles, assuming spherical particles. The light scattering software records an intensity-average size distribution that is then converted to number-average and volume-average size distributions. A Brookhaven BI-200SM light scattering system was used to perform the DLS experiments, with a measurement angle of 90°. Samples for measurement were prepared by diluting the magnetic fluid with deionized water to approximately 0.01 wt% magnetite and then filtering the samples with a 0.40 μm syringe filter to remove dust, which if present skews the measured data towards higher diameters than are actually present among the particle population.

Figure 2-4 shows the results of the measurement of one batch of magnetic fluid. Other batches were also tested with similar results. The hydrodynamic diameter measured corresponds to the full size of the magnetic nanoparticles, including the fully hydrated PAA-PEO/PPO polymer shell that coats the magnetite core.

The number-average distribution in Figure 2-4a shows significant polydispersity in the measured hydrodynamic diameter of the magnetic nanoparticles, with sizes ranging from approximately 25-60 nm. Such polydispersity was not unexpected given the polydispersity of the core sizes, as mentioned earlier. Using the number-average distribution, the average size of the polymer coated nanoparticles in water was 31.6 nm

with a standard error of ± 0.9 nm over all measured samples, with each particle weighted equally.

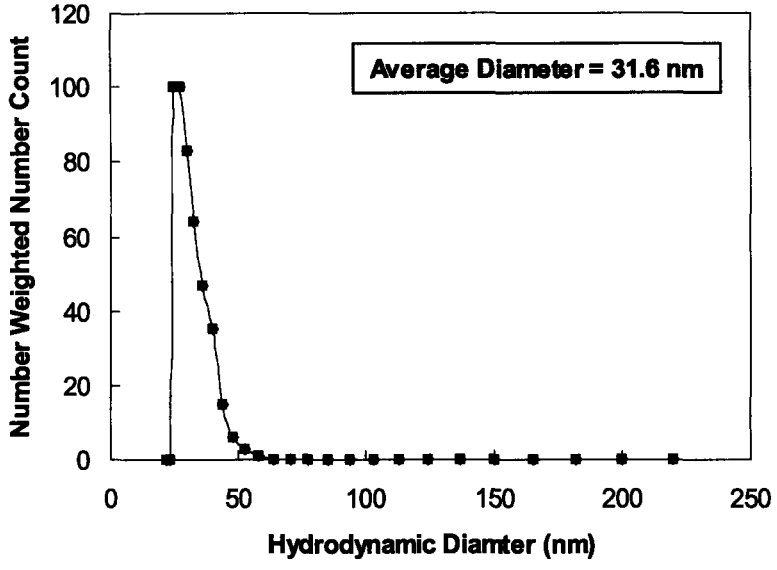

(a)

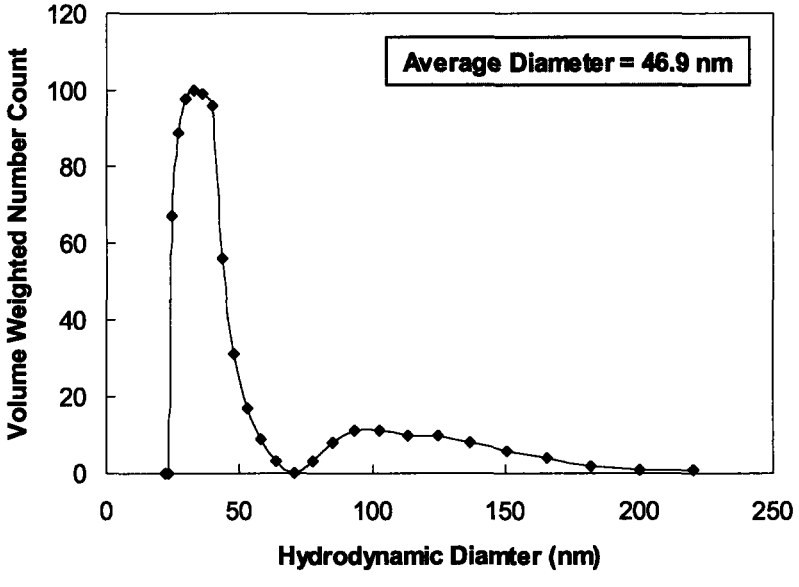

(b)

Figure 2-4. Size distribution of magnetic nanoparticles in magnetic fluid using dynamic light scattering, with (a) number average distribution and (b) volume average distribution.

The volume-average distribution differs from the number-average distribution in that each particle is weighted according to its size, with larger particles weighted more. This skews the average particle size towards higher values, but it also helps to uncover

the presence of larger magnetic particles that exist in such low concentrations as to be inconsequential in the number-average distribution. The volume-average distribution shown in Figure 2-4b shows the same polydisperse population of nanoparticles ranging in size from 25-60 nm, but it also shows a second polydisperse population with a size range of approximately 75-200 nm, leading to a total volume-weighted average particle size of 46.9 nm with a standard error of ± 3.6 nm over all measured samples.

For the two individual populations within the volume-weighted distribution, the 25-60 nm population has an average particle size of 34.9 nm with a standard error of ± 2.8 nm, while the 75-200 nm population has an average particle size of 118.5 nm ± 9.5 nm. Although the larger particles in the second population represent less than 1% of particles by number, they represent approximately 10% of the particle population by volume (and therefore also by weight). These larger particles consist of aggregates of single particles, where bridging of the PAA backbone on the graft copolymer occurred from one particle to another. Since the volume-average particle size is skewed towards the larger particles, the number-average mean particle diameter will be used throughout this work to represent the average size of the coated magnetite particles that make up magnetic fluid.

Using the mean number-average particle size of 31.6 nm, the thickness of the graft copolymer shell that stabilizes the magnetite core can be calculated by subtracting the average core size of 8 nm. This yields an average polymer thickness of approximately 12 nm around the magnetite core. Thus, the majority of the total volume of the magnetic nanoparticles, over 98%, is comprised of the graft copolymer layer surrounding the magnetite core.

2.4.3 Physical Properties

The density of 1 wt% magnetic fluid (1 wt% magnetite) was measured using a Mettler/Paar Calculating Digital Density Meter (DMA Model 45), and was found to be 1.0105 ± 0.0005 g/mL at ambient temperature (21.4°C). The density of 0.5 wt% magnetic fluid (0.5 wt% magnetite) was found to be 1.0040 ± 0.0005 g/mL at the same temperature. The viscosity of 1 wt% magnetic fluid (1 wt% magnetite) was measured

using a Zahn Cup-Type Viscosimeter (cup size 1) and was found to be approximately 4% higher than that of pure water, with a measured viscosity of roughly 0.995 cp at 22°C.

2.4.4 Magnetic Properties

Since it is the magnetic properties of a magnetic fluid that allow magnetophoretic clarification to take place, it is important to quantify these magnetic properties in order to utilize them effectively. Magnetic fluid as a whole is superparamagnetic,[4] meaning that the magnetic particles that make up magnetic fluid align in an applied magnetic field and exhibit significant magnetization while in the field, but exhibit no net magnetization in the absence of an applied field. Although the magnetite cores themselves are always permanently magnetic, the magnetic fluid as a whole exhibits no net magnetism outside of an applied field because the magnetization of each particle is randomly oriented with respect to the other particles in the fluid. This randomization is due to Brownian motion, which dominates the movement of the nano-sized magnetic particles in solution.[4]

The magnetite cores of the magnetic nanoparticles are also single-domain crystals, meaning that each core has only one direction of magnetization regardless of location on the core. Previous work using high-resolution transmission electron microscopy (TEM) showed this to be the case by imaging the atom planes in the cores directly and confirming visually that each core contained a single magnetite crystal with a single magnetic domain.[1] The presence of a single domain is important for the superparamagnetic properties of magnetic fluid.

The magnetization of the magnetic fluid was quantified in previous work using a Superconducting Quantum Interference Device (SQUID). SQUID was used to determine the induced magnetization (M) in a known concentration of magnetic fluid under changing applied magnetic fields (H). Figure 2-5 shows the magnetization curve obtained for 1 wt% magnetic fluid (1 wt% magnetite).[1] The magnetic fluid exhibits nearly linear magnetization behavior at low magnetic fields as the magnetic nanoparticles begin to align with the applied field. At high magnetic fields, a limiting or saturation value of the magnetization is reached as all the magnetic nanoparticles in the fluid become completely aligned with the field. This saturation magnetization, estimated by extrapolating the value of M as $H \rightarrow \infty$, was found to be 614 ± 49 A/m.[1] The SQUID

measurements also show zero residual magnetization at zero applied field, indicative of superparamagnetic behavior with no magnetic interactions between the particles. Previous work has also shown that because there are no magnetic interactions between the particles, the magnetization curves for different concentrations of magnetic fluids scale linearly by the weight fraction of magnetite in the fluid.[1]

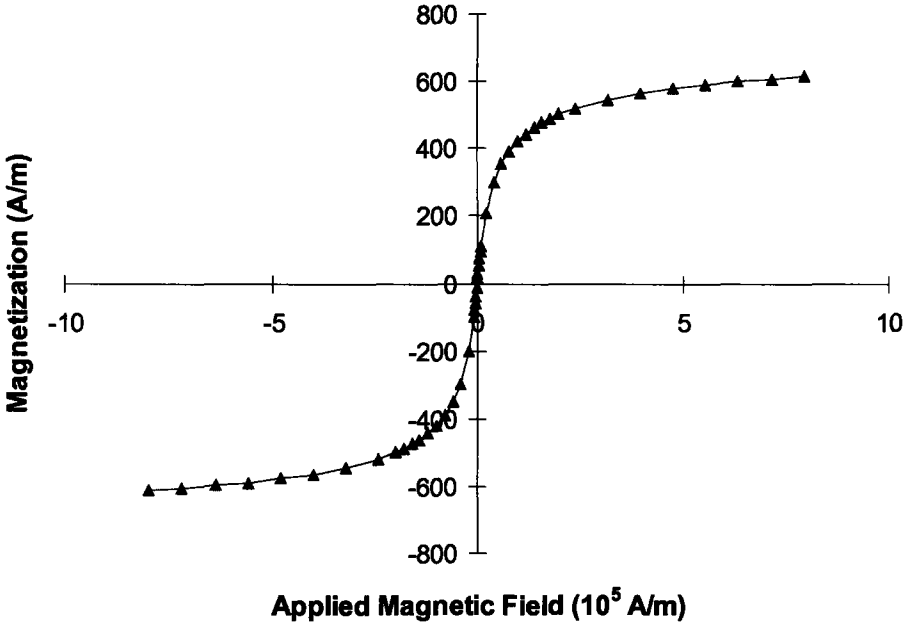

Figure 2-5. Magnetization response of 1 wt% magnetic fluid (1 wt% magnetite) under changing applied magnetic field. Negative values of the magnetic field indicate that the field was applied in the opposite direction. The SQUID measurements show zero residual magnetization at zero applied field, indicative of superparamagnetic behavior.[1]

2.4.5 Electrostatic Properties

Magnetic fluid is stabilized with a layer of graft copolymer that attaches to the magnetite core. The graft copolymer binds to the iron through the carboxylic acid groups (COOH) freely available along the backbone of the copolymer. Previous studies using IR spectrophotometry have shown that roughly 60% of the available COOH groups in the graft copolymer bind to the magnetite core, leaving approximately 40% of the carboxylic acid groups unattached.[1] These free acid groups become deprotonated to COO- in

aqueous solution, and result in a net negative charge on the surface of the magnetic nanoparticles.

The negative surface charge on the magnetic nanoparticles due to the presence of the COO- groups was measured using a Brookhaven ZetaPals Zeta Potential Analyzer, which allows for the quantification of the amount of charge near the surface of a particle or large molecule. The Brookhaven instrument uses a laser to measure optically the velocity of charged particles in solution as they move towards electrodes that produce a small electric field in the solution. At low electric field strengths, this drift velocity (V) is directly proportional to the applied field (E), as given by Equation 2-1:

$$V = \mu_e E \tag{2-1}$$

The proportionality constant (μ_e) is called the electrophoretic mobility and is calculated from the measured velocity and known electric field. Using the mobility, the zeta potential of the particles is calculated using the Smoluchowski limit, given by Equation 2-2:

$$\mu_e = \frac{e\zeta}{\eta} \tag{2-2}$$

where e is the dielectric constant of the solvent, η is the viscosity of the solvent, and ζ is the zeta potential. The sign and magnitude of the zeta potential correspond to the sign and number of free charges on the particle's surface. However, the zeta potential analyzer does not measure this charge at the exact surface of the particle, but instead at the particle's shear plane. As a particle moves through the solution, molecules of the solution travel with it (for example, water molecules in aqueous solutions), similar to a boundary layer that is associated with the particle. This is the shear plane, and it is here that the charge is measured. Under most conditions, the shear plane of the magnetic nanoparticles corresponds to the outside edge of the graft copolymer shell, which in this case is also considered to be the surface of the magnetic nanoparticles.

The Smoluchowski limit (Equation 2-2) is only valid for $\kappa a >> 1$, where a is the radius of the particle in solution and κ is the inverse Debye-Hückel screening length. The inverse of κ ($1/\kappa$) has units of length and corresponds to the thickness of the double layer surrounding a charged particle. Since the calculation of the zeta potential using the Smoluchowski limit assumes $\kappa a >> 1$, κ must be relatively large for very small particles

in order to achieve the most accurate zeta potential measurements. This is accomplished by increasing the ionic strength (I) of the solution through the addition of salt, as given by Equation 2-3:

$$\kappa = 3.288\sqrt{I} \quad \left(\text{nm}^{-1}\right) \tag{2-3}$$

with the ionic strength defined by Equation 2-4:

$$I = \frac{1}{2}\sum\left(c_i z_i^2\right) \tag{2-4}$$

where c_i is the molar concentration of the salt and z_i is the charge of each salt ion.[5] Thus, to accurately measure the zeta potential of magnetic fluid, which is a suspension of particles approximately 32 nanometers in diameter, the magnetic fluid was mixed with solutions having an ionic strength of at least 0.01 mol/L, in order to achieve a κa value of approximately 10.

The ionic strength of the solution of particles can not be too large, however. Under conditions of moderately low ionic strength, the shear plane of the magnetic nanoparticles corresponds to the outside edge of the graft copolymer shell. Under these conditions, the buildup of counterions around the particles occurs over a larger distance than the width of the shear plane, so more charge is seen at the shear plane, and thus the measured zeta potential will be higher. At very high ionic strengths, there are so many ions in solution that the counterions effectively mask the charge at the particle surface over a very short distance, leading to counterion buildup around the particle that can be less than the width of the shear plane, resulting in charge screening at the particle surface and a lower measured zeta potential. Thus, zeta potential measurements of magnetic fluid were not made in solutions with an ionic strength greater than 0.1 mol/L.

Samples were prepared by diluting magnetic fluid to 0.01 wt% magnetite in a salt solution with an ionic strength that varied from 0.001 M to 0.1 M. Roughly 1.5 mL of the sample were then added to the electrode cell. The electrophoretic mobility, and hence the zeta potential, was measured by averaging the results of ten electrode cycles. The results are given in Figure 2-6, which shows that the magnetic fluid nanoparticles are negatively charged over the working range of pHs used for magnetophoretic clarification in this work (6.4-7.4 pH), and that the negative charge on the particle surface increases with increasing pH.

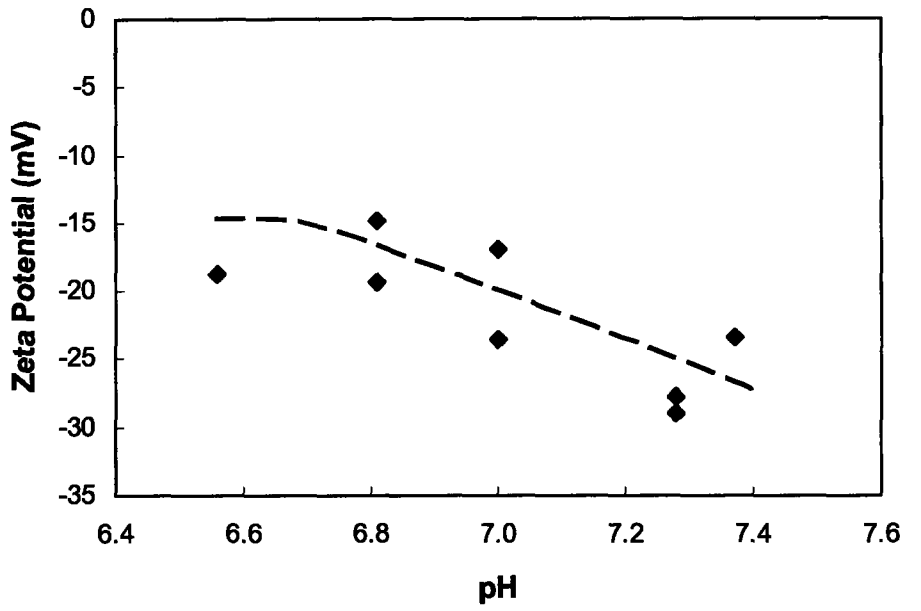

Figure 2-6. Zeta potential of dilute magnetic nanoparticles in the working pH range of the magnetic fluid for magnetophoretic clarification. The dashed line is present to indicate trends in the data.

2.5 Summary

The synthesis and stabilization of magnetic fluid has been described. The magnetic nanoparticles that made up the magnetic fluid used in this work consisted of a magnetite core surrounded by a polymer shell, which was composed of a comb graft copolymer with a polyacrylic acid (PAA) backbone onto which side chains of a polyethylene oxide (PEO)/polypropylene oxide (PPO) random block copolymer were attached. Magnetic fluid was synthesized in aqueous solution in a single batch reaction through chemical coprecipitation of iron(III) and iron(II) chlorides in the presence of the PAA-PEO/PPO graft copolymer, where the carboxylic acid groups on the PAA backbone of the graft copolymer were bound to the iron on the developing magnetite crystals, coating them and preventing further growth. The PEO/PPO side chains on the PAA backbone provided the stabilizing force that kept the coated magnetic nanoparticles stable in aqueous solution. A colorimetric iron analysis test was developed to accurately determine the concentration of magnetite in synthesized batches of magnetic fluid with a precision of 4-5%.

Synthesized magnetic fluid was characterized using different techniques to reveal particle size, stability, and other physical properties of the fluid. The magnetic nanoparticles were found to be colloidally stable over a wide range of conditions, including elevated temperatures and the full range of pH values of interest in this work. TEM imaging revealed an average magnetite core size of approximately 8 nm. Dynamic light scattering determined that the magnetic nanoparticles are polydisperse in size, with an average particle diameter of approximately 32 nm including the graft copolymer shell, but with a significant volume fraction of particles (~ 10%) also possessing diameters greater than 60 nm, indicating the presence of aggregates of magnetic particles in the magnetic fluid. The magnetization of magnetic fluid was determined using SQUID and scales linearly with the magnetite concentration of the fluid. Zeta potential measurements were also performed, with magnetic fluid exhibiting a negative surface charge in the pH range 6.4-7.4, which corresponds to the working pH range for the fluid in the magnetophoretic separation experiments.

2.6 References

1. Moeser, G.D., "Colloidal Magnetic Fluids as Extractants for Chemical Processing Applications", Ph.D. Thesis, Department of Chemical Engineering; Massachusetts Institute of Technology: Cambridge, MA, 2003.

2. Yoe, J.H. and A.L. Jones, "Colorimetric Determination of Iron with Disodium-1,2-dihydroxybenzene-3,5-disulfonate". *Industrial and Engineering Chemistry*, 1944. **16**(2): p. 111-115.

3. Shen, L.F., A. Stachowiak, S.E.K. Fateen, P.E. Laibinis and T.A. Hatton, "Structure of Alkanoic Acid Stabilized Magnetic Fluids. A Small-Angle Neutron and Light Scattering Analysis". *Langmuir*, 2001. **17**(2): p. 288-299.

4. Rosensweig, R.E., *Ferrohydrodynamics*. 1997, Mineola, NY: Dover Publications, Inc.

5. Hunter, R.J., *Introduction to Modern Colloid Science*. 1998, New York: Oxford University Press.

Chapter 3

E. coli Cell Growth and Characterization

3.1 Introduction

Magnetophoretic clarification has potential applications wherever solid, non-magnetic particles need to be removed from a bulk fluid. In particular, magnetophoretic clarification could be used in the biotechnological and pharmaceutical industries to remove cells from fermentation broth, where the cells have produced a certain product of interest that must then be recovered from the liquid broth. *E. coli* is a common bacteria that is currently used in industry to create a variety of biochemical products, particularly recombinant proteins.[1] *E. coli* cells are robust and easy to grow, and with a size of around 2 μm, are perfect candidates for successful magnetophoretic cell clarification.

Owing to their ideal size and ease of growth, *E. coli* cells were the biological entities exclusively tested in the magnetophoretic cell clarification devices. Since cells suspended in fermentation broth are complex bodies, control experiments were also initially performed using polystyrene beads, typically 2 μm in size, as a model particle for magnetophoretic clarification. This chapter discusses in detail the growth and characterization of the *E. coli* cells, as well as techniques used to analyze samples containing the cells both with and without the additional presence of the magnetic fluid. This chapter also discusses the characterization of the polystyrene beads and the techniques used to analyze the samples containing them.

3.2 *E. coli* Production

3.2.1 Safety and Sterilization Procedures

Wild strain BL21 was used in all cases for the *Escherichia coli* cells. Although this particular strain does not infect humans, standard sterilization and safety precautions consistent with a BL1 designation were followed to ensure the no living cells survived outside of the lab. Biohazardous waste was decontaminated prior to disposal either by

autoclaving with saturated steam at 2 atm and 121°C (250°F) or by chemical decontamination using an 80% ethanol solution or a 10% bleach solution. Laboratory benches and other similar surfaces were decontaminated using 80% ethanol, while glassware was sterilized primarily by autoclaving.

3.2.2 Shaker Flask Growth

The *E. coli* cells were grown exclusively in shaker flasks using a semi-defined growth medium. This growth technique resulted in consistently reproducible cell concentrations at amounts sufficient for experimentation without the need for complicated instrumentation and constant monitoring, as is required for cell growth in a fermentor. The materials required for shaker flask growth and the exact procedure followed for growing the cells are discussed in the next two sections.

3.2.2.1 Materials

The semi-defined growth medium used for the *E. coli* cells was the same in all cases and was created by mixing the appropriate amount of defined chemical stock solutions with the appropriate amount of sterile, deionized water. Table 3-1 lists the chemicals used to create these stock solutions, as well as the concentrations of the chemicals in the stocks and the final concentration of each chemical in the semi-defined growth medium.

The chemicals used to create the stock solutions were obtained from various sources. Sodium phosphate (dibasic, anhydrous – 99.8%), potassium phosphate (monobasic – 99.8%), ammonium chloride (99.9%), sodium chloride (99.7%), and D-Glucose (99%) were all obtained from Mallinckrodt (Paris, Kentucky). Magnesium sulfate (98%) was obtained from EM Science (Gibbstown, NJ), and Bacto Tryptone was obtained from Becton, Dickinson and Company (Sparks, MD). All chemicals were used as received. The trace metals stock solution was pre-prepared and generously donated by Professor Cooney's research group. The *Escherichia coli* BL21 cells were grown from glycerol-suspended cell stocks, and were also a generous gift from Professor Cooney's group.

Chemical Component	Stock Concentration (g/L)	Concentration in Medium
Salt Stock (10x) – titrated to pH 7.4 with NaOH		
Na_2HPO_4	60	42 mM
KH_2PO_4	30	22 mM
NH_4Cl	10	18.7 mM
NaCl	5	8.6 mM
$MgSO_4$ Stock (1 M)		
$MgSO_4$	120.4	1.0 mM
Tryptone Stock (10x)		
Bacto Tryptone	100	10 g/L
NaCl	50	86 mM
Glucose Stock (20%)		
D-Glucose	200	5 g/L
Trace Metals Stock (667x)		
$Na_2EDTA{\cdot}2H_2O$	20.3	81.8 μM
$CaCl_2{\cdot}2H_2O$	0.51	5.2 μM
$FeCl_3{\cdot}6H_2O$	16.9	93.8 μM
$CuSO_4{\cdot}5H_2O$	0.16	0.96 μM
$MnSO_4{\cdot}H_2O$	0.13	1.15 μM
$CoCl_2{\cdot}6H_2O$	0.18	1.15 μM
$ZnSO_4{\cdot}7H_2O$	0.18	0.91 μM

Table 3-1. Stock solutions used to create the semi-defined growth medium for the cells, listed with chemical concentrations for both the stock itself and for the final semi-defined growth medium.[2]

Stock solutions were prepared using deionized water in the concentrations given in Table 3-1 and were each autoclaved separately after preparation to ensure sterility. A separate bottle of deionized water was also autoclaved separately for use in making the final solutions of growth medium. All liquid solutions were steam autoclaved at 2 atm and 121°C (250°F) for 30 minutes, with the exception of the glucose solution, which was autoclaved for 20 minutes. Stock solutions were mixed with the appropriate amount of sterile, deionized water just prior to use to create the final growth medium.

Baffled shaker flasks were used for growing the cells. These flasks, as well as the pipet tips used to transfer the stock solutions to the shaker flasks, were either purchased pre-sterilized and individually wrapped, or were steam autoclaved prior to use at 2 atm

and 121°C (250°F) for 30 minutes and then dried in the autoclave for an additional 30 minutes.

3.2.2.2 Shaker Flask Procedure

The semi-defined growth medium was prepared using the stock chemical solutions given previously in Table 3-1. The quantity of each stock solution used to create the final growth medium in a sterile baffled flask is given in Table 3-2, which shows the procedure for preparing 100 mL of semi-defined growth medium.

For 100 mL of Growth Medium in a 500 mL flask, add:
• 77.0 mL sterile, deionized water
• 10 mL salt stock
• 10 mL Tryptone stock
• 2.5 mL glucose stock
• 150 μL trace metals stock
• 100 μL $MgSO_4$ stock

Table 3-2. Preparation of 100 mL the semi-defined growth medium from the chemical stock solutions for a 500 mL sterile baffled shaker flask.[2]

Once the growth medium in the flask was mixed and all of the components were at their appropriate concentration, the medium was innoculated with approximately 0.2 mL of *E. coli* (BL21) cells suspended in glycerol. These glycerol-suspended cell stocks were stored at –85°C and were each brought to 0°C by immersion in ice before being introduced to the growth medium. The innoculated shaker flask was then placed in a temperature-controlled forced air shaker (Queue Orbital Shaker Model 4730) at 37°C and rotated at 250 rpm. The cells were allowed to grow overnight for 13 hours under these conditions, after which they achieved an average concentration of 0.32 wt% on a dry cell basis ($OD_{600} \sim 9.7$).

Larger batches of *E. coli* cells were also grown using 400 mL of growth medium. The preparation of the medium was exactly the same as for the 100 mL batches, except that a 2000 mL baffled shaker flask was used, and exactly four times the amount of sterilized water and stock solutions were required. The amount of frozen cell stock added to the medium was kept the same at 0.2 mL. The larger batches were grown overnight at

37°C and 260 rpm for 14 ½ hours, after which they achieved an average concentration of 0.25 wt% on a dry cell basis (OD_{600} ~ 7.5). In all cases, the liquid volume in the shaker flasks was equal to one fifth the total volume of the flask to promote good oxygen transfer during mixing.

3.2.3 Processing of Cells and Fermentation Broth

E. coli cells were typically used in experiments at concentrations ranging from 0.5 wt% to 2.0 wt% on a dry cell basis. Since the cells were removed from the temperature-controlled shaker with an average cell content of 0.32 wt%, the cells were almost always concentrated before being used experimentally.

After removal from the temperature-controlled shaker, the cells were immediately put on ice to halt further growth. Once the cell suspension was sufficiently cool, centrifugation at 1700 rpm for 10 minutes (Eppendorf Centrifuge, Model 5810R) was performed at ambient temperature to sediment the cells, and enough of the fermentation broth supernatant was removed to achieve the desired cell concentration needed for experiments. Round bottom centrifuge tubes were used at all times to facilitate resuspension of the cells after removal of the supernatant. Aside from the concentration process using centrifugation, the cells and fermentation broth were otherwise not altered or processed in any way prior to the experiments. Experiments using the cells were all performed at ambient temperature. Cells not in immeditate use for experimentation were stored in a refrigerator at approximately 5°C, and cells more than 36 hours old were discarded.

3.3 Optical Density Measurements

The concentration of cells in fermentation broth was determined by measuring the absorbance (i.e. the optical density, or OD) of the cell suspension at 600 nm. Samples were measured using a Hewlett Packard UV-Visible Spectrophotometer (Model 8463), and were first diluted with deionized water to achieve an absorbance between 0 and 1.0 OD_{600}. A typical dilution was 0.05 mL cell suspension in 10 mL deionized water. Deionized water was also used as a blank prior to all measurements in the machine.

As determined in previous studies using *E. coli*, a correlation between the optical density at 600 nm and the dry cell weight of a cell suspension exists such that an OD_{600} of 1 is approximately equal to 0.34 g dry cell weight per liter when measured using a cuvette with a path length of 1 cm.[3] This optical measurement procedure was the primary method used in this work for determining cell concentration and has the advantage of being a real time technique, unlike dry cell weight measurements, which take a full day to obtain results. Optical density measurements also scale linearly at all concentrations and dilutions, as long as the dilution of the sample prior to measurement is enough to place the measured absorbance between 0 and 1.0.

Dry cell weight measurements were performed as a check to test the accuracy and consistency of the OD_{600} correlation. Supor-200 filters with 0.2 μm pores were used for the dry cell weight measurements. The filters were first rinsed with deionized water, and then set in an oven at 40°C to dry overnight. Dry filters were placed in a Buchner funnel and fully wetted with deionized water. A known volume of the cell suspension was added dropwise to the wet filter under vacuum, and the filter was then repeatedly washed with deionized water. The filters were placed back in the oven to dry overnight at 40°C. The dry cell weight was determined from the difference in mass between the dry, empty filter and the dry, sample filter. All tests performed using dry cell weight measurements showed that the OD_{600} correlation accurately determined cell concentration with a precision of ± 4% for *E. coli* cells, so a 2.00 wt% cell suspension would have an error associated with it of ± 0.08 wt%, which in all cases refers to the weight percent of cells on a dry cell basis.

3.4 Physical Characterization of *E. coli* Cells

Effective magnetophoretic clarification stems not only from the properties of the magnetic fluid, but also from the physical properties of the non-magnetic particles being separated. Particle size, density, and electrostatic properties all affect how strongly the particles react to the presence of magnetized magnetic fluid. The following two sections summarize the important physical properties of *E. coli* cells for magnetophoretic cell clarification.

3.4.1 Cell Size and Density

The size of the individual *E. coli* cells was determined by optical microscopy. Figure 3-1 shows a photograph of freshly grown *E. coli* cells using an optical microscope at 1000x resolution. The *E. coli* cells appear roughly cylindrical in shape, with a length of approximately 2-2.5 μm and a diameter of approximately 1 μm, which is consistent with literature values. The density of the individual cells suspended in fermentation broth is 1.04-1.06 g/mL, which represents the hydrated cell density. The density of the entire cell suspension encompassing both cells and fermentation liquid was measured using a Mettler/Paar Calculating Digital Density Meter (DMA Model 45). The density of a 0.5 wt% *E. coli* cell suspension was found to be 1.0054 ± 0.0005 g/mL at ambient temperature (21.2°C), and the density of a 1.0 wt% *E. coli* cell suspension was found to be 1.0177 ± 0.0005 g/mL at the same temperature.

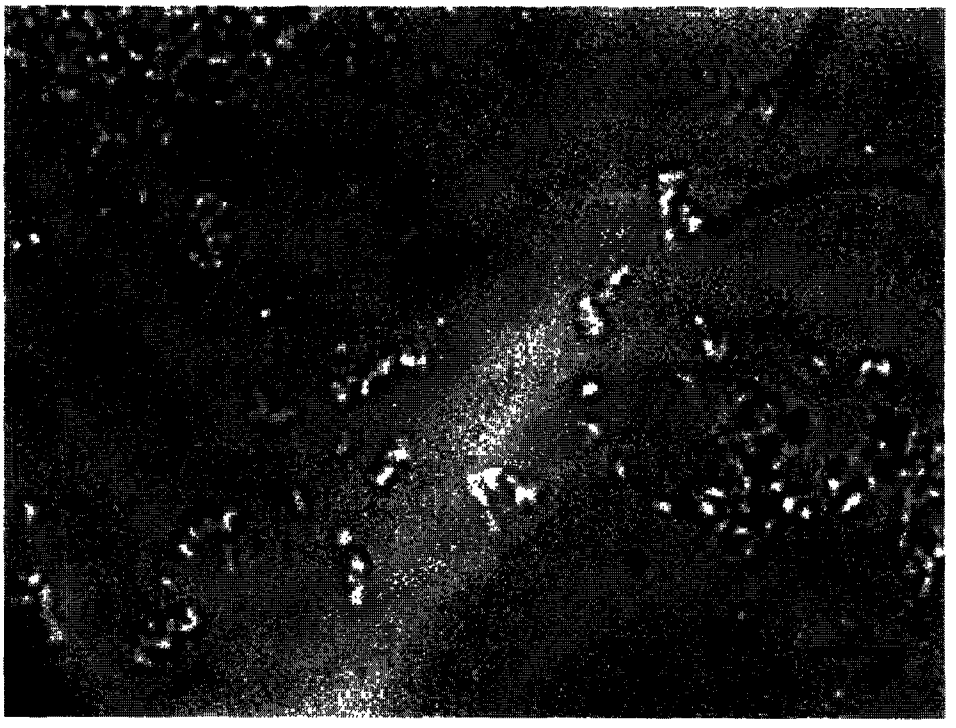

Figure 3-1. Photograph of *E. coli* cells using an optical microscope at 1000x resolution.

3.4.2 Electrostatic Properties

E. coli cells have a predominately negative surface charge at the pHs found in fermentation broth. This negative surface charge was determined by measuring the electrophoretic mobility of the cells using a Brookhaven ZetaPals Zeta Potential Analyzer (see Chapter 2 of this work for more details). The zeta potential was calculated from the electrophoretic mobility using the Smoluchowski limit:

$$\mu_e = \frac{e\zeta}{\eta} \tag{3-1}$$

where μ_e is the electrophoretic mobility, e is the dielectric constant of the liquid broth, η is the viscosity of the liquid broth, and ζ is the zeta potential. The sign and magnitude of the zeta potential correspond to the sign and number of free charges on the cell surface. The Smoluchowski limit is perfectly valid for measuring the zeta potential of micron size particles such as cells.

Samples were prepared by diluting the cells to 0.01 wt% in a salt solution with an ionic strength that varied from 0.001 M to 0.1 M. Roughly 1.5 mL of the sample were then added to the electrode cell. The electrophoretic mobility, and hence the zeta potential, was then measured by averaging the results of ten electrode cycles. Measurements using an ionic strength of 0.01 M proved the most reliable, and the *E. coli* cells were found to have a zeta potential of –67.6 ± 4.8 mV at a pH of 6.85 and a zeta potential of –68.2 ± 4.5 mV at a pH of 10.3, using an ionic strength of 0.01 M. Thus, increasing pH was shown to have little effect on the surface charge of the cells.

3.5 Analysis of Cell and Magnetic Fluid Mixtures

The feed fluid and the samples collected during magnetophoretic clarification experiments all contained a mixture of cells, magnetic fluid, and fermentation broth. The following three sections discuss how this mixture affected the procedures for measuring both cell and magnetic fluid concentrations in the samples.

3.5.1 Optical Density in the Presence of Magnetic Fluid

Optical density measurements at 600 nm were used with a high degree of accuracy (± 4%) to determine the concentration of cells in fermentation broth alone. For mixtures of both cells and magnetic fluid, optical density measurements still resulted in accurate determination of cell concentration, but additional steps were required to account for the presence of the magnetic nanoparticles.

The magnetic nanoparticles in magnetic fluid also show absorbance at 600 nm, in addition to the absorbance observed from the cells, and the two spectra were found to be additive. The cell concentration in the samples collected during experiments was therefore determined by first performing an initial measurement at 600 nm on a diluted solution of the experimental sample. A typical dilution was 0.05 mL sample in 10 mL deionized water. This measured absorbance provided the OD_{600} value for the total mixture of both cells and magnetic fluid. The diluted solution used for this initial measurement was then centrifuged at 4000 rpm for 40 minutes. This procedure sedimented only the cells, since the magnetic nanoparticles that make up magnetic fluid are not affected significantly by centrifugation. The absorbance of the magnetic fluid supernatant at 600 nm was measured, and the difference between the total optical density of the full mixture and the optical density of just the magnetic fluid supernatant yielded the optical density of the cells alone. Once the optical density was known for just the cells, the cell concentration was calculated as before using the OD_{600} correlation.

This technique for measuring cell concentration in the presence of magnetic fluid was shown to scale linearly with cell concentration and was independent of magnetic fluid concentration. Samples of cells alone and cells mixed with magnetic fluid were prepared from a freshly grown batch of cells of known concentration, and optical density measurements were performed on all the prepared samples. The results of the optical density analysis on each sample are shown in Figure 3-2. The optical density measurements taken in the presence of magnetic fluid were nearly indistinguishable from measurements taken with cells alone, demonstrating that the magnetic nanoparticle contribution to the optical density measurements is truly linearly additive. Further testing revealed the same level of accuracy for mixed OD_{600} measurements as was found for OD_{600} measurements of cells in fermentation broth alone (± 4%).

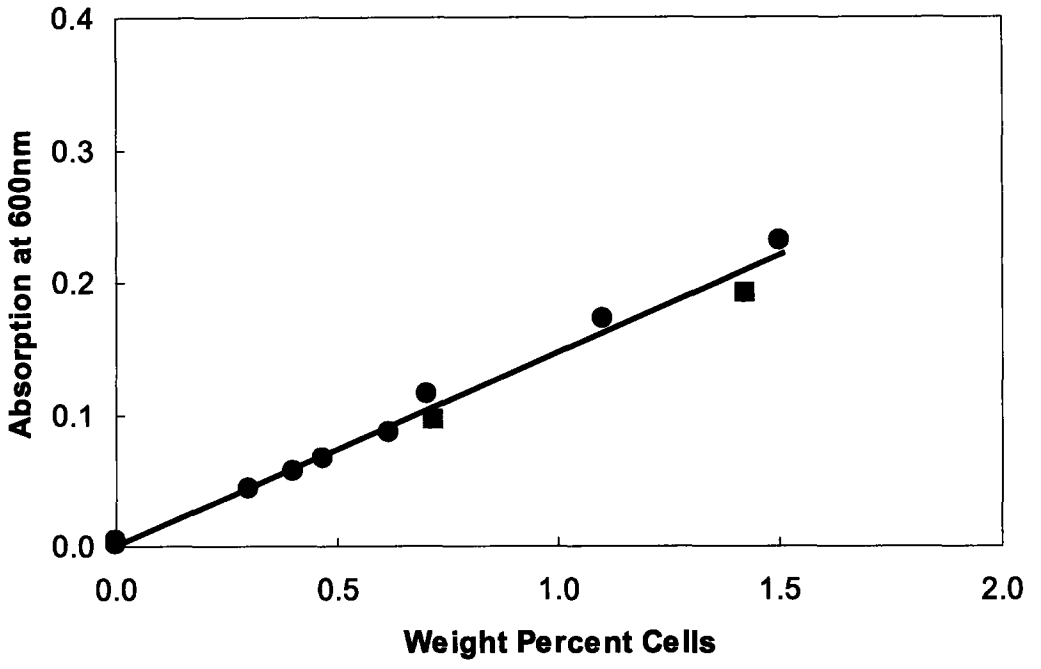

Figure 3-2. The absorption at 600 nm as a function of cell concentration for samples containing only cells (squares) and samples containing both cells and magnetic fluid (circles). The optical density measurements at 600 nm are either the pure measurements, for cells alone, or the corrected measurements, with the magnetic fluid contribution subtracted, for mixtures of cells and magnetic fluid.

3.5.2 Iron Analysis Test in the Presence of Cells

Experimental samples containing both cells and magnetic fluid were also tested to determine the magnetic fluid concentration of the samples, as measured by the concentration of magnetite. The iron analysis test (described in Chapter 2) can accurately determine the magnetite concentration in a batch of pure magnetic fluid with a precision of ± 4-5%.

Raw fermentation broth containing *E. coli* cells alone with no magnetic fluid was tested using the iron analysis test to determine if the presence of iron in the broth and cells could be detected by the test. Even though the growth medium for the cells contained 94 ppb Fe^{3+} ions, the iron analysis performed on the broth mixture did not detect any iron at this level, indicating that the presence of cells or broth in a mixture of magnetic fluid should have no effect on the accuracy of the iron analysis test for determining the magnetic fluid concentration. To confirm this, magnetic fluid samples

were made that each contained 1 wt% magnetic fluid (1 wt% magnetite) and different concentrations of cells in fermentation broth. Iron analysis testing was performed on each sample, and the results showed that the presence of the cells and broth, even at the most concentrated level of 1.5 wt% cells, did not have any affect on the determination of the magnetite content in the samples, with an average calculated concentration of 0.97 ± 0.01 wt% magnetite. Therefore, the iron analysis test is valid for determining the magnetite concentration in all experimental samples, both in the presence and absence of *E. coli* cells.

3.5.3 Physical Properties of Cell and Magnetic Fluid Mixtures

Mixing *E. coli* cells with magnetic fluid results in slight changes to the basic physical properties of the mixture. The density and viscosity of cell and magnetic fluid mixtures were both measured experimentally. The density of a solution containing 0.5 wt% cells and 1 wt% magnetic fluid (1 wt% magnetite), measured using a Mettler/Paar Calculating Digital Density Meter (DMA Model 45), was found to be 1.0170 ± 0.0005 g/mL at ambient temperature (21.2°C). This is a slight increase over the density of 1 wt% magnetic fluid alone, which was measured at 1.0105 g/mL at the same temperature. The viscosity of a solution containing 0.5 wt% cells and 1 wt% magnetic fluid (1 wt% magnetite) was measured using a Zahn Cup-Type Viscosimeter (cup size 1) and was found to be approximately the same as for 1 wt% magnetic fluid alone, with a measured viscosity 4% higher than that of pure water, at roughly 0.995 cp at 22°C.

The presence of magnetic fluid also affected the settling velocity of cells in the mixture. Theoretically, *E. coli* cells should have a settling velocity in fermentation broth of approximately 0.05 cm/hr. Experimentally, the measured settling velocity of cells in fermentation broth was determined to be 0.07-0.3 cm/hr by tracking the movement of the settling plane in columns filled with different concentrations of the cell suspensions. The settling plane was not sharply defined for the cell suspensions, however, so the measured settling velocity is a rough approximation. Additionally, more concentrated cell suspensions were observed to settle more rapidly than lower concentrations of cell suspensions, with the upper limit of the settling velocity observed from the settling of 1.1

wt% cells, and the lower limit observed from the settling of 0.5 wt% cells. Aggregation of cells in the broth is therefore more common for the higher cell concentrations.

When mixed with magnetic fluid, *E. coli* cells have a theoretical settling velocity of 0.04 cm/hr. Experimentally, however, cells mixed with magnetic fluid were shown to settle with a velocity of approximately 1.5 cm/hr at all cell concentrations tested, up to 1.1 wt% cells. This result indicates that the cells tend to aggregate more strongly in the presence of the magnetic nanoparticles. Based on the experimentally measured settling velocity, the cells appear to aggregate into loose clumps roughly 12 μm in diameter (assuming spherical aggregates), with an estimated number of cells per clump of approximately 151.

3.6 Polystyrene Beads as a Model Particle

E. coli cells in fermentation broth is a complex mixture that takes many hours to produce. Because of the complexity of the cells, simple non-magnetic particles of the same size as *E. coli* cells were used as a model system for all initial experiments involving magnetophoretic clarification. Polystyrene beads proved to be excellent model non-magnetic particles, possessing not only the appropriate size, but also many other physical properties similar to those of the cells. The following sections discuss the procurement of the polystyrene beads, their physical characteristics, and how polystyrene samples were analyzed, both with and without the additional presence of magnetic fluid.

3.6.1 Materials

Polystyrene beads were obtained from Spherotech, Inc. (Libertyville, IL). The beads were spherical in shape and were obtained in two sizes, with diameters of 1.17 ± 0.029 μm and 2.01 ± 0.05 μm. The 2 μm sized beads were used for the majority of the experiments, since that size most closely matched the size of the *E. coli* cells. The beads arrived as a solution of 5.0 wt% ± 0.2 wt% polystyrene in deionized water with 0.02% sodium azide added as bacteriostatic, and were used as received. The different sized beads were all manufactured by Spherotech using the same synthetic procedure, and so

except for their size, all other physical properties were identical, and the analysis techniques used to analyze the polystyrene samples worked equally well with both sizes.

3.6.2 Optical Density Measurements

Optical density measurements were used to measure the concentration of polystyrene beads in exactly the same manner as used for cells. The absorbance at 600 nm was measured using samples with known concentrations of polystyrene, and calibration curves were generated to determine the correlation coefficient relating optical density to polystyrene concentration. For the 2 μm polystyrene beads, an OD_{600} of 1 was found to correspond to 19.7 g polystyrene beads per liter when measured using a cuvette with a path length of 1 cm. For the 1 μm polystyrene beads, an OD_{600} of 1 was found to correspond to 11.1 g polystyrene beads per liter. In addition, the correlations were shown to be linear for both bead sizes up to 2 wt% polystyrene. For concentrations higher than 2 wt%, additional dilution (more dilute than 0.05 mL sample in 10 mL water) must be made to place the measured optical density value in the linear range between 0 and 1.0 OD_{600}.

Dry weight measurements were also performed as a check to test the accuracy and consistency of the OD_{600} correlation. Supor-200 filters with 0.2 μm pores were used for the dry weight measurements in the same manner as for the cells. All tests performed using dry weight measurements for polystyrene showed that the OD_{600} correlation accurately determined polystyrene concentration with a precision of ± 4%, the same accuracy level shown for the cells.

3.6.3 Physical Characterization of Polystyrene Beads

The polystyrene beads obtained from Spherotech were a good match for many of the physical properties of *E. coli* cells. The following two sections discuss the physical properties of the polystyrene beads, which were identical for both bead sizes.

3.6.3.1 Bead Size and Density

The size of the polystyrene beads was determined by Spherotech using a laser particle sizer, and each bead size was shown to be quite monodisperse, with a standard

deviation in bead diameter of ± 2.5%. In addition, scanning electron microscopy (SEM) imaging of the beads, also performed by Spherotech, showed them to be nearly perfectly spherical, which makes the beads ideal for comparison with theoretical calculations for magnetophoretic clarification, which typically assume the non-magnetic particles to be spherical in shape. The density of the individual polystyrene beads themselves was also reported by Spherotech to be 1.05 g/mL, the same as bulk polystyrene. This density is nearly identical to that of individual *E. coli* cells, further justifying the use of the polystyrene beads as model particles.

3.6.3.2 Electrostatic Properties

All of the polystyrene beads purchased from Spherotech were negatively charged due to the presence of sulfate groups on their surface. This negative surface charge was measured using a Brookhaven ZetaPals Zeta Potential Analyzer in exactly the same manner as used for the *E. coli* cells. Zeta potential measurements in solutions with an ionic strength of 0.01 M at a pH of 6.7 yielded an average zeta potential value of –104 ± 3 mV for the beads.

3.6.4 Analysis of Polystyrene and Magnetic Fluid Mixtures

The analysis techniques adapted to measure cells mixed with magnetic fluid were tested to ensure that they worked equally well with mixtures of polystyrene and magnetic fluid. The following three sections discuss the procedures for determining polystyrene and magnetic fluid concentration in experimental samples containing both types of particles.

3.6.4.1 Optical Density in the Presence of Magnetic Fluid

For mixtures of polystyrene and magnetic fluid, polystyrene concentration was determined using optical density measurements at 600 nm in exactly the same manner as for the cells, with an initial measurement of the full mixture followed by a measurement of the magnetic fluid supernatant after centrifugation. The difference between the two spectra yielded the absorbance at 600 nm for polystyrene alone. The polystyrene concentration for the sample was then calculated using the same OD_{600} correlation determined for polystyrene in water, as described earlier.

Experiments were performed to see if this technique scaled linearly with polystyrene concentration while being independent of magnetic fluid concentration, as was the case for the cells. Known concentrations of polystyrene in water and polystyrene mixed with magnetic fluid were prepared, and optical density measurements were performed on each sample. The results of the optical density analysis for the 2 μm polystyrene beads are shown in Figure 3-3.

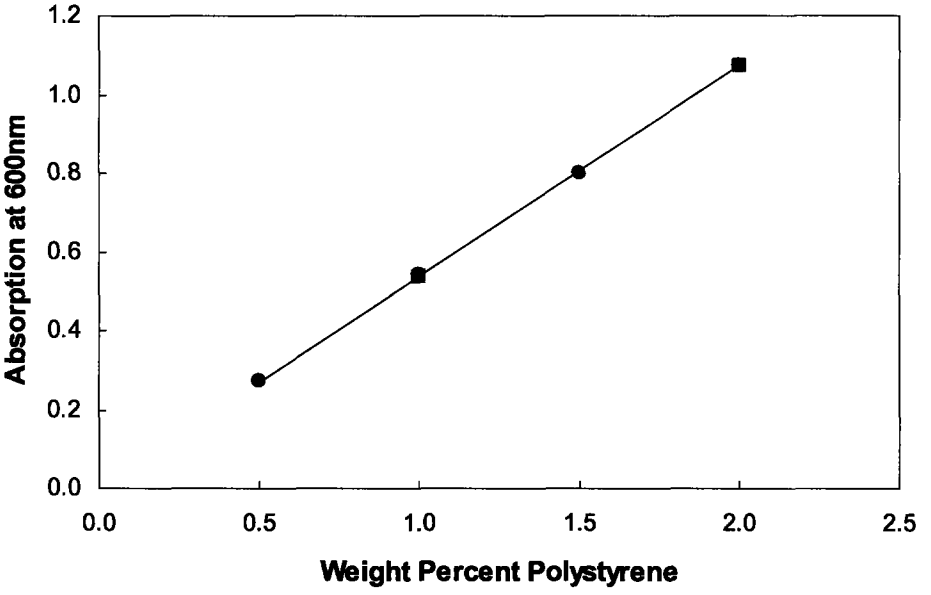

Figure 3-3. The absorption at 600 nm as a function of polystyrene concentration for samples containing 2 micron polystyrene beads in water (squares) and samples containing 2 micron polystyrene beads in magnetic fluid (circles). The optical density measurements at 600 nm are either the pure measurements, for polystyrene in water, or the corrected measurements, with the magnetic fluid contribution subtracted, for polystyrene in magnetic fluid.

Optical density measurements taken in the presence of magnetic fluid were indistinguishable from measurements taken with polystyrene alone, demonstrating that the magnetic nanoparticle contribution to the optical density measurements is truly linearly additive. Further testing revealed the same level of accuracy for polystyrene and magnetic fluid OD_{600} measurements as was found for polystyrene in pure water (± 4%).

3.6.4.2 Iron Analysis Test in the Presence of Polystyrene Beads

Experimental samples containing both polystyrene and magnetic fluid were also tested to determine the magnetic fluid concentration of the samples, as measured by the

concentration of magnetite. To ensure that the presence of the polystyrene in the samples did not affect the results of the iron analysis test, magnetic fluid samples were prepared containing 1 wt% magnetic fluid (1 wt% magnetite) with varying polystyrene concentrations. Iron analysis testing was performed on each sample, and the results showed that the presence of the polystyrene, even at the most concentrated level of 2 wt%, did not have any affect on the determination of the magnetite content in the samples, which yielded an average calculated concentration of 0.99 ± 0.01 wt% magnetite. Therefore, the iron analysis test is valid for determining the magnetite concentration in all experimental samples, both in the presence and absence of polystyrene beads.

3.6.4.3 Physical Properties of Polystyrene and Magnetic Fluid Mixtures

The density of a solution containing 1 wt% polystyrene and 1 wt% magnetic fluid (1 wt% magnetite) was measured using a Mettler/Paar Calculating Digital Density Meter (DMA Model 45), and was found to be 1.0111 ± 0.0005 g/mL at ambient temperature (20.8°C). The viscosity of a solution containing 1 wt% polystyrene and 1 wt% magnetic fluid (1 wt% magnetite) was measured using a Zahn Cup-Type Viscosimeter (cup size 1) and was found to be approximately the same as for 1 wt% magnetic fluid alone at 0.995 cp at 22°C.

The presence of the magnetic fluid did not significantly affect the settling velocity of either of the two polystyrene bead sizes, indicating that there are no interactions between the magnetic fluid particles and the polystyrene that would promote aggregation of the beads. For the 2 μm polystyrene beads, the theoretical settling velocity in magnetic fluid is 0.031 cm/hr, which is in good agreement with the experimentally determined settling velocity of 0.037 ± 0.001 cm/hr, as measured by tracking the movement of the settling planes in columns filled with different concentrations of the polystyrene beads. For the 1 μm polystyrene beads, the theoretical settling velocity in magnetic fluid is 0.011 cm/hr, which is in good agreement with the experimentally determined settling velocity of 0.017 ± 0.004 cm/hr, measured in the same manner as for the 2 μm beads. The settling velocities of both polystyrene bead sizes were independent of polystyrene concentration up to 2 wt%, the highest concentration tested.

3.7 Summary

E. coli cells in fermentation broth were produced with the shaker flask technique for use in magnetophoretic cell clarification experiments. The physical properties of the cells were characterized, with the cells determined to be roughly cylindrical in shape with a length of 2-2.5 μm and a diameter of approximately 1 μm. Zeta potential measurements showed the cells to have a negative surface charge in the pH range 6.8-10.3, which corresponds to the working pH range for the separation experiments. Optical density measurements were shown to be an accurate, real time method for determining cell concentration, when used both with cells alone in fermentation broth and with cells mixed with magnetic fluid. The iron analysis test for determining magnetic fluid concentration was also shown to be accurate even in the presence of cells and fermentation broth. The cells were therefore well characterized, and accurate methods were determined for analyzing all of the samples produced during experiments with the magnetophoretic clarification devices.

In addition to the use of the *E. coli* cells, polystyrene beads were used in the magnetophoretic clarification experiments as model particles. The beads were purchased in two sizes, and were spherical in shape with diameters of approximately 1.17 μm and 2.01 μm. As with the cells, zeta potential measurements indicated that the polystyrene beads carried a negative surface charge in the pH range 6.5-7.5. Optical density measurements were shown to be just as accurate when used with polystyrene beads as when used with cells, and this held true both for solutions of polystyrene in water and for polystyrene mixed with magnetic fluid. The iron analysis test was also shown to be accurate in the presence of polystyrene, with no loss in accuracy even for magnetic fluid samples containing up to 2 wt% polystyrene. With the exception of their size, the physical properties of all the beads and the analysis techniques used for each of them were identical. The polystyrene beads therefore served as excellent model particles for the magnetophoretic clarification experiments, and due to their ideal shape and physical properties, resulted in an upper bound on the separation performance of the magnetophoretic clarification devices when compared with the performance of the *E. coli* cells in the same devices.

3.8 References

1. Ogez, J.R., J.C. Hodgdon, M.P. Beal and S.E. Builder, "Downstream Processing of Proteins: Recent Advances". *Biotech. Adv.*, 1989. 7: p. 467-488.

2. Laska, M.E., "The Effect of Dissolved Oxygen on Recombinant Protein Degradation in *Escherichia coli*", Ph.D. Thesis, Department of Chemical Engineering; Massachusetts Institute of Technology: Cambridge, MA, 2001.

3. Winkler, S.A., "Development of a Fermentation Process for the Production of Recombinant Heparinase I in *Escherichia coli*", Ph.D. Thesis, Department of Chemical Engineering; Massachusetts Institute of Technology: Cambridge, MA, 1995.

Chapter 4

Continuous Counter Current Magnetophoresis

4.1 Introduction

Magnetophoretic clarification relies on the force that a non-magnetic particle feels when submersed in a magnetic fluid that is then magnetized by an applied magnetic field. This force pushes the non-magnetic particle away from areas of high magnetic field strength and into areas of low magnetic field strength. Thus, by carefully designing the magnetic field and its gradient for a specified system geometry, a clarification process can be developed that makes use of this magnetic force to concentrate non-magnetic particles, typically on the order of microns, and remove them from the bulk fluid.

Successful magnetophoretic clarification was first demonstrated using a continuous counter current flow process. In this system, pairs of permanent magnets moved in a direction opposite to the flow of the bulk feed mixture, and the traveling non-uniform magnetic field produced by the moving magnets captured the micron-sized non-magnetic particles from the bulk feed mixture and pushed them into a separate collection tube, resulting in clarified bulk feed fluid that then exited the counter current system. This chapter discusses first the physical system that comprises the counter current process, its specifications and magnetic field profile, and then discusses the results of the clarification experiments performed with the device.

4.2 Counter Current Device Specifications

4.2.1 Magnet Pairs

The counter current system consisted of a series of magnet pairs facing each other, spaced apart with an opening between them of 3.2 mm. This spacing was just wide enough to accommodate the tubing through which the feed mixture was pumped between the magnet pairs. The tubing used was Nalgene 180 Clear PVC Tubing, 1/16" (1.59 mm) ID and 1/8" (3.18 mm) OD. Neodymium Iron Boron 39 MGOe magnets, each having the

dimensions 11.7 x 11.7 x 5 mm, were used for the magnet pairs. The distance separating each of the pairs of magnets in the device was 12.7 mm, with a total of 36 magnet pairs (or 72 individual magnets). The magnets were mounted on an elliptical chain that was rotated by a motor, and they moved in a direction opposite to the motion of the fluid in the tubing. The speed of the magnets on the rotating chain was kept constant in all experiments at 5.3 cm/min, as this was the magnet speed that produced optimal separation at all feed flow rates used with the device.

The fluid feed mixture was introduced into the system through a T-junction located in the bottom right corner of the device, and was pumped through the tubing using a syringe pump (Sage Syringe Pump Model M365). Once pumped into the T-junction, the feed flowed to the right of the T-junction and up around the top of the apparatus, exiting at the opposite side from the feed inlet. The total length of the flow tubing was 60 cm. The tube to the left of the T-junction was closed at the far left end and experienced no real fluid movement, but instead served as a collection reservoir for the non-magnetic particles removed from the feed. The collection tube was 41 cm in length, and was filled at the start of each experiment with pure magnetic fluid of the same concentration used for the feed. A schematic of the full counter current device is shown in Figure 4-1, while Figure 4-2 shows a photograph of the complete counter current system, including the position of the syringe pump used to pump the fluid through the device.

4.2.2 Magnetic Field Profile

The use of equally spaced pairs of magnets in the counter current system generated an approximately sinusoidally shaped magnetic field profile along the length of the tubing, with a maximum field strength approaching 0.7 Tesla. This oscillating field was measured using a Gauss/Tesla meter (F. W. Bell, Model 4048), and is shown in Figure 4-3. The measurements were taken in between the two magnets that form the magnet pairs as well as in between the empty space between two pairs of magnets, along the same track that the tubing occupies in the device.

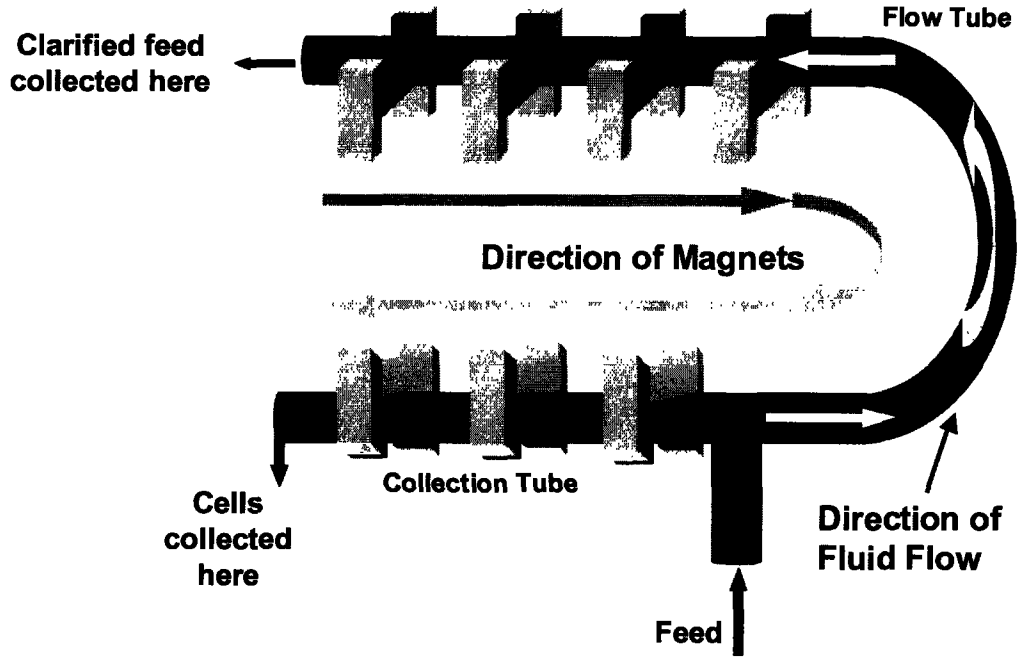

Figure 4-1. Schematic of the counter current device showing general geometry and direction of magnet movement and fluid flow.

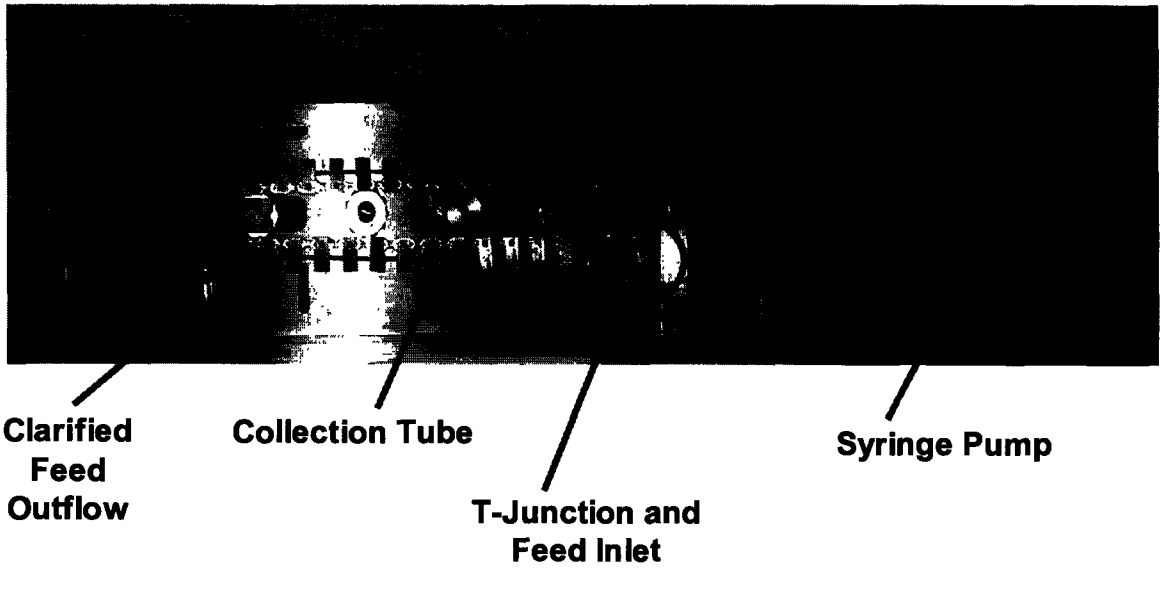

Figure 4-2. Complete counter current system, including tubing and syringe pump for pumping the feed fluid through the device.

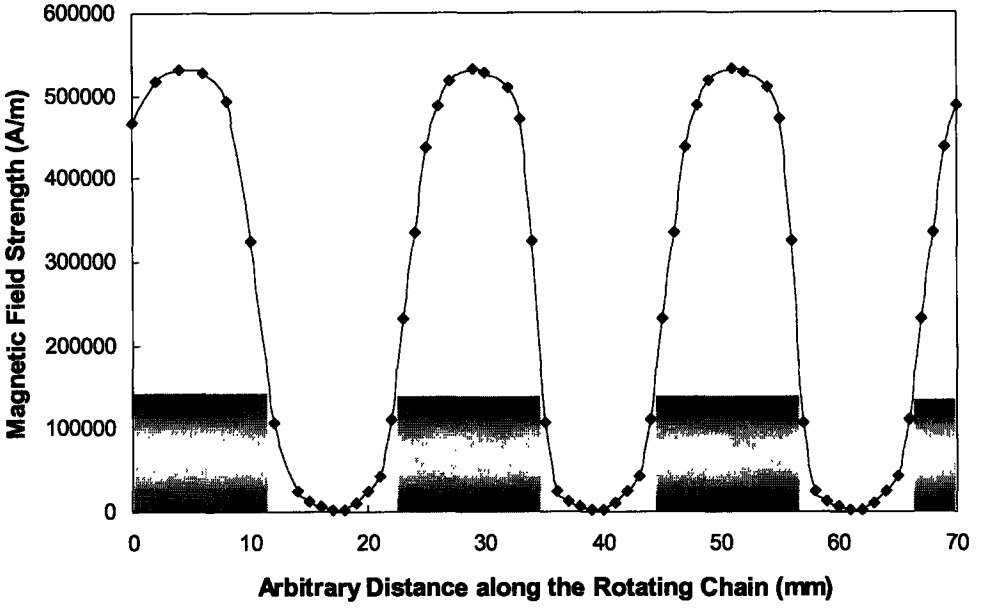

Figure 4-3. Measured magnetic field profile along the axis of the rotating chain in the counter current device. The boxes at the bottom of the graph represent the position of the magnet pairs. The peaks of strongest magnetic field occur in the center of the magnet pairs, while the troughs of weakest magnetic field occur in the middle of the space separating the magnet pairs.

The oscillating magnetic field profile shown in Figure 4-3 forced the micron sized non-magnetic particles in the feed fluid to move into the areas of weakest magnetic field, in this case between the magnet pairs. As the feed fluid flowed through the changing magnetic field, packets of non-magnetic particles collected between the magnet pairs. As the magnets moved in the direction opposite to the fluid flow, these packets of non-magnetic particles traveled with the magnets in order to stay in the areas of weakest field, analogous to surfing a magnetic wave. In this way, the particles traveled with the magnets against the flow of the bulk fluid, and were directed into the collection tube, where they were sequestered away from the feed fluid.

4.3 Counter Current Experiments

4.3.1 Experimental Procedure

Experiments using both polystyrene (PS) beads and *E. coli* cells as the non-magnetic particles of interest were performed with the counter current system. The procedure for performing the experiments was the same in all cases. First, magnetic fluid of a specified concentration was mixed either with a solution of polystyrene and deionized water, for the polystyrene experiments, or with raw fermentation broth containing freshly grown *E. coli* cells, for the cell experiments. Deionized water was the only water used in all of the experiments. This magnetic fluid/non-magnetic particle mixture was used as the feed, and the total volume of feed for all experiments was 5 mL.

The collection tube was filled with pure magnetic fluid of the same concentration as the magnetic fluid in the feed and was clamped shut at the far left end. The presence of the magnetic fluid in the collection tube enhanced the capture and sequestration of the non-magnetic particles that were carried into the tube by the movement of the magnets.

All of the tubing, together with the T-junction, was securely placed in the device between the pairs of magnets. A 5 mL syringe was filled with the feed, attached to a short inlet tube leading directly to the T-junction in the device, and placed in the syringe pump, which was used to pump the feed through the system at a specified flow rate (between 1.8 and 9.2 mL/hr). The clarified fluid that exited the device was collected using a glass sample vial. The syringe was turned at regular intervals to prevent the polystyrene beads or cells from settling in the syringe. Once the syringe was empty and all of the feed had been pumped into the device, the syringe pump was turned off. However, the magnets were left to rotate for another 15 minutes to enhance the collection of the non-magnetic particles from the 1.2 mL of feed fluid still entrained in the flow tube in the device. This enhancement procedure did not affect the analysis of the clarified feed that had already exited the system, but served only to deplete the concentration of non-magnetic particles retained in the flow tube and enhance the collection of these particles in the collection tube.

Once the magnets were turned off, all of the tubing was removed from the device, and the fluid still entrained in the flow tube was collected, along with the mixture of concentrated non-magnetic particles contained in the collection tube. The contents of the collection tube, the fluid entrained in the flow tube, and the clarified fluid that exited the system were then analyzed. The analysis procedure was the same for both polystyrene beads and cells, and is summarized in subsequent sections of this chapter. A detailed description of the analysis procedure for both polystyrene beads and cells can be found in Chapter 3 of this work.

4.3.2 Experiments with Polystyrene Beads

Experiments using the counter current processs were first performed using polystyrene (PS) beads as a model system. The beads, obtained from Spherotech, Inc. (Libertyville, IL), were spherical in shape with a diameter of 2.01 ± 0.05 μm. The beads arrived as a suspension of 5.0 wt% ± 0.2wt% beads in deionized water with 0.02% sodium azide added as bacteriostatic, and were used as received. The beads were negatively charged due to the presence of sulfate groups on their surface, and zeta potential measurements in 0.01 M NaCl (ionic strength 0.01 M) at a pH of 6.7 yielded an average zeta potential value of −104 ± 3 mV.

4.3.2.1 Analytical Measurements

The concentration of polystyrene beads in the samples collected during the experiments was determined by measuring the absorbance (i.e. the optical density, or OD) of the samples at 600 nm using a Hewlett Packard UV-Visible Spectrophotometer (Model 8463). Since the optical density measurements at 600 nm can be correlated with the optical density for known polystyrene concentrations (the correlation has been shown to be linear, see Chapter 3 of this work), the concentration of the polystyrene beads in the sample fluids can be calculated using this correlation.

The magnetic nanoparticles in magnetic fluid also show absorbance at 600 nm, in addition to the absorbance observed from the polystyrene beads, and the two spectra are additive. The polystyrene concentration in the samples collected during experiments was therefore determined by first performing an initial measurement at 600 nm on a diluted

solution of the experimental sample. A typical dilution was 0.05 mL sample in 10 mL deionized water. This measured absorbance provided the OD_{600} value for the total mixture of both polystyrene and magnetic fluid. The diluted solution used for this initial measurement was then centrifuged at 4000 rpm for 40 minutes. This procedure sedimented only the polystyrene, since the magnetic nanoparticles that make up magnetic fluid are not affected significantly by centrifugation. The absorbance of the magnetic fluid supernatant at 600 nm was measured, and the difference between the total optical density of the full mixture and the optical density of just the magnetic fluid supernatant yielded the optical density of the polystyrene alone. Once the optical density was known for just the polystyrene, the polystyrene concentration was calculated using the previously determined OD_{600} correlation.

4.3.2.2 Control Experiments

A control experiment was performed with the counter current system in which the feed consisted of 5 mL of 1 wt% polystyrene in water, with no magnetic fluid added. This experiment was performed to determine if there were any unanticipated flow patterns in the device that would cause non-magnetic particles to enter the collection tube in the absence of magnetic fluid. The 1 wt% polystyrene feed was pumped through the flow tube at a flow rate of 2.8 mL/hr. The samples collected at the end of the experiment were then analyzed, and the results showed that less than 1% of the polystyrene from the feed entered the collection tube. This result was as expected, with no separation of polystyrene observed, indicating that there were no flow anomalies associated with the counter current system.

4.3.2.3 Magnetic Fluid Experiments

Experiments were performed using magnetic fluid in the feed mixture to test the full separation capability of the counter current system. A feed mixture consisting of 5 mL of 1 wt% polystyrene (PS) and 1 wt% magnetic fluid (MF) was used. The feed was pumped through the counter current device at a flow rate of 2.8 mL/hr, which was the only flow rate used with the polystyrene beads. The samples collected at the end of the experiment were then analyzed, with the results shown in Figure 4-4.

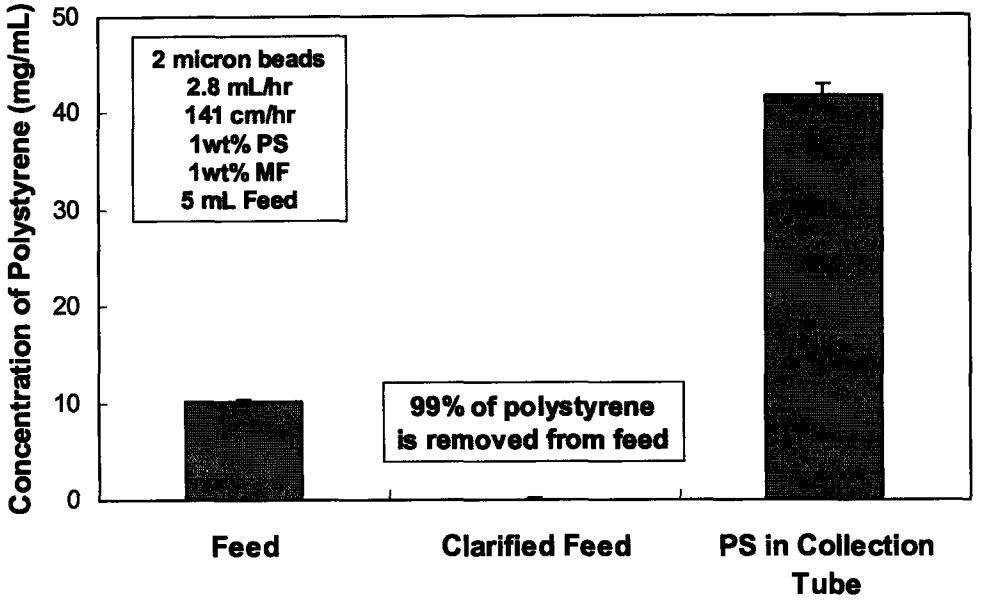

Figure 4-4. Results of the experiment using 5 mL of 1 wt% polystyrene and 1 wt% magnetic fluid as the feed. Clarified Feed represents the amount of the polystyrene collected in the fluid that exited the counter current device, and PS in Collection Tube represents the amount of polystyrene removed from the feed and collected in the collection tube.

The results show that excellent separation was achieved, with the clarified feed fluid containing less than 1% of the polystyrene originally present in the feed mixture. The material balance for the system also closed to within 1%, including the fluid retained in the flow tube in the device. This indicates that the analytical techniques used to determine the concentration of the polystyrene in the feed and fluid samples were accurate. Most importantly, the results showed that magnetophoretic clarification is successful with the counter current flow configuration. Subsequent experiments using polystyrene beads under the same experimental conditions proved to be highly reproducible, achieving 99.3% ± 0.2% removal of the polystyrene beads from the feed fluid. Since the proof of principle using polystyrene beads as a model system was achieved, no further polystyrene experiments were performed.

4.3.3 Experiments with *E. coli* Cells

The effectiveness of the counter current system for cell clarification was studied using *E. coli* cells (wild strain BL21) in raw fermentation broth. The cells were

cylindrically shaped and measured approximately 2-2.5 μm long by 1-1.5 μm in diameter, as determined by microscopy (see Chapter 3 of this work). The following sections discuss the results of the experiments performed using the cells in the counter current system.

4.3.3.1 Analytical Measurements

The concentration of cells in the samples collected during the experiments was determined using UV-Vis spectrophotometry (Hewlett Packard UV-Visible Spectrophotometer Model 8463) in the same manner as described previously for the polystyrene beads. The optical density at 600 nm was measured for both the raw experimental samples and the centrifuged samples, and the difference between the OD_{600} values was used to determine the optical density of just the cells alone. A linear correlation relating optical density to cell concentration was used to determine the concentration of the cells in each sample as wt% cells on a dry cell basis (see Chapter 3 of this work for more details of the analysis procedure).

4.3.3.2 Magnetic Fluid Experiments

No control experiments were performed in which the cells alone were suspended in pure fermentation broth, with no magnetic fluid added, since the importance of the magnetic fluid for separating non-magnetic particles from the bulk fluid had been demonstrated with the polystyrene beads.

The results of a typical experiment for cell clarification using the counter current process are shown in Figure 4-5 for a feed mixture composed of 1 wt% cells on a dry cell basis and 1 wt% magnetic fluid with a feed flow rate of 2.8 mL/hr. The results show that approximately 95% of the cells from the feed mixture were removed after one pass through the system, which clearly demonstrates that magnetophoretic cell clarification is successful with the counter current flow configuration. The importance of the operating parameters, such as feed flow rate, the concentration of magnetic fluid and the concentration of cells in the feed, was then tested in subsequent experiments, and the results were fit to an empirical model, as described in the next section.

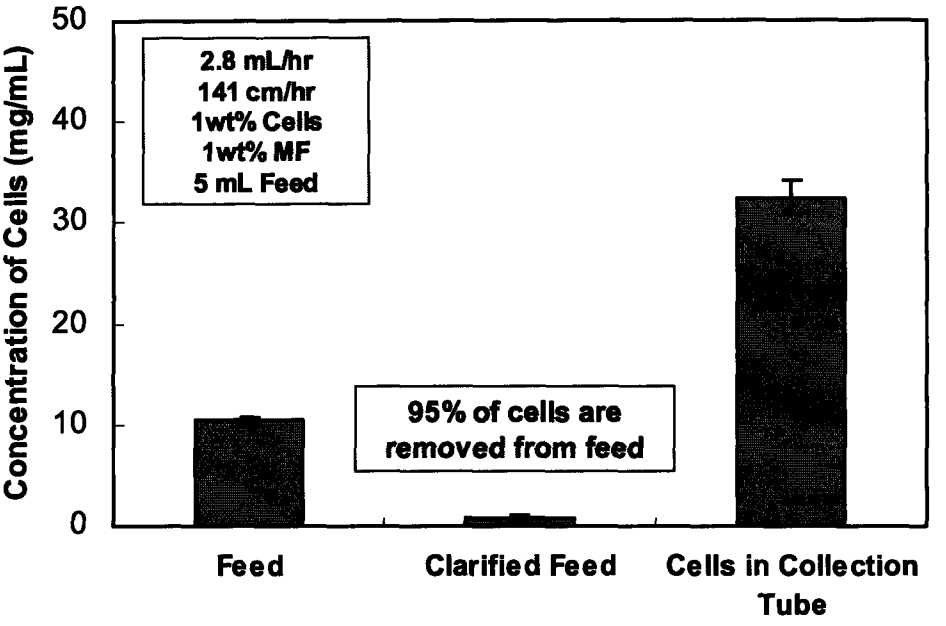

Figure 4-5. Results of the experiment using 5 mL of 1 wt% cells on a dry cell basis and 1 wt% magnetic fluid as the feed. Clarified Feed represents the amount of cells collected in the fluid that exited the counter current device, and Cells in Collection Tube represents the amount of cells removed from the feed and collected in the collection tube.

4.4 Importance of the Operating Parameters

To explore the importance of certain operating parameters on the separation capability of the counter current system, a Box Behnken experimental design was followed. For the case of three different parameters, the Box Behnken design assigns three values, or levels, to each of the three parameters in question. By performing experiments in various combinations of these levels, the effect of these parameters on the separation capability of the counter current device, as well as the repeatability of the experiments, can be assessed.

In this case, the three operational parameters explored were fluid flow rate, magnetic fluid concentration and cell concentration in the feed. The three values assigned to each parameter tested are shown in Table 4-1 below. The values for the cell concentration in the actual experiments varied over the range of 0.4 wt% to 1.9 wt% on a dry cell basis, but the values for the fluid flow rate and the concentration of magnetic

fluid in the feed were fixed in each experiment at one of the three levels indicated in Table 4-1.

Fluid Flow Rate (mL/hr)	wt% MF	wt% Cells
1.8	0.5	0.5
5.3	1.0	1.0
9.2	1.5	1.5

Table 4-1. Values of the operational parameters tested using a Box Behnken design for the counter current device.

The data gathered using these values in experiments, as well as data collected from earlier experiments, were then fit to an empirical correlation of the following form:

$$\%\ \text{Cells in Clarified Outflow} = b_1 + b_2x_1 + b_3x_2 + b_4x_3 + b_5x_1^2 + b_6x_2^2 + b_7x_3^2 + b_8x_1x_2 + b_9x_2x_3 + b_{10}x_1x_3$$

where x_1 is the normalized feed flow rate, with the fastest flow rate assigned a value of 1 and the lower flow rates normalized as fractions of the fast flow rate accordingly, x_2 is the magnetic fluid concentration in the feed in weight percent, x_3 is the *E. coli* cell concentration in the feed in weight percent on a dry cell basis, and "% Cells in Clarified Outflow" refers to the mass of cells collected in the clarified outflow divided by the total mass of cells in the feed, multiplied by 100. The feed flow rate was normalized so that all the operating parameters were of the same order of magnitude. The lower flow rates were normalized against the highest flow rate. For example, the lowest flow rate, 1.8 mL/hr, was 20% of the flow of the highest flow rate, 9.2 mL/hr, and thus had a normalized value of 0.2 (see Table 4-2). The Matlab code used to fit the experimental data to the empirical correlation is given in Appendix B. Figure 4-6 shows surface plots of the empirical correlation for various flow rates and magnetic fluid concentrations, with each plot depicting the results for a different cell concentration in the feed fluid.

The results of the empirical correlation show that the best separation (~4.5% cells remaining in the clarified feed, or 4.5% Cells in Clarified Outflow) resulted from the lowest flow rate (1.8mL/hr) at high magnetic fluid concentrations (>1.2wt%), as expected, but also for higher cell concentrations (0.7-1.1wt%). Thus, as shown graphically in Figure 4-6, cell concentration is not as important as flow rate and magnetic

fluid concentration in obtaining good cell separation. In addition, the higher the magnetic fluid concentration, the faster the flow can be while still maintaining approximately the same degree of separation.

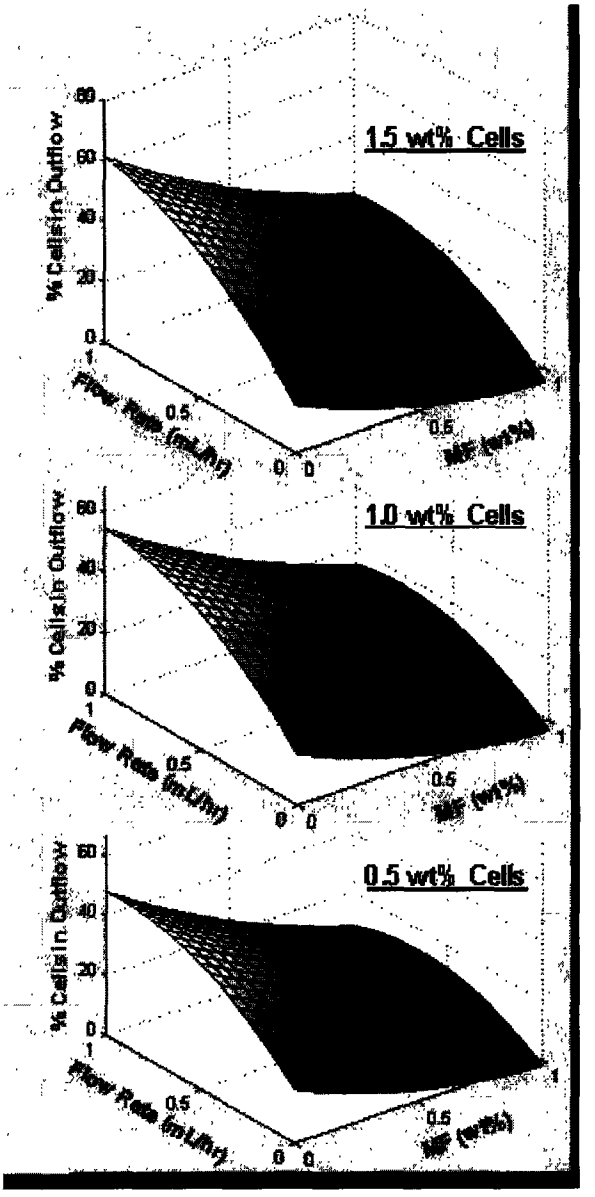

Figure 4-6. Surface plots showing the effects of magnetic fluid concentration and flow rate on the separation capability of the counter current device, with each plot representing a different cell concentration in the feed fluid.

The empirical correlation was not able to predict with better than 30% accuracy the specific percent of cell clarification that would be achieved in any one particular experiment when given the precise fluid flow rate, magnetic fluid concentration, and cell

concentration in the feed. It serves best as a good qualitative model, instead of a quantitative one. The results of all the valid experiments performed on the counter current system used in the empirical model are listed in Table 4-2.

The effect of the operating parameters on the separation capability of the counter current process can be correlated in terms of a dimensionless magnetic parameter, which gives the ratio of the magnetic force on the non-magnetic particles to the viscous drag force on the particles as they move through the counter current device, as shown schematically in Figure 4-7.

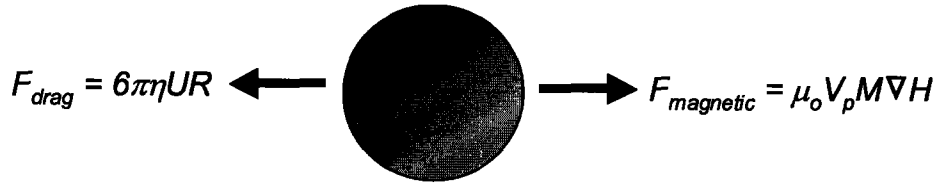

Figure 4-7. Force balance on a non-magnetic particle in the counter current device.

The magnetic and drag forces are given by Equations 4-1 and 4-2, respectively:[1-2]

$$F_m = \mu_o V_p M \nabla H \quad \text{where} \quad M = \frac{M_s}{H_t + H} H \tag{4-1}$$

$$F_d = 6\pi\eta U R_p \tag{4-2}$$

where μ_o is the permeability of free space, V_p is the volume of the non-magnetic particles, M is the magnetization of the magnetic fluid, ∇H is the magnetic field gradient, M_s is the saturation magnetization of the magnetic fluid at high magnetic field strengths, H is the magnetic field, H_t is the magnetic field strength at which the magnetization of the magnetic fluid is half the saturation magnetization (see Chapter 5 for a more detailed discussion of the magnetization of the magnetic fluid), η is the viscosity of the magnetic fluid and non-magnetic particle mixture, R_p is the radius of the non-magnetic particles, and U is the linear velocity of the non-magnetic particles relative to the fluid, which for the counter current system is the linear velocity of the bulk fluid plus the velocity of the moving magnets. The dimensionless magnetic parameter can then be defined to investigate the relative importance of the magnetic force compared to the viscous drag force:

$$D_{md} = \frac{\mu_o V_p M \nabla H}{6\pi\eta U R_p} \tag{4-3}$$

Changes to the magnetic force term of Equation 4-3 (numerator) can be made by changing the concentration of magnetic fluid in the feed. A higher concentration of magnetic nanoparticles in the feed fluid results in a larger magnetization, M, and thus a stronger magnetic force on the non-magnetic particles. Changes to the viscous drag term (denominator) can be made by changing the flow rate of the feed fluid and the velocity of the magnets, thus changing the relative linear velocity, U.

Flow Rate (mL/hr)	Normalized Flow Rate	wt% MF in Feed	wt% Cells in Feed	% Cells in Outflow
9.2	1.0	1.0	0.48	7.1
1.8	0.2	1.0	0.52	11.3
1.8	0.2	1.0	1.44	6.5
9.2	1.0	1.0	0.65	5.1
9.2	1.0	1.0	1.88	20.1
9.2	1.0	1.5	0.93	9.8
9.2	1.0	0.5	1.10	31.0
1.8	0.2	1.5	1.12	4.3
1.8	0.2	0.5	0.91	7.4
5.3	0.6	1.5	1.42	15.9
5.3	0.6	1.5	0.43	3.9
5.3	0.6	0.5	0.51	26.4
5.3	0.6	0.5	1.71	37.3
5.3	0.6	1.0	0.73	14.3
5.3	0.6	1.0	0.68	13.0
5.3	0.6	1.0	0.68	13.0
2.8	0.3	1.0	1.47	11.9
2.8	0.3	1.0	1.13	7.2
2.8	0.3	1.0	1.38	14.8
2.8	0.3	1.0	1.02	5.4
2.8	0.3	1.0	1.01	2.0
9.2	1.0	1.0	0.88	14.0
9.2	1.0	1.0	1.16	20.2
9.2	1.0	1.0	0.98	15.0
1.8	0.2	1.0	0.50	10.9

Table 4-2. Results from all experiments performed with the counter current device used to evaluate the importance of the feed flow rate, the concentration of magnetic fluid, and the concentration of cells in the feed on the separation capability of the device.

The dependence of the separation capability of the counter current device on the dimensionless magnetic parameter, D_{md}, is shown graphically in Figure 4-8, and depicts the percent of cells removed from the feed as a function of D_{md}, which was calculated from the values of the operating parameters used in each experiment. The percent of cells removed from the feed was calculated by dividing the mass of cells collected in the clarified feed fluid by the total mass of cells in the feed, then subtracting that ratio from 1, and multiplying by 100. The dashed line is present on the graph to indicate trends in the data and is not a theoretical prediction. The results show that better separation in the counter current device was achieved for increasing D_{md}, as expected, since increasing D_{md} corresponds to an increase in the magnetic force on the cells.

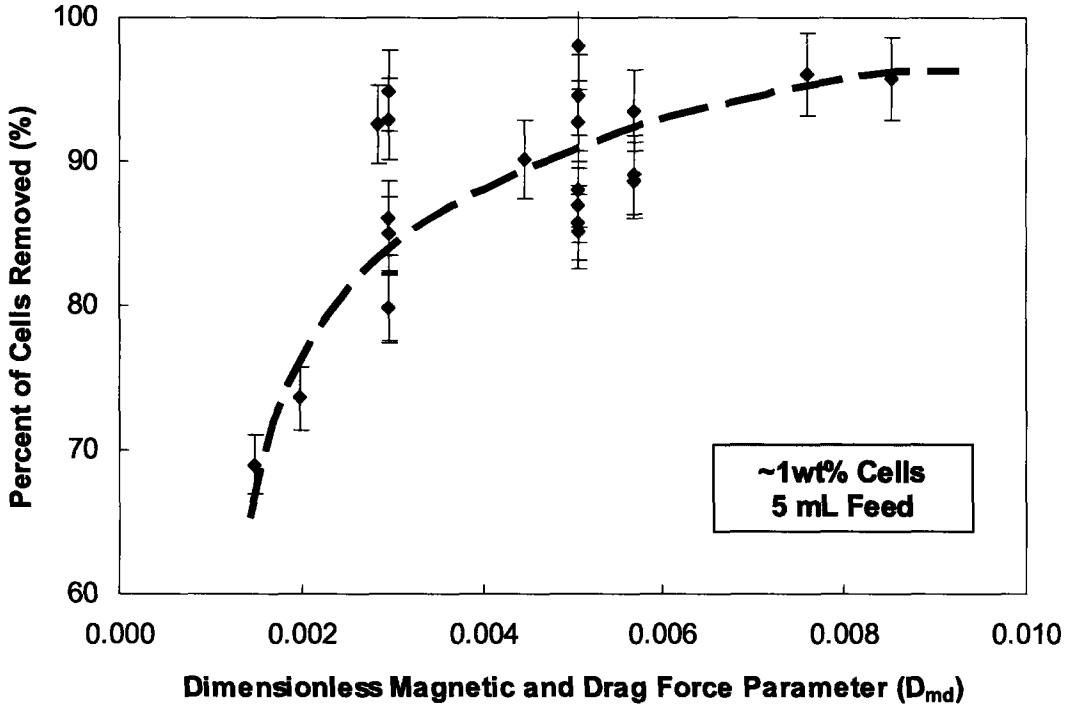

Figure 4-8. Dependence of the separation capability of the counter current device, in terms of the percent of cells removed from the feed fluid, on the dimensionless parameter (D_{md}). The dashed line is present to indicate trends in the data.

The percent of cells removed from the feed as a function of feed flow rate alone is shown in Figure 4-9 for constant magnetic fluid and cell concentration, with the dashed line present on the graph to indicate trends in the data. It is evident that good cell separation is more easily achieved at lower flow rates than at higher flow rates, since

higher flow rates translate into a stronger viscous drag force and a shorter residence time for the cells in the system, leading to less efficient capture of the cells by the traveling magnetic field.

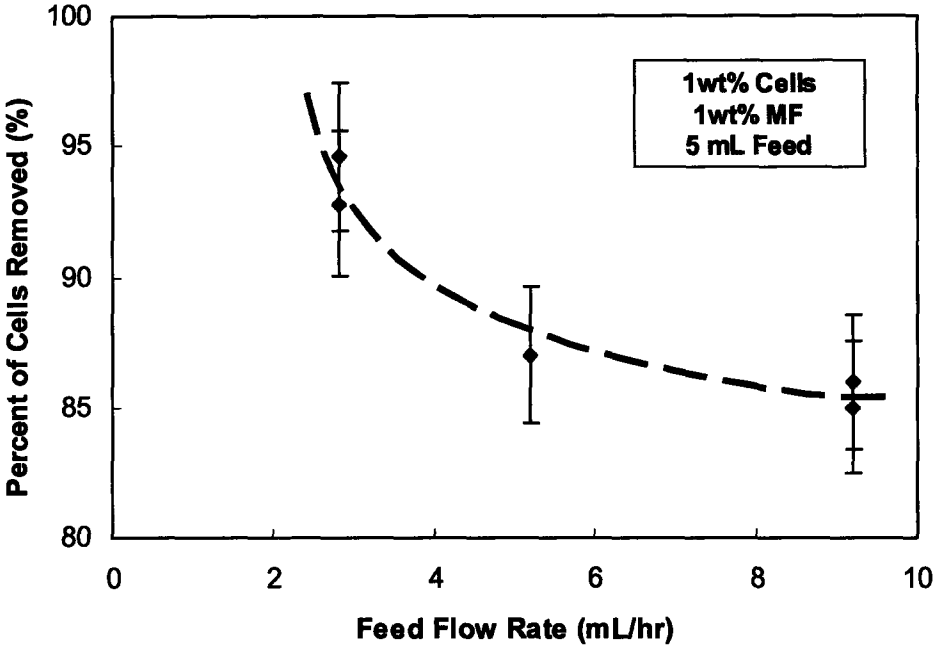

Figure 4-9. Percent of cells removed from the feed in the counter current device as a function of feed flow rate. The dashed line is present to indicate trends in the data.

The percent of cells removed from the feed as a function of magnetic fluid concentration alone is shown in Figure 4-10 for constant feed flow rate and cell concentration, with the dashed line present on the graph to indicate trends in the data. The flow rate used in these experiments was the highest flow rate used for all experiments with the counter current device, 9.2 mL/hr. Figure 4-10 shows that for constant feed flow rate and cell concentration, it is easier to achieve good cell separation with higher magnetic fluid concentrations than with lower magnetic fluid concentrations. In fact, the ability of the process to clarify cells from the feed drops dramatically with magnetic fluid concentrations less than 1 wt%. This result was anticipated, since it is the magnetization of the magnetic fluid that provides the magnetic force necessary for cell separation, and because magnetization scales linearly with the concentration of magnetic particles in the fluid (see Chapter 2 for more details), a lower concentration of magnetic fluid will result in a decreased magnetization of the fluid, and hence a smaller magnetic

force on the cells. Thus, the higher the magnetic fluid concentration, the stronger the magnetic force on the cells and the better the separation, even at higher flow rates. The experimental data in Figure 4-10 demonstrate this by asymptotically approaching 100% separation at higher magnetic fluid concentrations and rapidly approaching 0% separation (no separation) at lower magnetic fluid concentrations.

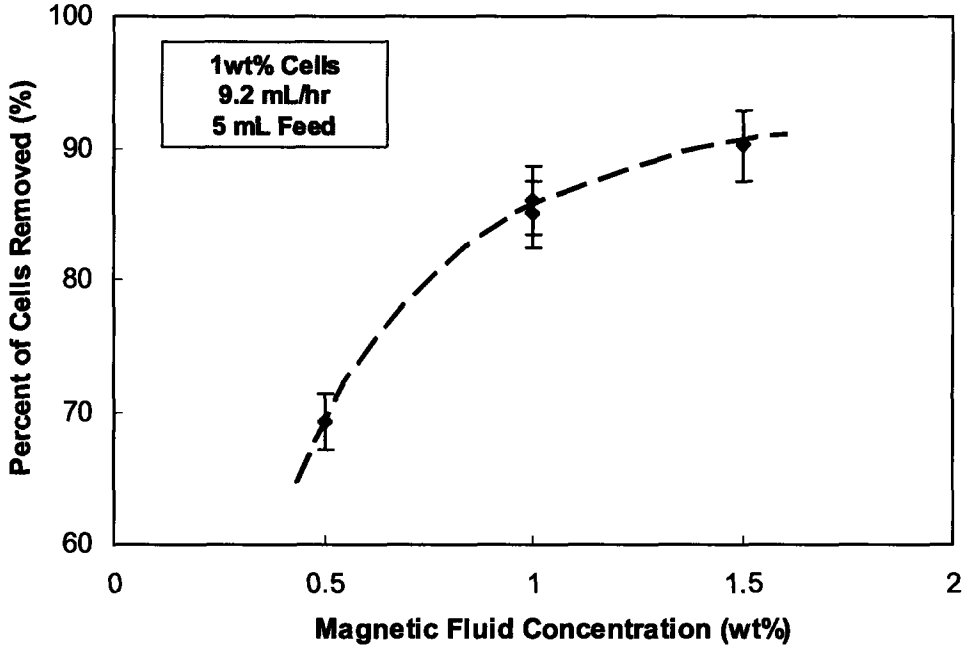

Figure 4-10. Percent of cells removed from the feed in the counter current device as a function of magnetic fluid concentration. The dashed line is present to indicate trends in the data.

4.5 Summary

The counter current process was shown to be successful in removing up to 95% of *E. coli* cells from the feed after one pass through the system. The importance of the operating parameters on the separation capability of the counter current system was determined, with the separation capability of the process increasing with decreasing flow rate and increasing with increasing magnetic fluid concentration. The concentration of the cells in the feed fluid was shown to have less impact on the separation capability of the counter current device than feed flow rate and magnetic fluid concentration.

The primary advantage of the counter current design is that the cells can be effectively removed from the fermentation broth without any significant loss of the bulk liquid. This is an important consideration when the biological product of interest in the bulk medium, such as a pharmaceutical compound or protein, is a high value product where all product losses must be minimized. An optimized counter current design would therefore have tremendous applications in the biotechnological and pharmaceutical industries for cell clarification.

4.6 References

1. Rosensweig, R.E., *Ferrohydrodynamics*. 1997, Mineola, NY: Dover Publications, Inc.

2. Deen, W.M., *Analysis of Transport Phenomena*. 1998, New York: Oxford University Press, Inc.

Chapter 5

Modeling Magnetophoresis

5.1 Introduction

A model for the magnetophoretic clarification technique was developed to aid in designing new processes for magnetophoretic cell clarification. This chapter discusses the basic theory behind magnetophoretic clarification, and includes an overall equation governing magnetophoresis as it was performed in this work. The chapter then discusses the application of these equations to the design and modeling of a second magnetophoretic clarification device, called the quadrupole device. A Matlab simulation of the quadrupole design is discussed, including its use in determining the final geometry and design of the custom-built quadrupole device.

5.2 Theory of Magnetophoresis

5.2.1 Assumptions for the Separation of Micron Sized Particles

Magnetophoresis results from the force that a non-magnetic particle feels when surrounded by a magnetized fluid. As discussed in Chapter 2, the magnetic fluid used in this work was a colloidal suspension of nanoparticles containing a magnetite core surrounded by a polymer shell, which acted as a stabilizer and kept the nanoparticles suspended in water. The average size of the magnetic nanoparticles, including the stabilizing polymer shell, was 32 nm, and it is the suspension of these particles in water that makes up magnetic fluid. The magnetic fluid was therefore treated as a continuum when compared to the non-magnetic particles separated during the magnetophoretic clarification process, since the magnetic nanoparticles that comprised the magnetic fluid were nearly two orders of magnitude smaller than the micron sized particles being separated.

In addition, although the magnetic fields used in this work were fairly strong (with magnetic flux densities on the order of one Tesla), the force on the tiny magnetic

nanoparticles due to the applied magnetic field was not able to compete with the Brownian motion of the particles. Thus, the density and concentration of magnetic fluid was assumed to remain constant during magnetophoresis.

As discussed in more detail in Chapter 3, the non-magnetic particles separated in this work were either *E. coli* cells or polystyrene beads, and each had a net negative surface charge. Therefore, at the concentrations of non-magnetic particles explored in this work, electrostatic interactions between particles were not negligible and had to be considered in the theoretical framework for magnetophoresis.

5.2.2 Magnetic Force on Non-magnetic Particles

The force that makes magnetophoresis possible is the magnetic force, which acts on a non-magnetic particle that is surrounded by a magnetized fluid in a non-uniform magnetic field, and is given to leading order by Equation 5-1:

$$F_m = \mu_o V_p M \underline{\nabla} H \tag{5-1}$$

where μ_o is the permeability of free space, V_p is the volume of the non-magnetic particle, M is the magnetization of the magnetic fluid, and H is the magnetic field.[1] Equation 5-1 incorporates the assumptions of constant magnetic fluid density and concentration and treats the magnetic fluid as a continuum relative to the larger non-magnetic particles. The equation further assumes that the magnetization of the magnetic fluid is collinear with the magnetic field, such that the magnetic nanoparticles become magnetized in the same direction as the applied field. This expression is therefore not valid for high-frequency, alternating magnetic fields. Other assumptions incorporated in Equation 5-1 include constant temperature or temperature far from the Curie temperature of magnetite, negligible electrical conductivity of the magnetic fluid, a total magnetization of the magnetic fluid that is much less than the magnitude of the magnetic field strength ($M << H$), low concentration of the non-magnetic particles in the fluid, nearly constant H and $\underline{\nabla} H$ through the non-magnetic particle volume such that the presence of the non-magnetic particles does not distort the magnetic field lines, and that the micron sized particles have nearly zero magnetization in the presence of a magnetic field (the particles

are completely non-magnetic).[2] Equation 5-1 is valid both for stationary non-magnetic particles and for particles moving at a constant velocity through the magnetic fluid.

Equation 5-1 shows that the force on a non-magnetic particle that is surrounded by a magnetized fluid is proportional to the volume of the non-magnetic particle, the magnetization of the surrounding magnetic fluid, and the gradient of the magnetic field. Thus, the non-magnetic particles experience a force that pushes them away from areas of high magnetic field and into areas of low magnetic field, and this force is stronger for larger non-magnetic particles. The particles will continue to migrate due to the magnetic force until they encounter a region where either the magnetic field or the magnetic field gradient is zero.[2]

5.2.3 The Flux Relationship Defining Magnetophoresis

Using the assumptions outlined in the previous section, a force balance on the non-magnetic particles can be performed to develop an overall expression for the molar diffusive flux of the micron sized non-magnetic particles. The major forces acting on the non-magnetic particles are the magnetic force, the viscous drag force, the gravitational force, and a diffusive force, given as the negative of the gradient of the chemical potential of the non-magnetic particles. By rearranging the terms of the force balance and incorporating the electrostatic repulsion force through the gradient of the chemical potential of the particles (as the excess chemical potential), the molar diffusive flux of the non-magnetic particles relative to the mass average velocity can be stated as follows in Equation 5-2, from the derivation by Gonzalez, et al.

$$\underline{J}_p = \frac{-W_f C D_p}{\rho RT}\left(RT\underline{\nabla}C_p + C_p\Psi^2\underline{\nabla}C_p + C_p\overline{V}_p\rho g(1-\frac{\rho_p}{\rho}) + C_p\mu_o\overline{V}_p M\underline{\nabla}H \right) \qquad (5\text{-}2)$$

where W_f is the molecular weight of the magnetic fluid solvent, C is the total concentration of the fluid, D_p is the diffusivity of the non-magnetic particles in the magnetic fluid, ρ is the density of the magnetic fluid solvent, R is the gas constant, T is temperature, C_p is the molar concentration of the non-magnetic particles, $\overline{V}_p$ is the partial molar volume, g is the gravitational constant, ρ_p is the density of the non-magnetic particles, μ_o is the permeability of free space, M is the magnetization of the magnetic

fluid, and H is the magnetic field. The term Ψ^2 represents the electrostatic force constants, given by:

$$\Psi^2 = 16\pi^2 \varepsilon \psi_o^2 R_p^2 \kappa^{-2} (1 + 2\kappa R_p) N_A^2 \tag{5-3}$$

where ε is the electric permittivity of the fluid, ψ_o is the electric potential at the surface of the non-magnetic particles, R_p is the hydrodynamic radius of the non-magnetic particles, κ^{-1} is the Debye length, and N_A is Avogadro's number.

Aside from the assumptions previously mentioned, Equation 5-2 also assumes that the non-magnetic particles are spherical. For Equation 5-3, the assumptions include a low concentration of non-magnetic particles, that the volume exclusion contribution of the particles is considerably smaller than the electrostatic contribution, and that the double-layer theory is valid for the non-magnetic particles. For the double-layer theory to be valid, the magnetic fluid must be non-conducting, the magnetic field applied to the system must not vary with time, and the migration of the charged non-magnetic particles through the magnetic fluid must be slow enough not to induce any significant fields in the fluid.[2] All of these conditions hold true for the magnetophoretic clarification systems studied in this work, so Equations 5-2 and 5-3 are both valid for these systems.

Table 5-1 summarizes the assumptions that were used to derive Equations 5-2 and 5-3, all of which are valid for the non-magnetic particles and magnetophoretic clarification devices studied in this work. It is important to note that in Equations 5-2 and 5-3 the non-magnetic particles can be either stationary or moving in the magnetic fluid, and the magnetization can be any function of the applied magnetic field ($M = M(H)$).

Using the molar diffusive flux equation given by Equations 5-2 and 5-3, the overall species conservation equation describing magnetophoresis for micron sized non-magnetic particles in magnetic fluid is given by[3]:

$$\frac{\partial C_p}{\partial t} + \underline{v}_f \cdot \underline{\nabla} C_p = -\underline{\nabla} \cdot \underline{J}_p \tag{5-4}$$

where $\underline{v}_f$ is the velocity of the magnetic fluid relative to the coordinate system of interest, and $\underline{J}_p$ is given by Equation 5-2.

Assumptions for the Flux Equation Describing Magnetophoresis:

- Constant magnetic fluid density
- Constant magnetic fluid viscosity
- Constant magnetic fluid concentration
- Constant temperature, or temperature far from the Curie temperature
- The magnetic fluid is a continuum when compared to the non-magnetic particles
- The magnetization of the magnetic fluid is collinear with the magnetic field ($M \times H = 0$)
- The magnetic field applied to the system does not vary with time
- Negligible electrical conductivity of the magnetic fluid
- No free electrical currents ($\nabla \times H = 0$)
- A total magnetization of the magnetic fluid that is much less than the magnetic field ($M << H$)
- Low concentration of the non-magnetic particles in the fluid
- The non-magnetic particles are spherical
- The non-magnetic particles have nearly zero magnetization in the presence of a magnetic field (the particles are non-magnetic)
- Nearly constant H and ∇H through the non-magnetic particle volume
- The presence of the non-magnetic particles does not distort the magnetic field lines
- Migration of the charged non-magnetic particles is slow enough not to induce any significant fields in the magnetic fluid
- The volume exclusion contribution is considerably smaller than the electrostatic contribution for the charged non-magnetic particles
- The double-layer theory is valid for the charged non-magnetic particles

Table 5-1. Assumptions for the molar diffusive flux equation relative to mass average velocity for micron sized non-magnetic particles surrounded by magnetic fluid.

5.3 Model for Quadrupole Magnetophoresis

Equations 5-2 and 5-4 provide the general equations describing magnetophoresis for micron sized non-magnetic particles surrounded by magnetic fluid, and were used to model a new quadrupole magnetophoretic separation device. The next few sections describe the overall geometry of the new quadrupole design, the application of the general equation, and the results of the modeling study for the quadrupole flow configuration.

5.3.1 Geometry of the Quadrupole Design

The quadrupole design consists primarily of four permanent bar magnets arranged around a central column as depicted in Figure 5-1 (not shown to scale). The alternating north/south, north/south orientations of the four magnets create a magnetic field in which the outer wall of the column inside the magnets experiences a strong magnetic field while the center of the column experiences a low magnetic field. Thus, non-magnetic particles traveling through the column will experience a force that pushes them towards the center of the column where the magnetic field is weakest, concentrating the particles at the centerline of the column. The concentrated particles can then be removed through a coaxial tube present at the outlet end of the main column.

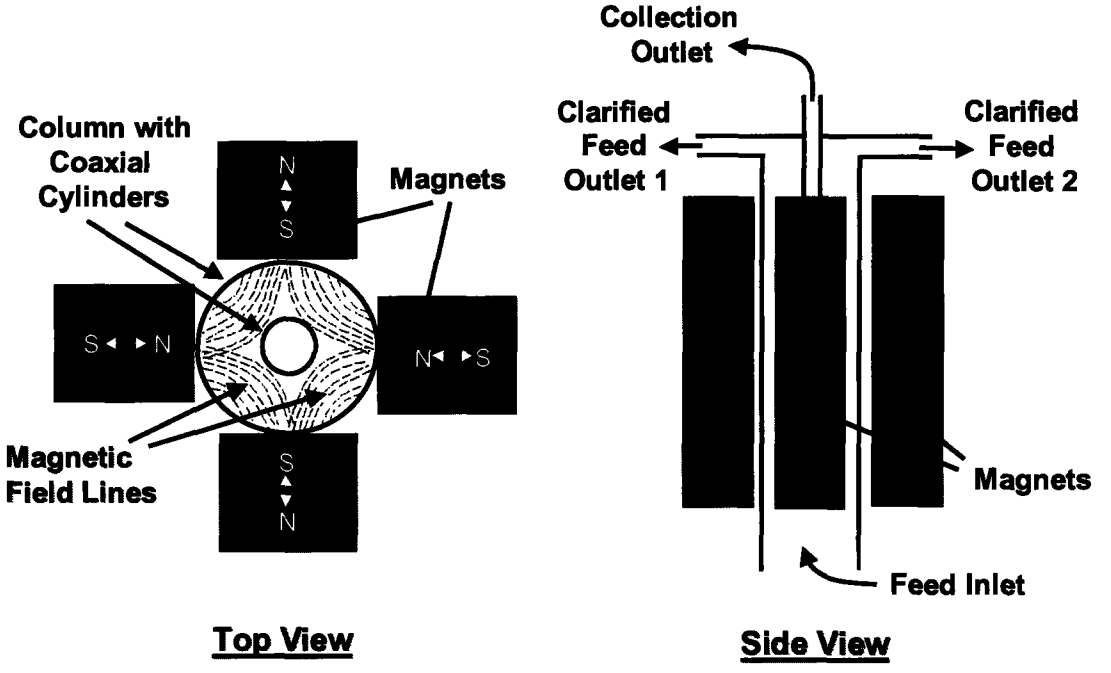

Figure 5-1. Schematic of the quadrupole design, showing an overall cylindrical geometry that is radially symmetric.

5.3.2 Quadrupole Model for Magnetophoresis

As shown in Figure 5-1, the quadrupole device was cylindrical in design, and the magnetic field was designed to be radially symmetric and constant along the length of the

column inside the magnets. The force balance on the magnetic particles in the quadrupole design suggests that the particles experience a radial magnetic force pushing them towards the centerline of the column that is balanced in part by diffusion and by electrostatic repulsive forces. Along the length of the column, the particles experience a viscous drag force from the flow of the fluid through the column that is balanced in part by a buoyancy, or gravitational, force opposing the fluid flow and encouraging settling of the non-magnetic particles in the column. Both the radially directed forces (magnetic, electrostatic, and diffusive) and the axially directed forces (drag and buoyancy) are assumed to be completely decoupled and independent from each other, which is a reasonable assumption for the case of low Reynolds number flow. In addition, the magnetic, electrostatic, and diffusive forces are assumed to be significant only in the radial direction, and the drag and buoyancy forces are assumed to be significant only in the axial direction. Axial diffusion and dispersion effects are neglected, and the total fluid concentration (C) is assumed to be constant.

Using these assumptions and the general cylindrical geometry of the quadrupole design, the overall magnetophoresis equation given by Equation 5-4 reduces to:

$$\frac{\partial C_p}{\partial t} + v_z(r)\frac{\partial C_p}{\partial z} - \frac{W_f C D_p \bar{V}_p g}{RT}\left(1 - \frac{\rho_p}{\rho}\right)\frac{\partial C_p}{\partial z} = \frac{W_f C D_p}{\rho RT}\frac{1}{r}\frac{\partial}{\partial r}r\left(RT\left(\frac{\partial C_p}{\partial r}\right) + \Psi^2\left(C_p\frac{\partial C_p}{\partial r}\right) + \mu_o \bar{V}_p M(H,r)\frac{\partial H(r)}{\partial r}C_p\right) \tag{5-5}$$

This governing equation for quadrupole magnetophoresis (Equation 5-5) takes into account two spatial dimensions (radial and axial) plus time. This equation can be solved for the concentration profiles of non-magnetic particles in the quadrupole device, thus yielding predictions about the performance of the design based on initial operating parameters such as feed flow rate and concentration.

5.4 Matlab Model for the Quadrupole Design

Equation 5-5 gives the overall governing equation for the specific case of quadrupole magnetophoresis. Assuming steady state operation and neglecting axial diffusion and dispersion effects, Equation 5-5 was modified to obtain:

$$v_z(r)\frac{\partial C_p}{\partial z} - \frac{W_f C D_p \bar{V}_p g}{RT}\left(1-\frac{\rho_p}{\rho}\right)\frac{\partial C_p}{\partial z} = \frac{W_f C D_p}{\rho RT}\frac{1}{r}\frac{\partial}{\partial r}r\left(RT\left(\frac{\partial C_p}{\partial r}\right)+\Psi^2\left(C_p\frac{\partial C_p}{\partial r}\right)+\mu_o \bar{V}_p M(H,r)\frac{\partial H(r)}{\partial r}C_p\right) \quad (5\text{-}6)$$

where Ψ^2 represents the electrostatic force constants given by Equation 5-3. This was the form of the equation solved using Matlab's PDE solver, PDEPE.

To solve this equation for the concentration profile of non-magnetic particles as they pass through the quadrupole device, numerical values or relationships for estimating each of the parameters in the equation were required to achieve a full solution. The following two sections describe how Equation 5-6 was adapted for Matlab's PDE solver, and includes a discussion of all the numerical values and relationships used for each of the parameters in the Matlab model.

5.4.1 Quadrupole Model Parameters

To solve Equation 5-6, numerical values or relationships for estimating all of the parameters in the equation were needed. Numerical values such as fluid density and viscosity, non-magnetic particle size and density, and other physical property values were determined as discussed in detail in Chapters 2 and 3 of this work. The following sections discuss how relationships describing the velocity profile, the non-magnetic particle diffusivity, the magnetization of the magnetic fluid, and the magnetic field profile were all determined for use in solving Equation 5-6.

5.4.1.1 Velocity Profile and Particle Diffusivity

The velocity profile used for Equation 5-6 was assumed to be parabolic in shape with a fluid velocity of zero (no slip) at the column walls. The velocity profile was further assumed to be constant in the axial (z) direction and to depend only on the radial direction ($v_z = v_z(r)$ only). Both of these assumptions are generally valid for the geometry of the system modeled in this work and for the low Reynolds number flows used ($Re << 1$). The overall form of the fluid velocity profile used with Equation 5-6 is given below by Equation 5-7:

$$v_z = v_{max}(1 - r^2) \tag{5-7}$$

where v_{max} is the maximum linear velocity for the fully developed profile, and r is the radial distance through the center of the column, where $r = 0$ corresponds to the centerline and $r = 1$ corresponds to the column wall.

The Stokes-Einstein equation, used to estimate the diffusivity (D_p) of the non-magnetic particles in the magnetic fluid, is given by:

$$D_p = \frac{RT}{6\pi\eta R_p N_A} \tag{5-8}$$

where R is the gas constant, T is temperature, η is the viscosity of the magnetic fluid, R_p is the hydrodynamic radius of the non-magnetic particles, and N_A is Avogadro's number. The Stokes-Einstein equation is valid for dilute solutions of spherical solutes where the moieties that make up the solvent are so small as to be considered a continuum when compared to the solute,[3] a criterion that is certainly met when using 32 nm sized magnetic fluid particles in aqueous suspension as the fluid phase in which the micron sized non-magnetic particles are immersed.

5.4.1.2 Magnetization of Magnetic Fluid

The magnetic nanoparticles that make up magnetic fluid become collinearly magnetized when exposed to an applied magnetic field, meaning that the magnetic dipoles in the magnetite cores of the nanoparticles, which are normally randomly oriented, begin to spend more time in an orientation parallel to the applied field than at other angles to the field, fluctuating along the direction of the applied magnetic field lines. The magnetization of the magnetic fluid increases as the applied magnetic field

increases, as more and more of the magnetic nanoparticles become aligned with the applied field. Eventually, at a high enough magnetic field, the average of the fluctuations of the magnetic dipoles corresponds directly to the direction of the applied magnetic field lines, indicating that the magnetic particles are fully aligned, and the magnetization reaches a maximum value and can not increase further even when stronger magnetic fields are applied to the system. This maximum magnetization value is called the saturation magnetization (M_s). Although rigorous models have been developed for the dependence of magnetic fluid magnetization on applied magnetic fields, a simpler, more easily applied empirical model that describes the magnetization data well was chosen instead:

$$M = \left(\frac{M_s}{H_t + H} \right) H \tag{5-9}$$

where M_s is the saturation magnetization, H is the magnetic field, and H_t is the magnetic field at which the magnetization of the magnetic fluid is equal to half the saturation magnetization ($M_s/2$). As Equation 5-9 shows, the magnetization is not simply linearly proportional to the magnetic field, but has a definite nonlinear dependence on the strength of the magnetic field ($M = M(H)$). The experimental magnetization data and the empirical model given by Equation 5-9 are plotted for comparative purposes in Figure 5-2 for a 1 wt% magnetic fluid solution.[4]

5.4.1.3 Quadrupole Magnetic Field Profile

The orientation of the four magnets shown in Figure 5-1, which is the essence of the quadrupole design, creates a radially symmetric magnetic field that is strongest next to the magnets and weakest in the center of the magnet assembly. The spatially non-uniform magnetic field generated by the alternating north/south, north/south orientations of the four magnets was modeled using the Maxwell 3-D Electromagnetic Field Simulator program (Ansoft Corporation), which calculated the field lines of the magnetic flux density (B) produced by the quadrupole orientation of the four permanent magnets.

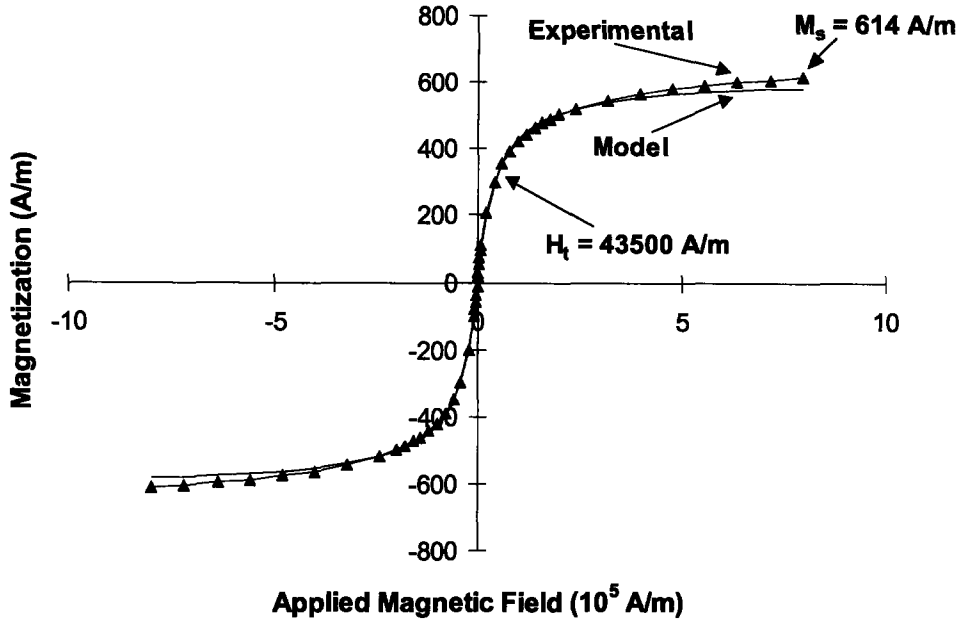

Figure 5-2. Magnetization response of 1 wt% magnetic fluid (1 wt% magnetite) under changing applied magnetic field, including the fit of the experimental data to the empirical model. Negative values of the magnetic field indicate that the field was applied in the opposite direction.[4]

The Maxwell Field solver creates a simulation by taking a user-defined geometry, incorporating the appropriate magnetic properties into the defined geometry, discretizing the geometry using a defined mesh (or set of grid points), and then solving Maxwell's equations to determine the magnetic flux density at each point on the mesh (at each grid point). The magnetic flux density calculated by the solver can then be used to determine the magnetic field profile (H) for the geometry of interest, since the magnetic flux density is directly proportional to the magnetic field and differs only by the constant μ_o, the permeability of free space, under conditions where the magnetization is much less than the applied field strength ($M << H$), as is the case for the magnetic fluids used in this work. The results of the Maxwell simulation for the geometry inherent in the quadrupole design are shown in Figure 5-3, using a central column diameter of 2 cm.

The Maxwell simulation showed that the magnetic flux density (B), and hence the magnetic field (H), is indeed radially symmetrical and constant along the axial dimension of the quadrupole design, with the strongest field lines next to the magnets (at a magnetic flux density of 0.63 Tesla) and the weakest field in the center (with a magnetic flux density of less than 0.1 Tesla). The simulation was performed for Neodymium Iron

Boron 35 MGOe permanent magnets, which is one of the strongest permanent magnet materials available for purchase commercially, and was also the strongest permanent magnet with physical properties readily available in the Maxwell solver.

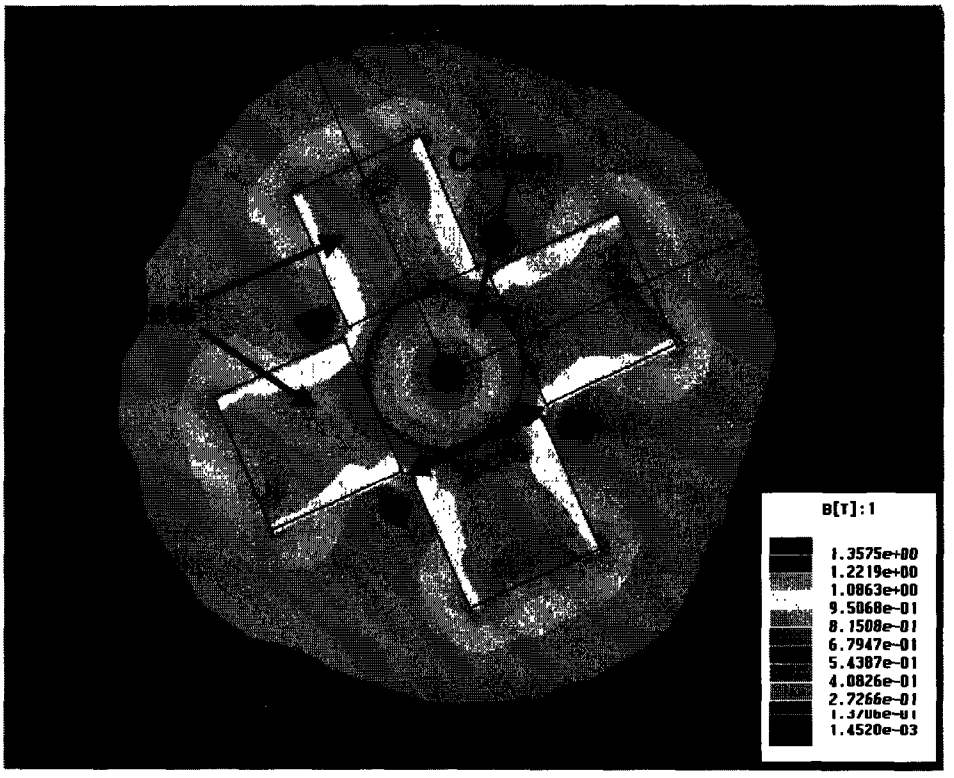

Figure 5-3. Contour plot of the magnetic flux density produced by the quadrupole orientation of the four permanent magnets. Lighter colors represent a stronger magnetic flux density. The units are in Tesla.

Since the magnetic flux density was shown by the Maxwell simulation to be radially symmetric and constant in the axial direction, the magnetic field profile could be modeled as one-dimensional, depending only on the radial distance in the quadrupole column ($H = H(r)$ only). To develop a relationship describing this one-dimensional dependence, the numerical results of the Maxwell simulation were plotted as cross sections through the center of the quadrupole column. The resultant magnetic flux density profiles along these cross sections were found to be nearly identical, and were fit to a second order polynomial function, as shown in Figure 5-4.

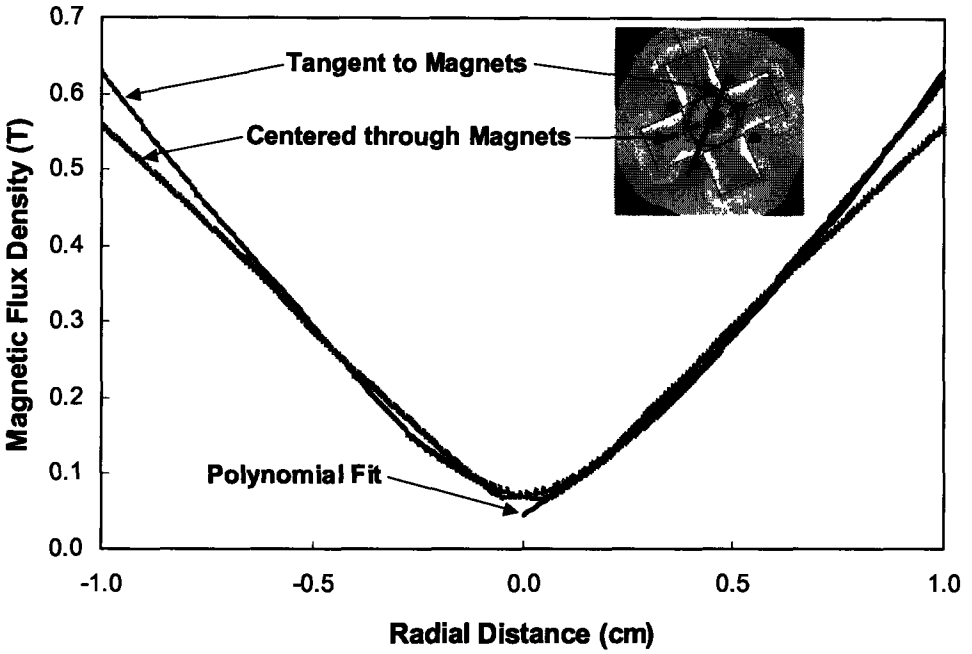

Figure 5-4. Cross sectional profiles of the magnetic flux density shown centered through the faces of the magnets and tangent to the edges of the magnets, with the polynomial fit to the magnetic flux density included in the positive r direction.

The magnetic flux density profile is almost perfectly radially symmetric, with nearly identical cross sectional profiles both centered through the faces of the magnets and tangent to the edges of the magnets, as shown in Figure 5-4. The best second order polynomial fit to the magnetic flux density profile (B) in the positive r direction is given by Equation 5-10, with units of B in Tesla:

$$B = 0.2212r^2 + 0.3662r + 0.0436 \tag{5-10}$$

where $r = 0$ corresponds to the centerline and $r = 1$ corresponds to the column wall. The magnetic field profile can then be calculated as shown in Equation 5-11:

$$H = B/\mu_o = (0.2212r^2 + 0.3662r + 0.0436)/\mu_o \tag{5-11}$$

This was the overall form of the magnetic field profile that was used with Equation 5-6 for modeling magnetophoresis in the quadrupole design. For calculating the magnetic field gradient, a parabolic fit of the magnetic field was used:

$$H = B/\mu_o = (0.5633r^2 + 0.1146)/\mu_o \tag{5-12}$$

Although Equation 5-11 provides a better fit to the magnetic field profile over the whole range from $r = 0$ to $r = 1$, the parabolic fit was necessary for calculating the magnetic

field gradient in order to ensure that the gradient approached zero at the centerline of the column.

5.4.2 Non-dimensional Quadrupole Model for Matlab

To facilitate the solution of Equation 5-6 in Matlab, the equation and its associated parameters were non-dimensionalized as follows, where the ~ symbol over the parameter indicates that it is the non-dimensional form of that parameter:

$$\tilde{C}_p = \frac{C_p}{C_{po}} \tag{5-13}$$

$$\tilde{r} = \frac{r}{R_o} \tag{5-14}$$

$$\tilde{z} = \frac{z}{L} \tag{5-15}$$

$$\tilde{v}_z = \frac{v_z}{v_{\max}} \tag{5-16}$$

$$\tilde{M} = \frac{M}{M_s} \tag{5-17}$$

$$\tilde{H} = \frac{H}{H_o} \tag{5-18}$$

where C_{po} is the initial concentration of non-magnetic particles, R_o is the full radius of the column, L is the full length of the column, v_{max} is the maximum linear velocity of the non-magnetic particles in the column, M_s is the saturation magnetization, and H_o is the maximum magnetic field applied to the system. Substituting these quantities into Equation 5-6 and rearranging yields:

$$\left(\tilde{v}_z(\tilde{r}) - \tilde{g}\right)\frac{\partial \tilde{C}_p}{\partial \tilde{z}} = \frac{1}{\tilde{r}}\frac{\partial}{\partial \tilde{r}}\tilde{r}\left(\tilde{D}\frac{\partial \tilde{C}_p}{\partial \tilde{r}} + \tilde{\Psi}^2 \tilde{C}_p \frac{\partial \tilde{C}_p}{\partial \tilde{r}} + \tilde{\beta}\,\tilde{M}(\tilde{H},\tilde{r})\frac{\partial \tilde{H}(\tilde{r})}{\partial \tilde{r}}\tilde{C}_p\right) \tag{5-19}$$

where the non-dimensional groups are defined as:

$$\tilde{D} = \frac{W_f C D_p L}{v_{\max} R_o^2 \rho} \tag{5-20}$$

$$\tilde{g} = \frac{W_f C D_p \overline{V}_p g}{v_{max} RT}\left(1 - \frac{\rho_p}{\rho}\right) \tag{5-21}$$

$$\tilde{\Psi}^2 = \frac{16\pi^2 \varepsilon \psi_o^2 R_p{}^2 \kappa^{-2}(1+2\kappa R_p) N_A^2 C_{po} W_f C L D_p}{RT\rho R_o^2 v_{max}} \tag{5-22}$$

$$\tilde{\beta} = \frac{\mu_o \overline{V}_p M_s H_o W_f C L D_p}{RT\rho R_o^2 v_{max}} \tag{5-23}$$

Equation 5-19 describes the overall equation for magnetophoresis in the quadrupole design, and was used in this form in Matlab's PDE solver, PDEPE, to solve for the concentration profile of the non-magnetic particles as they moved through the column in the quadrupole device. Table 5-2 lists the values for all the constant parameters used for solving Equation 5-19 (see Chapters 2 and 3 for more detail concerning the physical properties of both the magnetic fluid and the non-magnetic particles used in this work).

Constant Parameter	Value
μ_o	1.257 x 10^{-6} T·m/A
W_f	0.02 kg/mol
C	5.08 x 10^4 mol/m^3
ρ	1.017 x 10^3 kg/m^3
R	8.314 J/(mol·K)
T	294 K
g	9.80665 m/s^2
ρ_p	1.05 x 10^3 kg/m^3
ε	6.95 x 10^{-10} A·s/(V·m)
ψ_o	0.083 V
κ^{-1}	9.61 x 10^{-7} m
M_s	614 A/m
H_i	43500 A/m
H_o	499905 A/m
η	0.995 x 10^{-3} kg/(m·s)
R_o	0.01 m
L	0.18 m

Table 5-2. Values for the constant parameters used for solving the overall equation for magnetophoresis for the quadrupole system.

5.5 Model Results for the Quadrupole Design

Equation 5-19 was solved using Matlab's PDE solver, PDEPE, subject to the following initial and boundary conditions:

$$\widetilde{C}_p = 1 \text{ for } \widetilde{z} = 0 \text{ (all } r) \tag{5-24}$$

$$\frac{\partial \widetilde{C}_p}{\partial \widetilde{r}} = 0 \text{ for } \widetilde{r} = 0, \widetilde{r} = 1 \text{ (all } z) \tag{5-25}$$

where z = 0 refers to the feed inlet portion of the column. Thus, the axial boundary condition sets the concentration at the column inlet equal to the initial non-magnetic particle concentration for all r, and the radial boundary conditions set the concentration flux equal to zero both at the centerline of the column and at the column walls for all z. Appendix C contains the details of the Matlab code used to solve Equation 5-19.

The Matlab model for the quadrupole design was initially constructed for use as a diagnostic tool to test slightly different geometries of the quadrupole design. Although most of the overall geometry of the quadrupole device was predetermined by outside factors, such as the overall length and outer diameter of the column, the geometry of the interior of the column had not been set. Equation 5-19 was solved in Matlab to determine how the concentration profile of the non-magnetic particles was predicted to develop down the length of the column in order to determine when the concentration profile was fully developed (how far down the column) for a particle linear velocity. Based on the size and shape of the concentration profile, the dimensions of the inner cylinder that was designed to run coaxially inside the column at the outlet end (to remove the concentrated non-magnetic particles from the centerline of the column) could then be determined so the maximum amount of non-magnetic particles could be removed while minimizing the amount of bulk fluid removed from the system.

The predetermined dimensions of the quadrupole design were a column diameter of 2 cm and a column length of 20 cm, of which 18 cm was positioned directly within the four permanent magnets, which were each 18 cm long. The extra 2 cm of column length was used on the inlet side of the column to ensure that the velocity profile of the feed fluid was fully developed before entering the magnetic portion of the device. For the Matlab model, the point of zero column length (z = 0) corresponds to the entrance into

the magnetic field, which occurs 2 cm above the actual inlet of the column. Using this coordinate system, the outlet end of the column corresponds to 18 cm above the entrance to the field ($z = 18$).

The results of the Matlab model for a feed fluid composed of 1 wt% non-magnetic particles in 1 wt% magnetic fluid with a maximum linear velocity along the centerline of 31.8 cm/hr, corresponding to a flow rate of 50 mL/hr, are shown in Figure 5-5 below, using 2 μm polystyrene beads as the non-magnetic particles for the system.

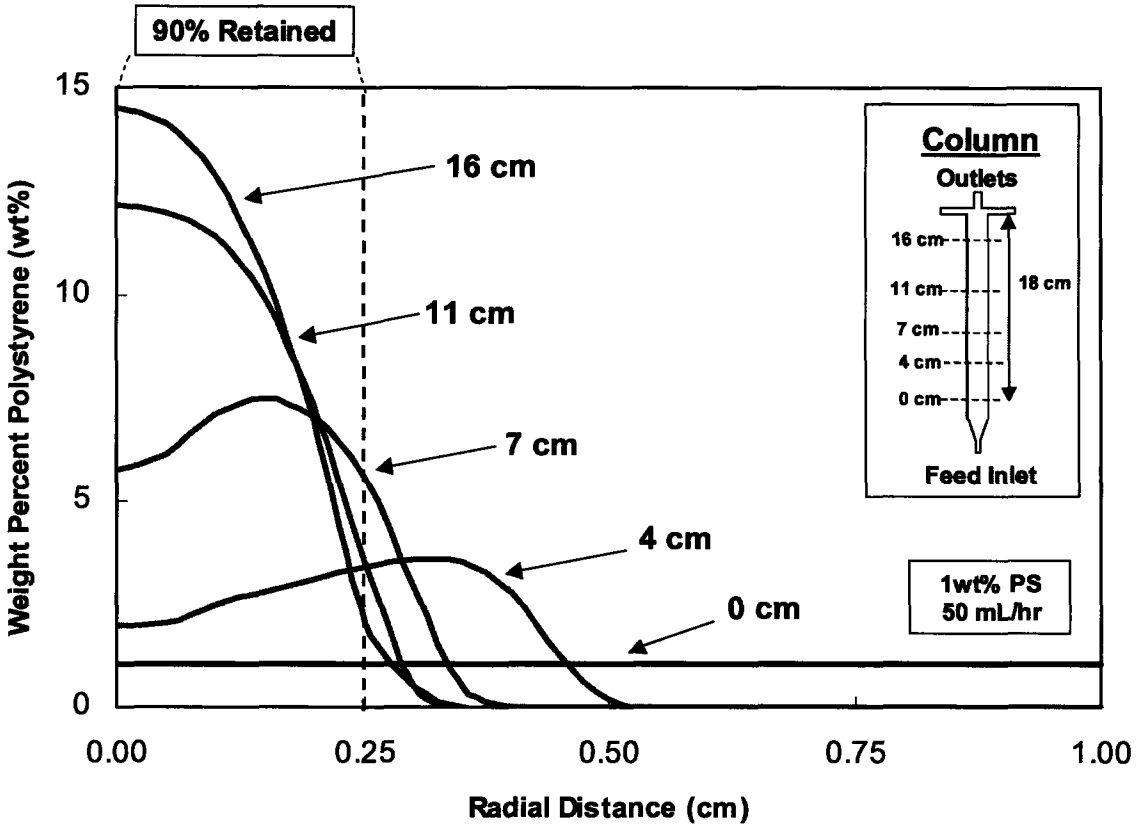

Figure 5-5. The predicted concentration profiles of 2 micron polystyrene beads at different points along the length of the quadrupole column for an initial feed concentration of 1 wt% polystyrene in 1 wt% magnetic fluid with a maximum linear velocity along the centerline of 31.8 cm/hr (50 mL/hr).

The concentration profiles for the polystyrene beads, as shown in Figure 5-5, are nearly fully developed by the time the feed reaches 16 cm up the length of the column, and the results of this simulation were used establish the inner coaxial cylinder dimensions. Since the concentration profile was predicted to be fully developed by 16 cm, the inner coaxial cylinder was designed to extend 2 cm into the column from the

outlet end. This allowed the concentrated non-magnetic particles at the center of the column to be removed from the bulk fluid at a point where their concentration was at a maximum (fully defined profile), but before the fluid hit the top wall of the cylinder, where the fluid flow profiles would be distorted. Thus, the extension of the inner coaxial cylinder into the column served to remove the concentrated non-magnetic particles while they were at their most concentrated with the minimum disruption of the flow pattern.

The Matlab model predicted that approximately 90% of the polystyrene beads would be concentrated in a area roughly 0.5 cm in diameter through the centerline of the column, where the peak of the concentration profile formed. Thus, an inner coaxial cylinder with a diameter of 0.5 cm was predicted to remove approximately 90% of the polystyrene beads from the feed while removing only 7% of the total volume of the bulk feed fluid.

The geometry of the flow column positioned inside the four magnets for the quadrupole design was therefore fully determined. The length of the column inside the magnets was 18 cm, with an extra 2 cm at the inlet to allow the velocity profile to be fully developed before the feed fluid entered the magnetic portion of the system. The overall length of the column was 20 cm, with a diameter of 2 cm. The inner coaxial cylinder at the outlet end of the column was 0.5 cm in diameter and extended 2 cm into the interior of the column to remove the maximum amount of concentrated non-magnetic particles from the centerline of the column while removing only 7% of the bulk fluid. This was the final column design that was used for experimental testing.

5.6 Summary

The overall non-dimensionalized equation governing magnetophoretic clarification using magnetic fluids was applied to the specific case of a quadrupole design. The results of the quadrupole model were used to define the final geometry of the flow column needed for the custom-built quadrupole device, with an estimated recovery rate of 90% of 2 μm sized non-magnetic particles after one pass through the system, for a feed concentration of 1 wt% particles and a feed flow rate of 50 mL/hr.

The Matlab model for the quadrupole design can be used to calculate the non-magnetic particle concentration profiles at various points down the length of the

quadrupole column for different initial feed concentrations, non-magnetic particle sizes and densities, and for different feed flow rates. Accumulation of material in the column, e.g. settling of the particles in the column, can not be taken into account by this steady state model. However, the steady state predictions are accurate for certain flow regimes in the quadrupole device where particle accumulation in the column is negligible, and a comparison between the model predictions and the experimental results is described in detail in Chapter 6 of this work.

5.7 References

1. Rosensweig, R.E., *Ferrohydrodynamics*. 1997, Mineola, NY: Dover Publications, Inc.

2. Gonzalez, L., S.E.K. Fateen, K. Smith and T.A. Hatton. "Magnetophoresis of Nonmagnetic, Submicrometer Particles in Magnetic Fluids". in *Singapore-MIT Alliance (SMA) Symposium*. 2004. Singapore.

3. Deen, W.M., *Analysis of Transport Phenomena*. 1998, New York: Oxford University Press, Inc.

4. Moeser, G.D., "Colloidal Magnetic Fluids as Extractants for Chemical Processing Applications", Ph.D. Thesis, Department of Chemical Engineering; Massachusetts Institute of Technology: Cambridge, MA, 2003.

Chapter 6

Continuous Quadrupole Magnetophoresis

6.1 Introduction

The success of the first flow configuration for magnetophoretic cell clarification, the counter current system, led to the development of a second process for exploring this new technology, a quadrupole system. The quadrupole process was designed to explore a different methodology for magnetophoretic clarification, and to allow for the continuous clarification of larger volumes of feed fluid than was feasible with the counter current system.

The quadrupole system made use of four permanent magnets arranged around a central column in such a way that the outer wall of the column experienced a strong magnetic field while the center of the column experienced a low magnetic field. Thus, non-magnetic particles traveling through the column experienced a force that pushed them towards the center of the column where the magnetic field was weakest, concentrating the particles at the centerline of the column. The concentrated particles could then be removed through a specially designed coaxial central outlet at the far end of the column.

Chapter 5 discusses the theory behind magnetophoretic clarification and describes the Matlab model that was used to develop the final design for the quadrupole system. This chapter discusses first the final quadrupole design itself, its specifications and magnetic field profile, and then discusses the results of the experiments performed with the quadrupole device and how they compare to the model predictions.

6.2 Quadrupole System

6.2.1 Magnet Assembly

The quadrupole system consisted of two major components for the separation of micron-sized non-magnetic particles from a feed mixture, the permanent magnets that

supplied the magnetic field, and the cylindrical column used to contain the feed fluid as it passed through the magnetic field. Each is discussed in detail in this section.

Four nickel-plated Neodymium Iron Boron 40 MGOe permanent magnets were arranged in a cross shape equidistant from one another, with the cylindrical column placed in the middle of the four magnets. The size of each magnet was 7.086" (18 cm) long x 0.708" (1.8 cm) wide x 0.708" (1.8 cm) thick (this last dimension was also the direction of magnetization). Due to the high magnetic field strength of the magnets, each one was glued onto a stainless steel plate, and the plates were then bolted together to form a solid, permanent housing for the four magnets. This stainless steel housing kept the magnets permanently arranged as a quadrupole while also preventing them from snapping together and breaking at such close proximity. Both the magnets and the steel housing box were manufactured by Dura Magnetics, Inc. (Sylvania, OH). A technical schematic of the magnets and the steel housing box is shown in Figures 6-1 and 6-2, and Figure 6-3 shows a picture of the completed magnet assembly manufactured by Dura Magnetics.

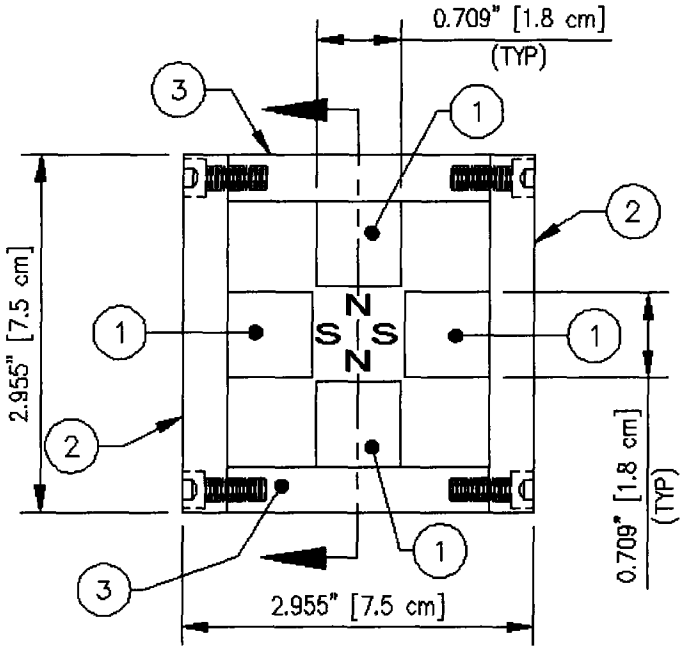

Figure 6-1. Technical schematic of the four permanent magnets and their stainless steel housing box, top view, where 1 indicates the magnets, 2 and 3 indicate the stainless steel plates needed to construct the housing box for the magnets, and N/S indicates the polarity of the magnetic field for each magnet in the finished magnet assembly.

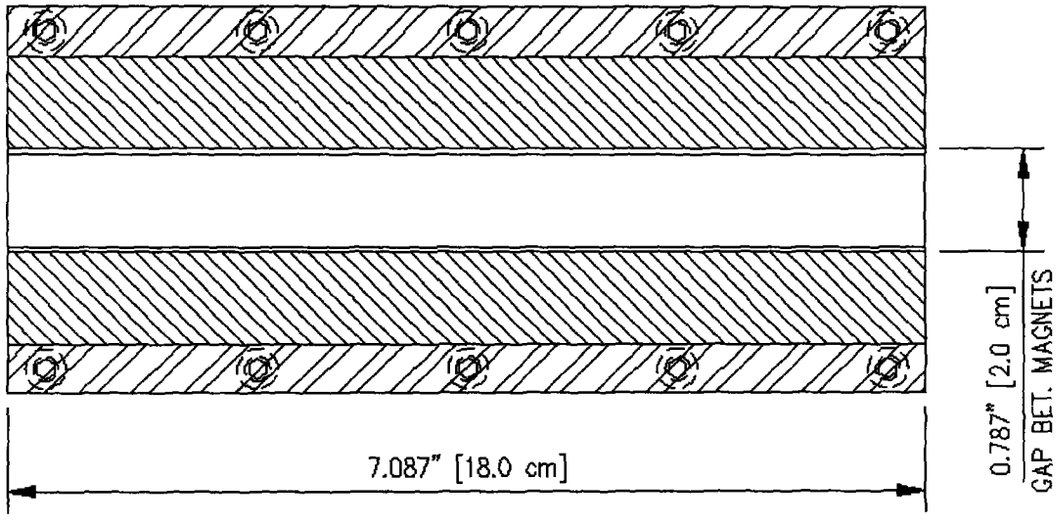

Figure 6-2. Technical schematic of the four permanent magnets and their stainless steel housing box, side view.

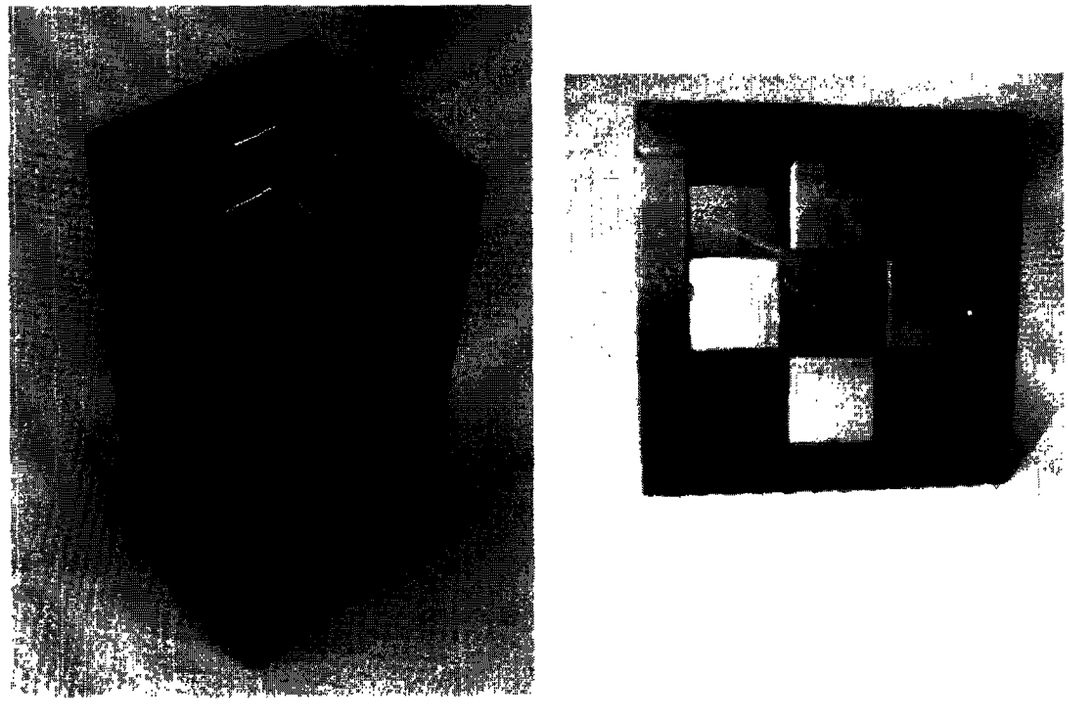

Figure 6-3. A photo of the completed magnet assembly manufactured by Dura Magnetics.

6.2.2 Magnetic Field Profile

The orientation of the four magnets shown in Figure 6-1, which is the essence of the quadrupole design, creates a radially symmetric magnetic field that is strongest next to the magnets and weakest in the center of the magnet assembly. As discussed in more detail in Chapter 5, the Maxwell 3-D Electromagnetic Field Simulator program (Ansoft Corporation) was used to model the field lines of the magnetic flux density produced by the alternating north/south, north/south orientation of the four magnets. The magnetic flux density is directly proportional to the magnetic field and differs only by the constant μ_o, the permeability of free space, under conditions where the magnetization is much less than the applied field strength ($M << H$), which is the case for the magnetic fluids used in this work. The results of the simulation for the quadrupole orientation of the magnets are given in Figure 6-4, which clearly shows that the magnetic flux density, and hence the magnetic field, is radially symmetric and constant along the length of the magnets, with the strongest field lines next to the magnets (with a magnetic flux density of 0.63 Tesla) and the weakest field in the center of the magnet assembly (with a magnetic flux density of less than 0.1 Tesla). The field gradient, or how fast the magnetic flux density decays over distance, is roughly 0.56 Tesla/cm. The simulation was performed using Neodymium Iron Boron 35 MGOe, which was the strongest permanent magnet material whose physical properties were readily available for use in the Maxwell solver, and is a slightly weaker magnetic material than the Neodymium Iron Boron 40 MGOe used to manufacture the magnets for the actual quadrupole device.

Experimental measurements of the magnetic flux density generated by the Neodymium Iron Boron 40 MGOe magnets in the quadrupole device does show a slightly stronger magnetic field than the one predicted by the Maxwell simulation using the Neodymium Iron Boron 35 MGOe magnets. The measurements show that the magnetic flux density is radially symmetrical and constant along the length of the magnets, as expected, with the strongest field lines next to the magnets at a magnetic flux density of approximately 0.73 Tesla, and the weakest field in the center of the magnet assembly, with a magnetic flux density of less than 0.1 Tesla. Using these measurements, the field gradient was calculated to be 0.62 Tesla/cm. Thus, the Neodymium Iron

Boron 40 MGOe permanent magnets are both slightly stronger than the magnets used for the simulation and have a slightly higher field gradient.

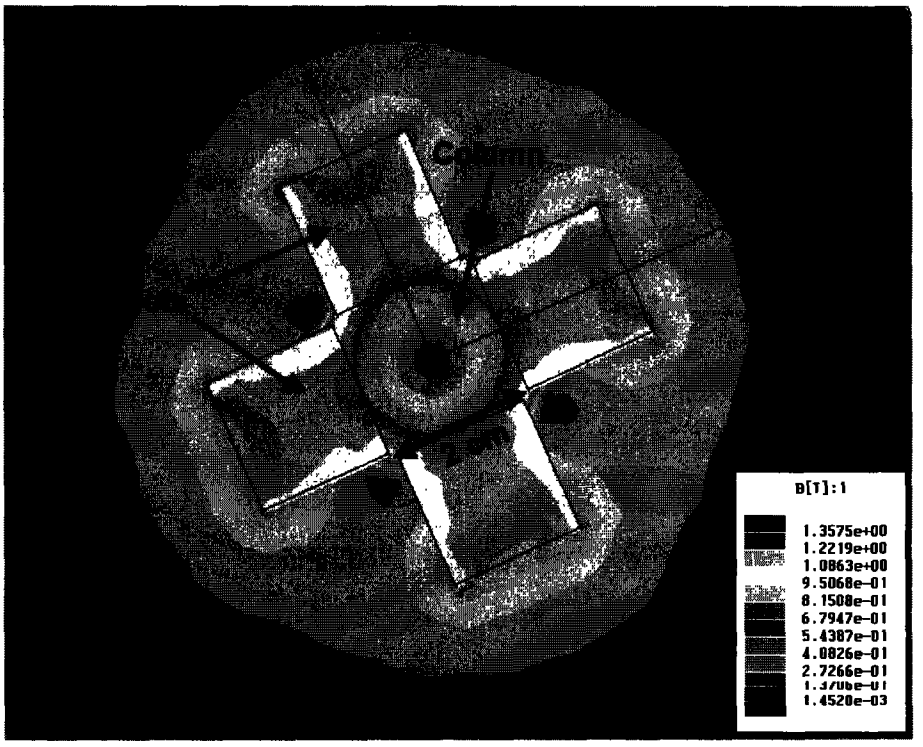

Figure 6-4. Contour plot of the magnetic flux density produced by the quadrupole orientation of the four permanent magnets. Lighter colors represent a stronger magnetic flux density. The units are in Tesla.

6.2.3 Cylindrical Column

The cylindrical column was constructed to fit inside the magnet assembly so that the feed fluid could be pumped through the magnetic field created by the quadrupole magnets without actually contacting the magnets directly. Since the magnetic field is weakest in the center of the magnet assembly, the micron-sized non-magnetic particles in the feed are forced by the magnetization of the surrounding magnetic fluid to move to the center of the column, once the column is placed inside the magnet assembly. The column was therefore designed with a coaxial inner cylindrical tube located near the outlet end of the column, from which the concentrated non-magnetic particles could be collected and removed from the bulk fluid.

The column itself was constructed out of aluminum. Other construction materials, such as steel and various plastics, were also available, but aluminum provided the ideal choice of material for the column. Unlike steel, aluminum is non-magnetic, and the insertion of an aluminum column into the magnet assembly does not distort the magnetic field produced by the magnets. Although plastic is also non-magnetic, aluminum is rigid and fairly easy to machine down to very thin wall thicknesses, so the final column could be constructed with walls as thin as 0.5 mm while still maintaining rigidity. Such thin walls were not possible with the plastic materials available for constructing the column. Thin column walls were extremely important for the coaxial inner tube, as thinner walls have less of an effect on flow patterns in the column than thicker walls do, and any distortions in the fluid flow would interfere with the separation of the non-magnetic particles as they are pushed towards the centerline of the column.

A technical schematic of the aluminum column is given in Figure 6-5, which shows that the coaxial inner cylinder extends 2 cm into the column and has an inner diameter of 0.5 cm. The extension of the coaxial inner tube into the column allows the concentrated non-magnetic particles at the center of the column to be removed from the bulk fluid before the fluid hits the top wall of the column, where the fluid flow profiles would be distorted. Thus, the extension of the inner cylinder into the column serves to remove the concentrated non-magnetic particles while they are still in their fully formed flow profile.

An inner diameter of 0.5 cm for the coaxial inner tube was chosen based on the results of the Matlab model for the quadrupole system (see Chapter 5 for more detail), which predicted that 90% of the non-magnetic particles would be concentrated in an area roughly 0.5 cm in diameter through the centerline of the column. Thus, a coaxial inner cylinder with a diameter of 0.5 cm should remove approximately 90% of the non-magnetic particles from the feed while removing only 7% of the total volume of the bulk feed fluid.

The schematic given in Figure 6-5 also shows the inlet end of the cylindrical column as a tapered aluminum cone that then connects to the main body of the column. Flexible tubing was connected to the tapered end, and the feed mixture was introduced into the column through this tubing. The cone shape was chosen to lessen entrance

effects as the feed entered the column. Flexible tubing was also connected to the three outlets present at the opposite end of the tube, and the outlet streams exited the column through these tubes.

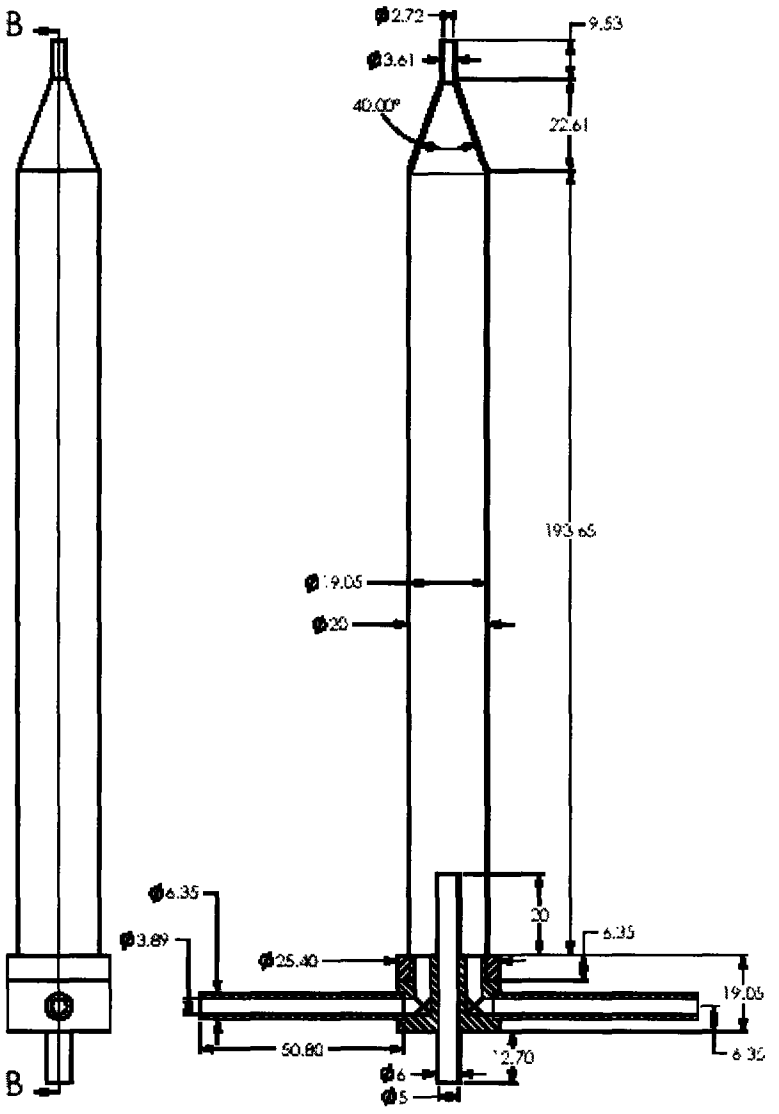

Figure 6-5. Technical schematic of the aluminum column used with the magnet assembly, shown at two different side views, each at 90 degrees to one another. The units are in millimeters.

Figure 6-6 shows a picture of the completed aluminum column, and Figure 6-7 shows a picture of the column sitting in the magnet assembly, exactly as it appears for performing the magnetophoretic clarification experiments. The feed was pumped

through the device against the flow of gravity in all cases, with the feed inlet always positioned on the bottom and the outlets always positioned at the top.

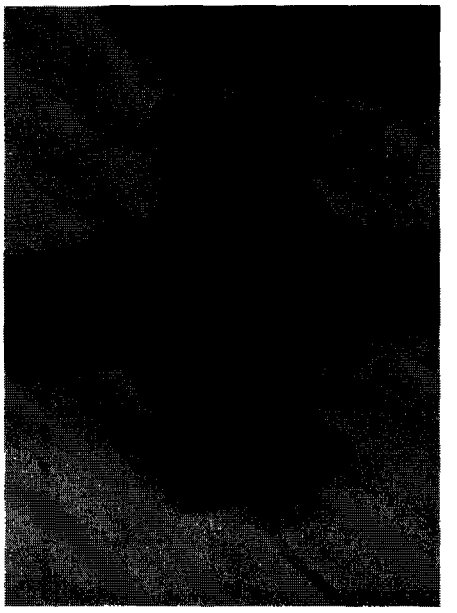

Figure 6-6. Completed aluminum column with tubing shown attached. The body of the column is uniform in diameter, not tapered as the reflected light on the column body makes it appear in the photograph.

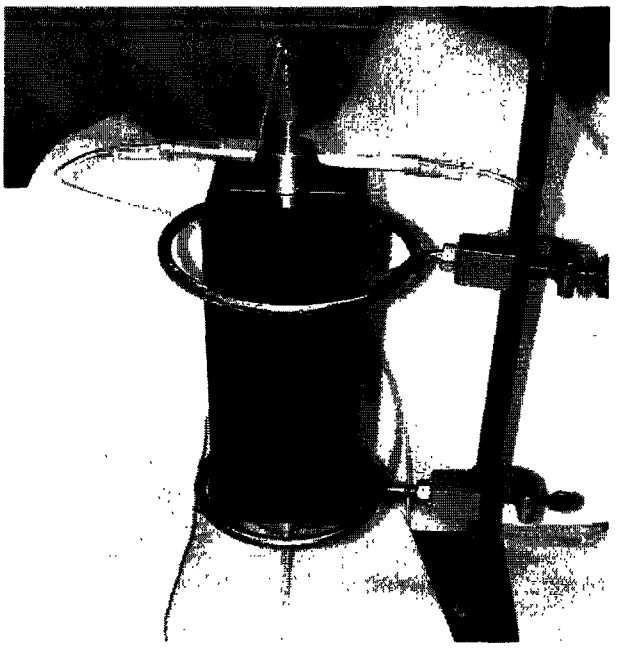

Figure 6-7. Aluminum column sitting in the magnet assembly in the orientation used for all experiments, with the feed flow directed against gravity.

6.2.4 Completed Quadrupole System

The separation components of the quadrupole system consisted of the permanent magnets in their steel magnetic housing assembly and the aluminum column used to pass the feed fluid through the magnetic field provided by the magnets. The entire quadrupole system consisted of these two separation components, a peristaltic pump used to pump the feed mixture through the column, clear PVC tubing used for the inlet feed and for the three outlets, and three needle valves used to regulate the flow rate of the fluid exiting through the three outlets.

The peristaltic pump used was a VWR Low Flow Variable Flow Mini-Pump, with a maximum pumping capacity of 75 mL/hr. The tubing used for the inlet to the column was flexible Nalgene 180 Clear PVC Tubing, 2/16" (3.17 mm) ID, 3/16" (4.76 mm) OD, with 69.1 cm of tubing used. Two tubing sizes were used for the outlets. Approximately 3 cm of Nalgene 180 Clear PVC Tubing, 3/16" (4.76 mm) ID, 5/16" (7.94 mm) OD, was connected directly to the outlets. In order to minimize the volume of fluid in the tubing and reduce the total entrained volume of the system, Nalgene 180 Clear PVC Tubing, 2/16" (3.17 mm) ID, 3/16" (4.76 mm) OD, was then glued to the inside of the 3/16" (4.76 mm) ID tubing. The two tubing sizes nested into each other almost perfectly, and clear RTV silicone glue was used at the junction to ensure a watertight seal.

The concentrations measured from the two side outlets represented the concentration of the bulk, clarified feed, and these concentrations were always averaged to obtain a consistent overall concentration from the column that was independent of slight variations in the outlet tubing lengths and orientations. The concentrations measured from the central outlet, which contained the concentrated non-magnetic particles removed using the coaxial inner tube in the column, were not averaged or altered in any way.

In order to accurately control the flow rate of the fluid exiting each of the three outlets, stainless steel Swagelok needle valves were installed approximately at the midpoints of the tubing that was connected to each outlet. The valves allowed for precise regulation of the flow rates exiting each outlet.

Figure 6-8 shows a picture of the complete quadrupole system taken during an experiment involving the separation of 2 μm polystyrene beads, and includes the

peristaltic pump, the tubing, and the valves. With the addition of the tubing to the system, the total entrained volume for the entire device was 79.0 mL.

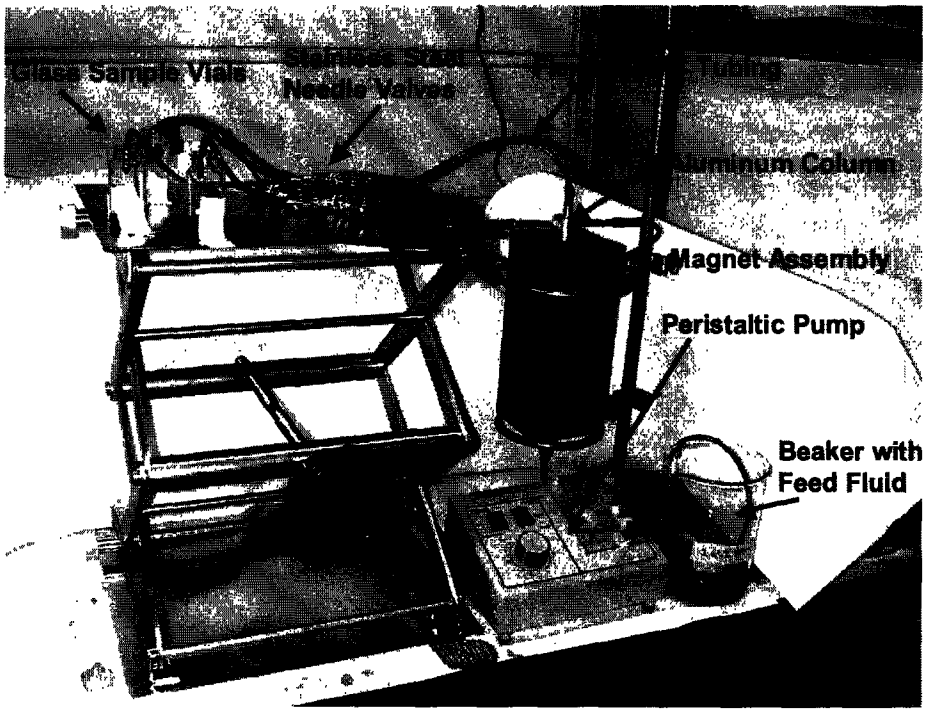

Figure 6-8. The complete quadrupole system, including the magnet assembly, the aluminum column, the peristaltic pump, the tubing, and the valves. A beaker used to hold the feed and glass vials used to collect the samples from the outlets are also shown.

6.3 Quadrupole Experiments

6.3.1 Experimental Procedure

The experimental procedure used for the quadrupole system was the same for all experiments performed. Two batches of fluid were prepared, the feed fluid itself (with a typical feed fluid volume of 160 mL) and the initial column fluid (typically 80 mL, the entrained volume of the device). The initial column fluid contained the same concentration of magnetic fluid as the feed but without the non-magnetic particles. The pH of each fluid was measured and recorded. The aluminum column and all tubing in the device were then quickly filled by hand with the initial column fluid, using a syringe attached to the inlet feed tube.

Once the entire system was full of magnetic fluid of the same concentration as the feed, the syringe was removed from the inlet feed tube, and the tube was place in the beaker containing the feed fluid. The peristaltic pump was turned on at a specified feed flow rate, and the needle valves attached to the outlets were adjusted so that 20% of the feed fluid exited from the central outlet and the remaining 80% of the feed exited through the two side outlets, 40% through each outlet. Although the coaxial inner tube that corresponds to the central outlet had a cross sectional area that was only 7% of the total cross sectional area of the column, a removal rate of 20% of the volumetric flow rate of the feed was selected to ensure that all concentrated non-magnetic particles would be removed, as an initial check of the separation capability of the quadrupole system. The flow patterns associated with this choice of flow rate for the central outlet are shown schematically in Figure 6-9. The feed was also pumped through the device against the flow of gravity in all cases, with the feed inlet always positioned on the bottom and the outlets always positioned at the top. This configuration allowed for more efficient removal of the non-magnetic particles than if the feed were pumped in the same direction as the gravitational force.

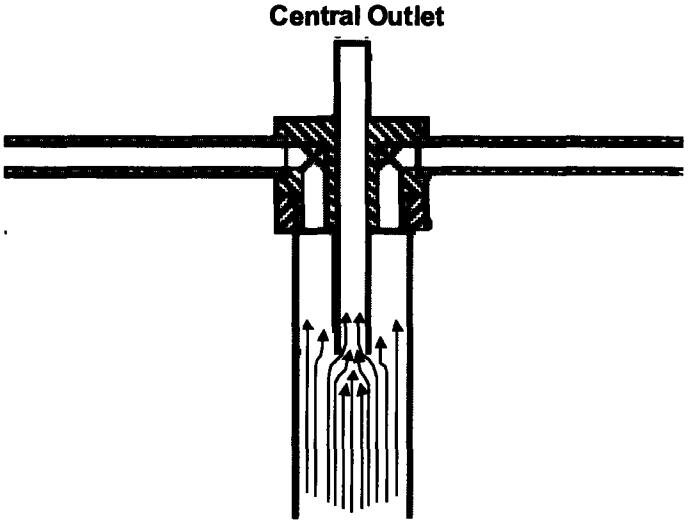

Figure 6-9. Flow pattern in the quadrupole column associated with a 20% flow rate for the central outlet.

The feed fluid in the beaker was stirred at regular intervals to prevent settling of the non-magnetic particles during the experiments. The fluid exiting the quadrupole

device through each outlet was collected in glass sample vials and analyzed using UV-Vis spectrophotometry to determine the concentration of the non-magnetic particles in the outlet streams. At the end of the experiments, the aluminum column was removed from the magnet assembly and drained, and UV-Vis spectrophotometry was used to determine the concentration of the non-magnetic particles retained in the device.

6.3.2 Experiments with Polystyrene Beads

Experiments using the quadrupole system were first performed using polystyrene (PS) beads as a model system. The beads, obtained from Spherotech, Inc. (Libertyville, IL), were spherical in shape with diameters of 2.01 ± 0.05 μm and 1.17 ± 0.029 μm. The beads each arrived as a suspension of 5.0 wt% ± 0.2 wt% beads in deionized water with 0.02% sodium azide added as bacteriostatic, and were used as received. The beads were negatively charged due to the presence of sulfate groups on their surface, and zeta potential measurements in 0.01 M NaCl (ionic strength 0.01 M) at a pH of 6.7 yielded an average zeta potential value of -104 ± 3 mV.

6.3.2.1 Analytical Measurements

The concentration of polystyrene beads in the samples collected during the experiments was determined by measuring the absorbance (i.e. the optical density, or OD) of the samples at 600 nm using a Hewlett Packard UV-Visible Spectrophotometer (Model 8463). Since the optical density measurements at 600 nm can be correlated with the optical density for known polystyrene concentrations (the correlation has been shown to be linear, see Chapter 3 of this work), the concentration of the polystyrene beads in the sample fluids can be calculated using this correlation.

The magnetic nanoparticles in magnetic fluid also show absorbance at 600 nm, in addition to the absorbance observed from the polystyrene beads, and the two spectra are additive. The polystyrene concentration in the samples collected during experiments was therefore determined by first performing an initial measurement at 600 nm on a diluted solution of the experimental sample. A typical dilution was 0.05 mL sample in 10 mL deionized water. This measured absorbance provided the OD_{600} value for the total mixture of both polystyrene and magnetic fluid. The diluted solution used for this initial

measurement was then centrifuged at 4000 rpm for 40 minutes. This procedure sedimented only the polystyrene, since the magnetic nanoparticles that make up magnetic fluid are not affected significantly by centrifugation. The absorbance of the magnetic fluid supernatant at 600 nm was measured, and the difference between the total optical density of the full mixture and the optical density of just the magnetic fluid supernatant yielded the optical density of the polystyrene alone. Once the optical density was known for just the polystyrene, the polystyrene concentration was calculated using the previously determined OD_{600} correlation.

6.3.2.2 Control Experiments

The quadrupole process was first tested for its flow and magnetic properties to ensure that the physical system itself behaved as expected and introduced no anomalies during the separation process. Experiments were therefore performed using non-magnetic particles in the absence of magnetic fluid, to test the flow properties of the system alone, and magnetic fluid in the absence of non-magnetic particles, to test the magnetic properties of the system alone.

6.3.2.2.1 Polystyrene in Water

A control experiment was performed with the quadrupole system in which the feed consisted of 160 mL of 1 wt% polystyrene in water, with no magnetic fluid added. This experiment was performed to determine if the polystyrene would be evenly distributed throughout the quadrupole system in the absence of the magnetic force caused by the presence of the magnetic nanoparticles. The size of the polystyrene beads used was 2.0 μm.

The quadrupole column and all tubing were filled with deionized water, after which 160 mL of 1 wt% polystyrene were pumped through the column at a flow rate of 44 mL/hr. The effluent exiting the top of the system from the three outlet streams was collected and analyzed using UV-Vis spectrophotometry to determine the concentration of polystyrene in the outlet streams. The results are shown in Figure 6-10, and the concentration of polystyrene was found to be approximately the same in each outlet for the control experiment. At steady state, the inlet feed concentration was 9.8 ± 0.4 mg

PS/mL, the central collection outlet concentration was 9.8 ± 0.4 mg PS/mL, and the two side outlets had an average concentration of 9.7 ± 0.4 mg PS/mL. This was exactly the result that was expected, as no increase in concentration of the polystyrene beads was observed at the center of the column. There was also very little retention of polystyrene in the column during the experiment, with less than 3% of the polystyrene in the feed being retained in the device at the conclusion of the experiment. The overall material balance for the system also closed to within 5%, indicating that the analytical techniques used to determine the concentration of the polystyrene in the feed and fluid samples were accurate.

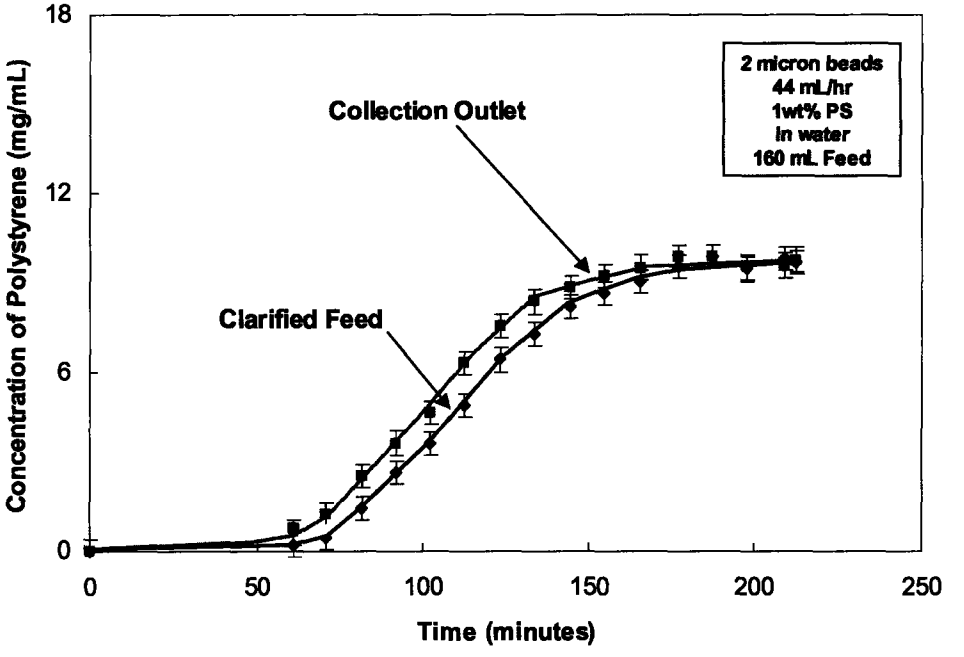

Figure 6-10. Concentration profile of the polystyrene content in the quadrupole outlets for a control experiment using 160 mL of 1 wt% polystyrene as the feed with no magnetic fluid present in the system. Clarified Feed represents the average concentration of the polystyrene collected at specific time intervals from the two side outlet streams, and Collection Outlet represents the polystyrene concentration collected at specific time intervals from the central outlet stream.

Figure 6-10 shows that breakthrough of the polystyrene occurred at roughly 55 minutes and steady state concentration was achieved at approximately 160 minutes, as anticipated for a feed flow rate of approximately 44 mL/hr though a total device volume of 80 mL. Breakthrough of the polystyrene also occurred first through the central outlet

(or collection outlet), which was also expected since the centerline of the column contains the fastest moving particles for a parabolic velocity profile. Thus, the quadrupole system was shown to function perfectly well on a physical flow level, and the analysis procedures for polystyrene content were also shown to be accurate.

6.3.2.2.2 Magnetic Fluid Alone

Control experiments were conducted to test the magnetic properties of the system and determine how the strong magnetic field in the device affects the magnetic fluid itself, in the absence of non-magnetic particles.

The quadrupole column and all tubing were filled with 1 wt% magnetic fluid (MF), after which 150 mL of 1 wt% magnetic fluid were pumped through the column at a flow rate of 61 mL/hr. The effluent exiting the top of the system from the three outlet streams was collected and analyzed using colorimetric iron analysis and dynamic light scattering (DLS) to determine the concentration of magnetite in the fluid and the size of the magnetic nanoparticles in the outlet streams (see Chapter 2 of this work for more details about colorimetric iron analysis and dynamic light scattering). The results are given in Figure 6-11, which shows that the concentration of magnetic fluid, defined as the concentration of magnetite in the fluid, increases in the column as the magnetic fluid feed is pumped through the device. For this experiment, 1.1 wt% ± 0.04 wt% MF entered the column, 0.95 wt% ± 0.04 wt% MF exited through the central outlet, and an average of 1.0 wt% ± 0.04 wt% MF exited through the two side outlets. Statistically, the outlet concentrations were all the same at approximately 1.0 wt%. These concentrations occurred immediately at the start of the experiment and remained steady for the duration. There was no breakthrough curve of any sort for the magnetic fluid concentration, indicating that the magnetic force inside the column immediately acted to retain approximately 10% of the magnetic nanoparticles as they entered the device.

Dynamic light scattering analysis showed that the particles retained in the column by the magnetic field were all the larger-sized nanoparticles. As discussed in more detail in Chapter 2 of this work, magnetic fluid is composed of magnetic nanoparticles with an average hydrodynamic diameter of 31.6 nm ± 0.09 nm, but less than 1% of the particles on a number basis have a diameter greater than 60 nm. On a volume basis, and thus also

on a weight basis, magnetic nanoparticles greater than 60 nm make up roughly 10% of the particles. The volume-average distribution differs from the number-average distribution in that each particle is weighted according to its size, with larger particles weighted more. This skews the average particle size towards higher values, but it also helps to uncover the presence of larger magnetic particles that exist in such low concentrations as to be inconsequential in the number-average distribution. It is these larger particles that are being retained in the column in the quadrupole system, as demonstrated by the statistically higher particle size of the retained fluid (39.8 nm ± 2.3 nm versus 32.1 nm ± 0.8 nm in the feed) and the statistically lower nanoparticle size of the fluid exiting the device (27.3 nm ± 1.8 nm in the two side outlets and 25.6 nm ± 0.8 nm in the central outlet versus 32.1 nm ± 0.8 nm in the feed).

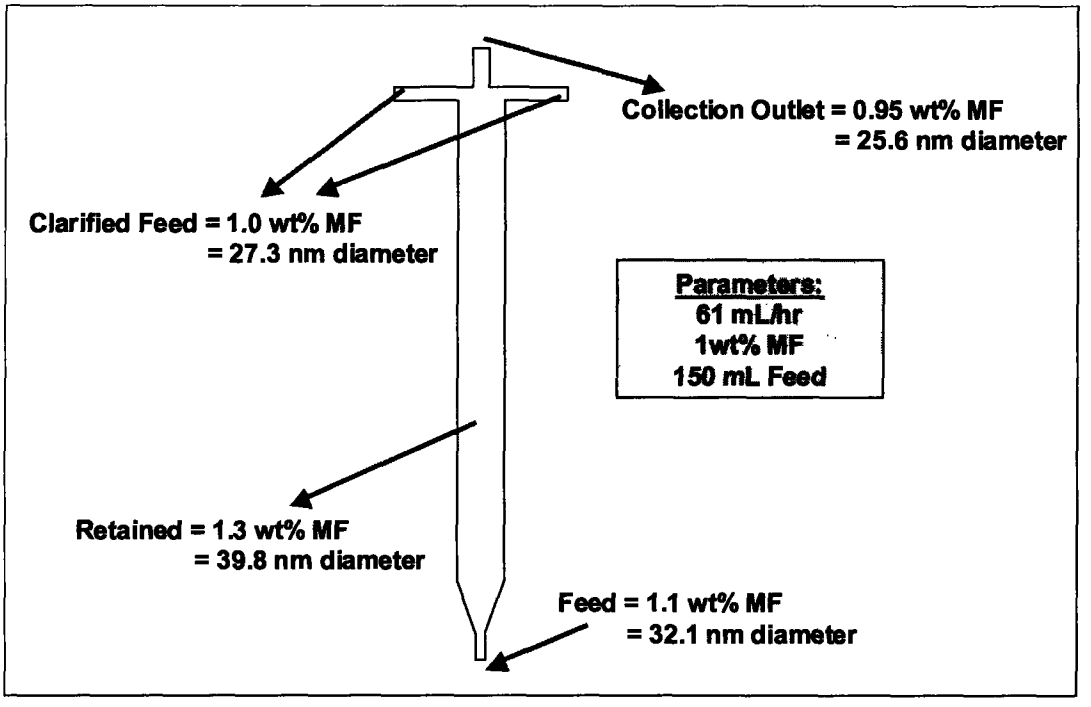

Figure 6-11. Results for the control experiment using 150 mL of 1 wt% magnetic fluid as the feed, with 1 wt% magnetic fluid present in the device at the start of the experiment. Clarified Feed represents the average magnetite concentration and nanoparticle size collected from the two side outlet streams, Collection Outlet represents the magnetite concentration and nanoparticle size collected from the central outlet stream, Feed represents the magnetite concentration and nanoparticle size of the feed fluid, and Retained represents the magnetite concentration and nanoparticle size of the fluid retained in the column at the end of the experiment.

The retention of the larger particles in the column can be seen more clearly by looking at the volume-average distribution of magnetic particle size. The volume-average distributions for the feed, the outlets, and the fluid retained in the column at the end of the experiment are given in Figure 6-12, which clearly shows how the smaller particles are eluted and the larger ones are retained in the column.

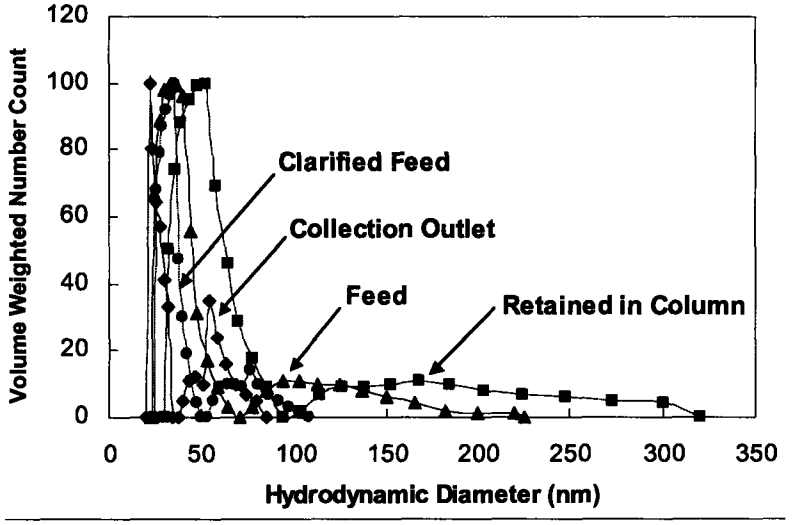

(a)

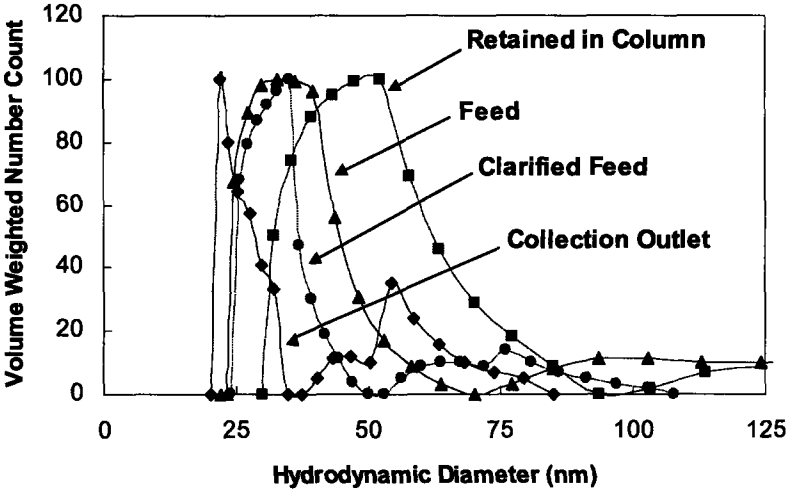

(b)

Figure 6-12. The volume-average distribution of the hydrodynamic diameter of magnetic particles in the feed, the outlets, and the fluid retained in the column at the end of the control experiment. Feed represents the feed fluid, Clarified Feed represents the fluid collected from the two side outlet streams, Collection Outlet represents the fluid collected from the central outlet stream, and Retained in Column represents the fluid retained in the device at the end of the experiment, with (a) depicting the full curves and (b) showing a close up of the front half of the curves to show detail.

For the feed itself, roughly 10% of the particles by volume are larger than 60 nm, and approximately 6% are larger than 100 nm. For the clarified feed outlet (the two side outlets), roughly 8% of the particles by volume are larger than 60 nm, while only 2% are larger than 100 nm. Similarly, for the collection outlet (the central outlet), roughly 4% of the particles by volume are larger than 60 nm, and there are no particles present greater than 80 nm. However, for the retained fluid, approximately 20% of the particles are larger than 60 nm, with 11% by volume larger than 100 nm. This clearly shows that the larger magnetic particles in the feed fluid are being retained in the column. The retention of 20 vol% of particles larger than 60 nm is therefore expected, since the amount of feed fluid passed through the column was twice the working volume of the system, so twice the concentration of large particles in the feed should be retained.

The larger particles are retained because they represent aggregates of two or more single particles (those less than 60 nm in diameter) and therefore have a larger combined size for the magnetite core than do the single particles. This larger effective core size results in a stronger magnetic force attracting these particles to areas of high magnetic field in the system. Thus, the larger nanoparticles move towards the outer walls of the column towards the magnets, where they are retained by the strong magnetic field, while the smaller magnetic particles are left at the center of the column where the magnetic field is weakest.

The results of this control experiment demonstrate that the strength of the permanent magnets in the quadrupole device is sufficient to retain approximately 10 vol% of the magnetic particles that enter the device. This results in a higher concentration of magnetic fluid in the column, particularly near the column walls next to the magnets. This in turn helps to more efficiently push any non-magnetic particles in the column away from the walls, slightly enhancing the separation capability of the quadrupole process.

6.3.2.3 Polystyrene and Magnetic Fluid Experiments

Experiments using feed mixtures of magnetic fluid and non-magnetic 2 μm polystyrene beads showed that, in general, the quadrupole system operated according to expectations. Depending on flow conditions, the outlet streams exiting the device were

of significantly different concentrations, with one of the streams being essentially clarified and the other containing a concentrated amount of the polystyrene particles.

The quadrupole column and all tubing were filled with 1 wt% magnetic fluid, after which 160 mL of 1 wt% polystyrene (2 μm) and 1 wt% magnetic fluid were pumped through the column at a flow rate of 50 mL/hr. The effluent exiting the top of the system from the three outlet streams was collected and analyzed using UV-Vis spectrophotometry to determine the concentration of polystyrene in each outlet stream. The results are given in Figure 6-13, which shows that the polystyrene was effectively removed from the feed through the central outlet. The overall material balance for the system closed to within 5% for this experiment.

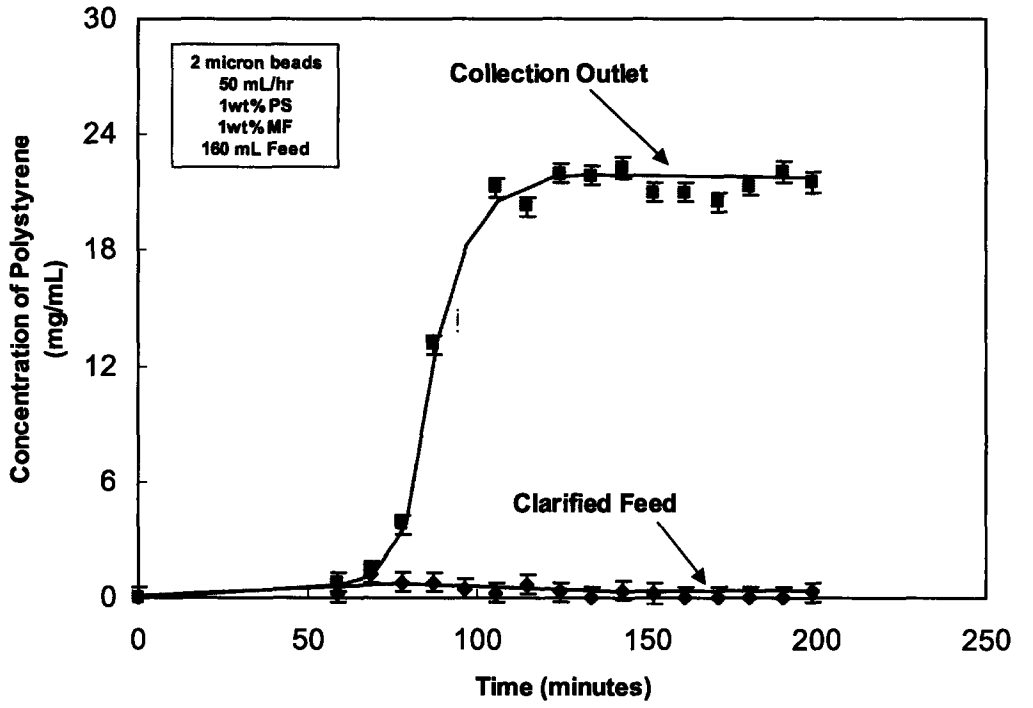

Figure 6-13. Concentration profile of the polystyrene content in the quadrupole outlets for 2 micron polystyrene beads using 160 mL of 1 wt% polystyrene and 1 wt% magnetic fluid as the feed with 1 wt% magnetic fluid present in the system. Clarified Feed represents the average concentration of the polystyrene collected at specific time intervals from the two side outlet streams, and Collection Outlet represents the polystyrene concentration collected at specific time intervals from the central outlet stream.

The inlet feed concentration for the experiment was 9.6 ± 0.4 mg PS/mL, the central collection outlet concentration was 21.5 ± 0.9 mg PS/mL, and the two side outlets had an average concentration of 0.3 ± 0.1 mg PS/mL. Additionally, at a flow rate of 50

mL/hr, the average residence time of the polystyrene in the system should be approximately 100 minutes, with initial breakthrough expected at 50 minutes for a parabolic velocity profile ($Re << 1$ for the device). This is essentially the behavior shown in Figure 6-13, and in this case the polystyrene exited the column fairly sharply, indicating a buildup in polystyrene concentration as the beads traveled through the column. However, although the collection stream exiting the column was concentrated in polystyrene and the other effluent stream was essentially completely clarified, only approximately 40 percent of the polystyrene particles fed to the device were recovered in the outlets. The remainder of the polystyrene was retained in the system.

The significant retention of the polystyrene beads in the column was not the result of settling due to gravitational, or buoyancy, forces on the polystyrene beads. The theoretical settling velocity of the 2 μm beads, given by the terminal velocity of the beads as they settle in the magnetic fluid, was calculated using Equation 6-1[1]:

$$v_{settling} = \frac{2R_p^2 g(\rho_{part} - \rho_{fluid})}{9\eta} \tag{6-1}$$

where R_p is the radius of the beads, g is the gravitational constant, ρ_{part} is the density of the beads, ρ_{fluid} is the density of the surrounding fluid, and η is the viscosity of the magnetic fluid and polystyrene mixture. For the 2 μm polystyrene beads, the theoretical settling velocity in magnetic fluid is 0.031 cm/hr, which is in good agreement with the experimentally determined settling velocity of 0.037 ± 0.001 cm/hr, as measured by tracking the movement of the settling planes in columns filled with different concentrations of the polystyrene beads. This settling velocity is orders of magnitude smaller than the typical linear velocities used in this work, which were on the order of 20 cm/hr, and indicate that gravitational settling was not the cause of the retention of the beads within the device. Instead, the force acting on the polystyrene beads that causes the retention in the column appears to be magnetic in origin.

The same magnetic force that succeeds in separating the non-magnetic particles once they are in the device also acts as a barrier force against entry into the magnetic portion of the system. When the feed is first pumped into the column, it travels up through the cone at the inlet and then along 2 cm of the column length before reaching the magnet assembly, as shown in Figure 6-14. Although the magnetic field inside the

magnet assembly itself is radially symmetric and does not change along the length of the column, this is not true at the entrance to the assembly, where the magnetic field wraps around the long ends of the magnets. The resulting axial magnetic field gradients at the magnet edges cause end effects in which the downward magnetic force overcomes the upward drag force at certain radial positions in the column, which prevents the non-magnetic particles from entering the magnetized zones within the device, and so the axial magnetic field gradients provide a barrier to particle entry. The particles will migrate inwards towards the column centerline, however, owing to the radial components of the field gradient at these points within the column, and should eventually end up at a radial position where the drag force is sufficient to overcome the axial magnetic force, and the particle is able to enter the column. This upstream buildup of particles due to the axial magnetic gradient at the entrance to the magnet assembly in the device is most likely responsible for the retention of the particles observed within the column over the course of a run.

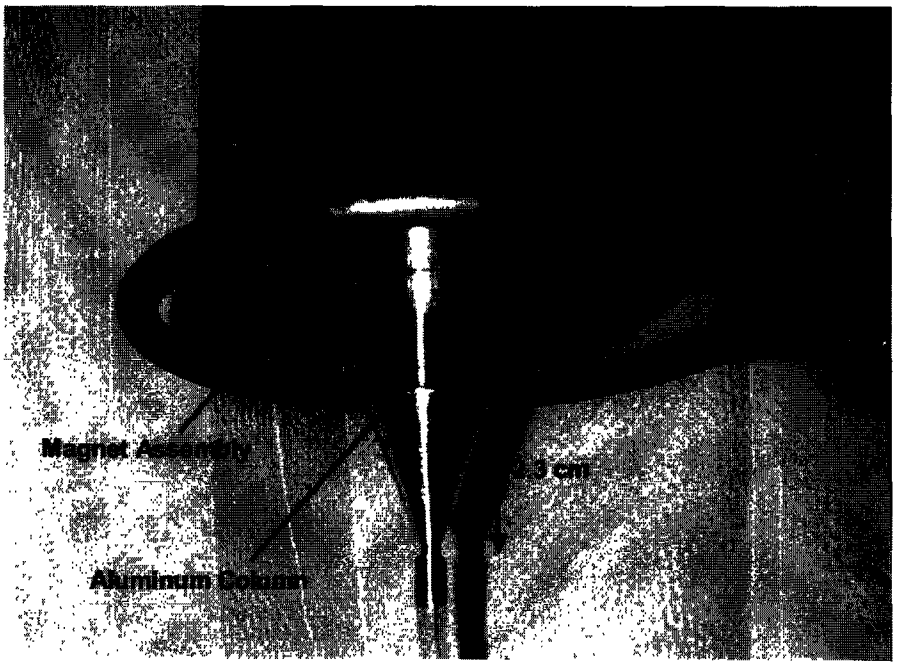

Figure 6-14. Close up of the inlet section of the aluminum column in the magnet assembly.

The magnetic barrier force can be quantified by modeling the axial and radial dependence of the magnetic field in the column at the entrance to the magnet assembly.

Using the Maxwell 3-D Electromagnetic Field Simulator program (Ansoft Corporation), the magnetic flux density at the entrance to the magnet assembly was modeled for the quadrupole geometry. Figure 6-15 shows a contour plot of the magnetic flux density established by the magnets at the entrance region into the magnet assembly, and the resultant axial field lines at the entrance are shown in Figure 6-16. The simulation results, which were confirmed experimentally using a Gauss/Tesla meter, show a very sharp axial magnetic field gradient that occurs at the magnet edges and extends a quarter centimeter both into and out of the column, centered at the magnet edges. This sharp field gradient is strongest near the column walls and weakest at the column centerline, with the magnetic field degrading linearly along the radial axis. This axial magnetic field gradient is in addition to the expected radial magnetic field gradient established by the quadrupole orientation of the magnets.

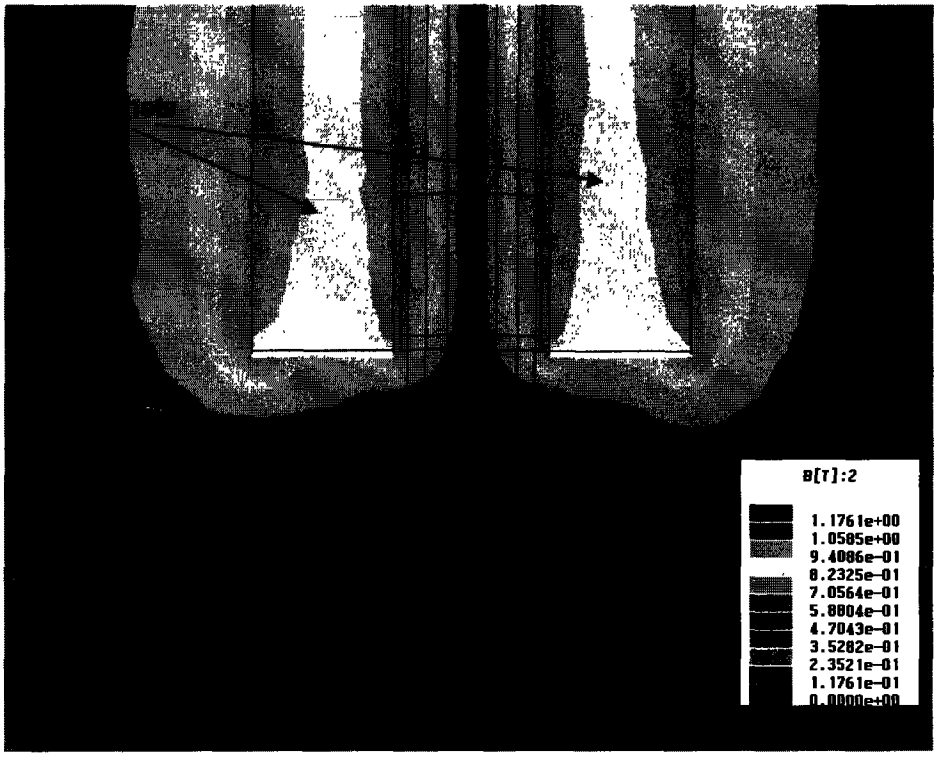

Figure 6-15. Contour plot showing the magnetic flux density (B) along an axial cross section of the quadrupole column and magnets. The axial magnetic flux density gradient extends approximately a quarter centimeter on either side of the magnet edges through the column. The units are in Tesla.

The axial field lines were used to estimate the magnetic barrier force via Equation 6-2:

$$F_m = \mu_o V_p M \nabla H \quad \text{where} \quad M = \frac{M_s}{H_t + H} H \tag{6-2}$$

where μ_o is the permeability of free space, V_p is the volume of the non-magnetic particles, M is the magnetization of the magnetic fluid, ∇H is the magnetic field gradient, M_s is the saturation magnetization of the magnetic fluid at high magnetic field strengths, H is the magnetic field, and H_t is the magnetic field strength at which the magnetization of the magnetic fluid is half the saturation magnetization (see Chapter 5 for a more detailed discussion of the magnetization of magnetic fluid). The magnetic force is constant for constant non-magnetic particle size and constant magnetic fluid concentration.

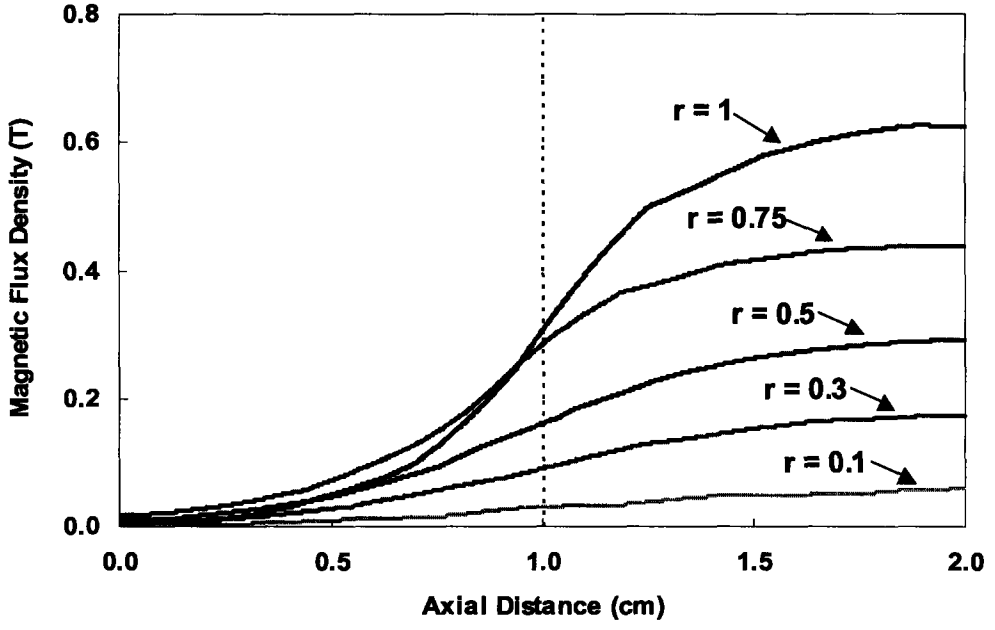

Figure 6-16. Axial field lines for the magnetic flux density at different points along the radius of the column, with r = 1 corresponding to the column walls and r = 0 corresponding to the column centerline. The dashed line at an axial distance of 1 cm corresponds to the edges of the magnets, or the entrance into the magnet assembly.

A force balance on the non-magnetic particles at various locations in the entrance region to the magnet assembly was used to determine the trajectories of the non-magnetic particles as they entered the column and flowed through the device. The magnetic forces in both the axial and radial directions were opposed by the drag force from the motion of the particles, with the drag force in the axial direction enhanced by the fluid flow up the

column. Figure 6-17 shows the magnitudes and directions of the net migration velocities the particles would experience if they were to be placed at different positions within the column. It is clear that at some locations within the column, the net migration of the particles is downward, and hence the particle motion would be reversed, particularly at low flow rates, with the particles near the column wall affected most because of the lower flow velocities and higher field gradients present there. These particles will accumulate at points just where the downward magnetic forces are balanced by the upward drag associated with the local flow within the column. Complete retention is not predicted, however, as there would still be small radial components of the magnetic force that ensure some radial migration of the particles to the faster flowing regions near the column centerline.

Particle trajectories for particles entering the column at different radial positions were determined by integrating the equation:

$$\underline{v}(t) = \frac{d\underline{r}(t)}{dt} \quad i.e. \quad \underline{r}(t) = \{r(t), z(t)\} = \underline{r} + \int_0^t \{v_r(r,z), v_z(r,z)\} dt \tag{6-3}$$

where $r(t)$ and $z(t)$ are the radial and axial positions, respectively, for a particle at a time t after being introduced to the column at position $\underline{r}_0$ at time $t = 0$, and v_r and v_z are the components of the particle velocities at position $\{r(t),z(t)\}$, as shown in Figure 6-17. The calculated trajectories for 2 μm non-magnetic particles are shown in Figure 6-18 for different average flow rates through the column.

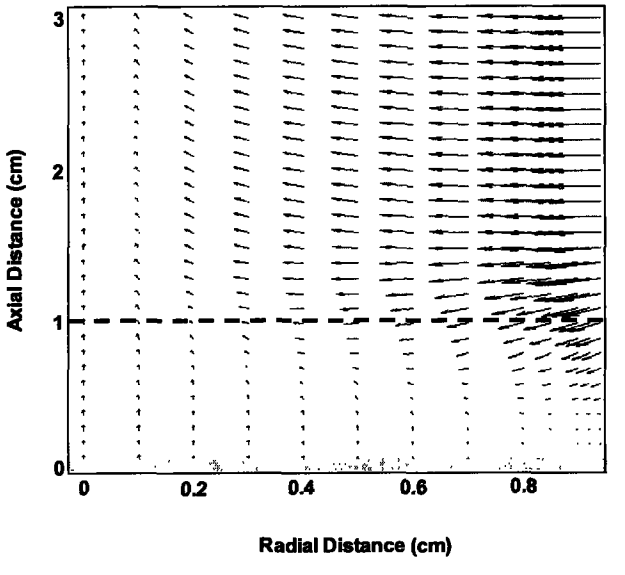

(a)

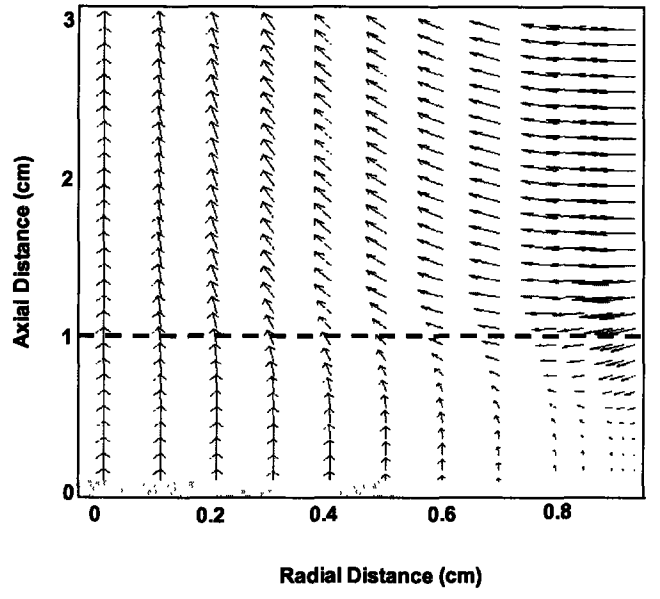

(b)

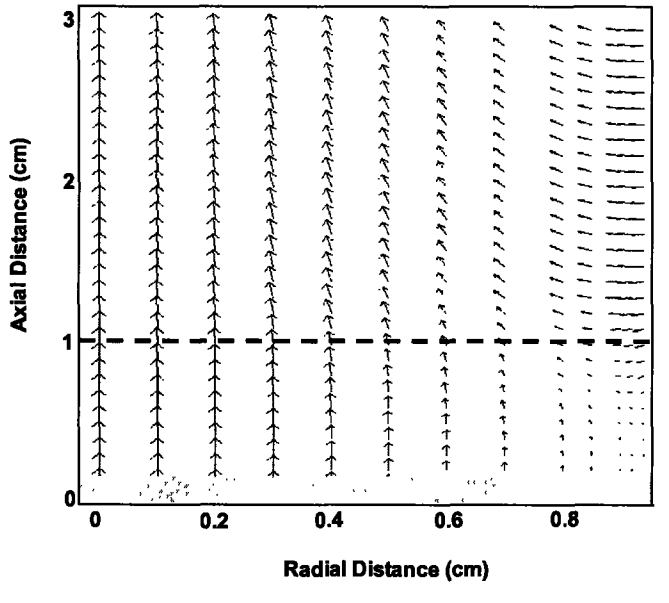

(c)

Figure 6-17. Velocity field profile for 2 micron particles at different flow rates, (a) 2 mL/hr, (b) 10 mL/hr, and (c) 30 mL/hr. The thick dashed line at an axial distance of 1 cm corresponds to the edges of the magnets, or the entrance into the magnet assembly. The velocity field profile is unchanged from approximately 2 cm (1 cm after entry into the magnet assembly) to the top of the column, shown here up to 3 cm. The arrows representing the fluid velocity have been normalized as v/v_{max}, where v_{max} is the maximum linear velocity of the fluid through the column.

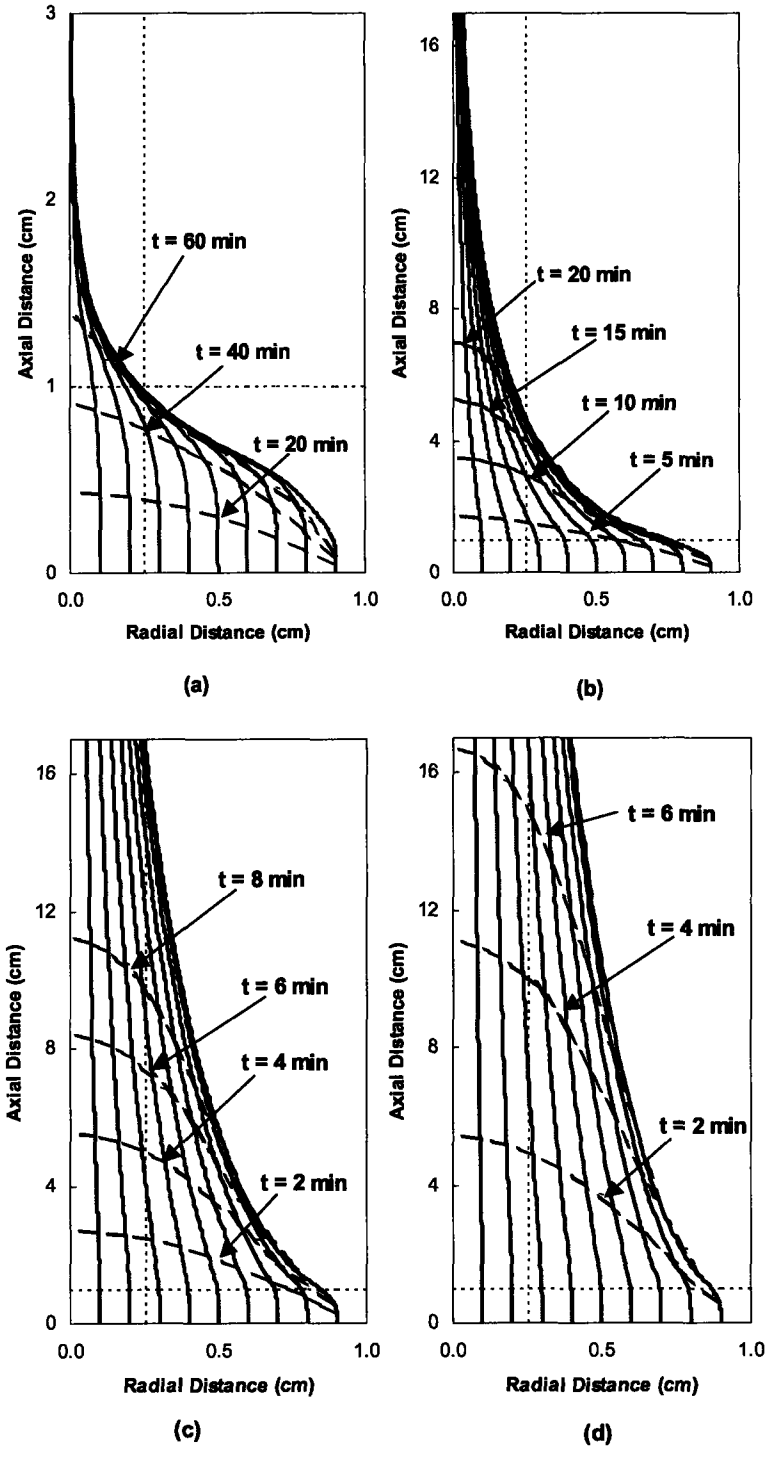

Figure 6-18. Particle trajectories at different flow rates, (a) 2 mL/hr (axial scale changed to enhance detail), (b) 30 mL/hr, (c) 120 mL/hr, (d) 240 mL/hr. The thick dashed lines represent position in the column at constant time. The dashed line at an axial distance of 1 cm corresponds to the edges of the magnets, or the entrance into the magnet assembly. The dashed line at a radial position of 0.25 cm corresponds to the position of the coaxial inner cylinder at the top of the column.

Figure 6-18 clearly shows that the particles are deflected by the axial and radial magnetic forces at the entrance to the magnet assembly and become substantially concentrated in the first few centimeters of the column at lower flow rates, due to the relative dominance of the magnetic force over the drag force in this region. At higher flow rates, only the slowest moving particles at the column walls experience a significant enhancement in concentration, due to the overall dominance of the drag force at higher flow rates. The trajectories show that lower flow rates will result in better separation of the non-magnetic particles, and although the greatest extent of enhanced particle concentration in Figure 6-18 occurs at flow rates significantly lower than those used in this work, the trajectories clearly show how the particles can become very concentrated at the centerline even for moderate flow rates. Clearly, at the low flow rates, it would also be best to draw off only a small amount of the fluid flowing through the central collection outlet in order to maximize the concentration in the collected fraction while minimizing the loss of the bulk fluid.

Also shown for comparison in Figure 6-19 are the trajectories the particles would follow for low flow rates in the absence of the axial magnetic field gradient in the entrance region while still in the presence of the radial entrance gradient, as well as for the case of no radial or axial entrance magnetic field gradients. The trajectories clearly show the large effect on particle movement and concentration that the magnetic gradients have in the entrance region. For a flow rate of 2 mL/hr, a particle at the column wall will travel from 0 to 3 cm up the column (with the magnets present at 1cm) in 515 minutes for the case that excludes both axial and radial entrance fields. For the case that includes only the radial entrance fields, a non-magnetic particle will take 276 minutes to travel the same distance, while for the case including the full axial and radial magnetic field gradients at the entrance, a particle will take 420 minutes to travel that distance. The particle trajectories represent single particles calculated in the absence of particle-particle interactions, and thus do not describe the full behavior of particle flow and retention in the column; however, even this single particle force balance clearly shows that the axial gradients present in the entrance region in the device do have a retarding effect on the motion of the particles, which increases their residence time in the column when compared to the case where only radial entrance gradients are present.

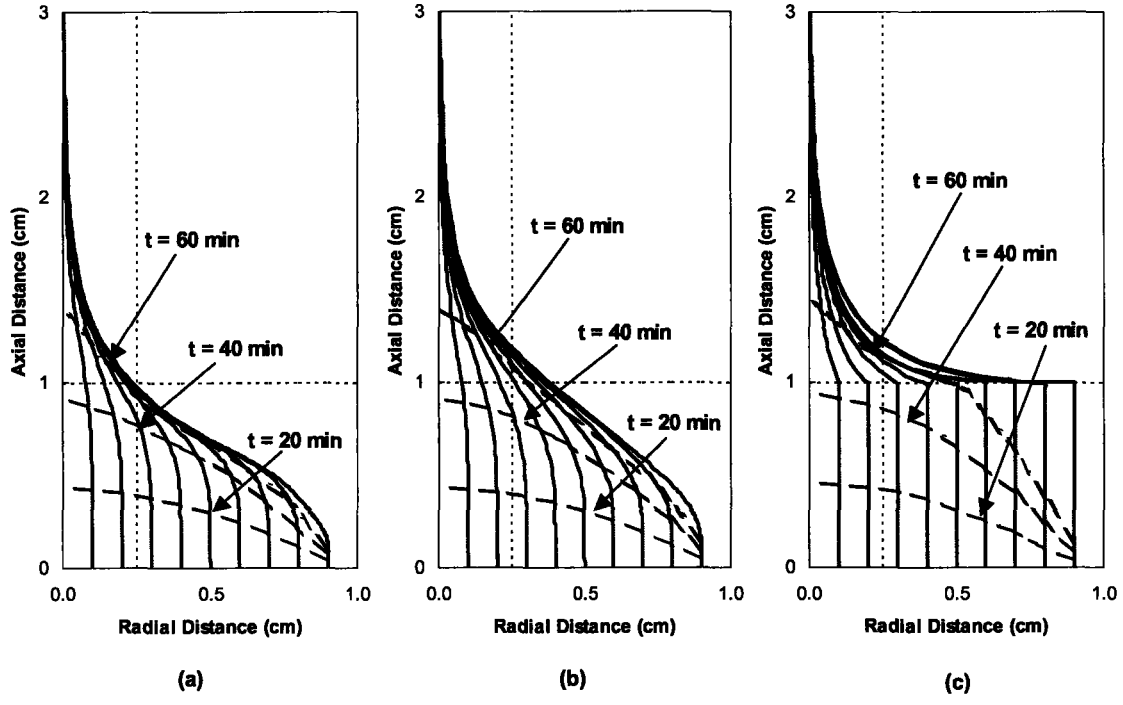

Figure 6-19. Particle trajectories at 2 mL/hr, (a) calculated with the presence of the axial and radial magnetic field gradients at the entrance to the magnet assembly, (b) calculated in the absence of the axial gradients but in the presence of the radial gradients at the entrance, and (c) calculated in the absence of both the axial and radial gradients at the entrance to the magnet assembly. The thick dashed lines represent position in the column at constant time. The dashed line at an axial distance of 1 cm corresponds to the edges of the magnets, or the entrance into the magnet assembly. The dashed line at a radial position of 0.25 cm corresponds to the position of the coaxial inner cylinder at the top of the column.

Experimental proof of the presence of the magnetic barrier force was provided by passing a feed fluid composed of 1 wt% 2 μm polystyrene beads in 1 wt% magnetic fluid through the system at 30 mL/hr in both the presence and absence of the magnetic field. The polystyrene beads were retained in the column when the magnets were in place, but without the magnets, all of the polystyrene exited the system, with a mass balance closure to within 2%. No polystyrene separation was achieved, as expected, but the negligible retention rate in the absence of the magnets showed that the accumulation of polystyrene in the magnetized column is the result of the balance of forces between the magnetic force at the entrance to the magnet assembly and the drag force exerted by the fluid flow.

6.3.2.4 Effects of Operating Parameters on Polystyrene Particle Separation and Concentration

Fluid flow rate and polystyrene bead size were both varied in the quadrupole system to determine how differences in these operating parameters affected the separation capability and ideal operating range of the device. Polystyrene beads with a diameter of 1.17 μm were used to determine the effect of particle size on the separation capability of the quadrupole process. The quadrupole column and all tubing were filled with 1 wt% magnetic fluid, after which 160 mL of 1 wt% polystyrene (1 μm) and 1 wt% magnetic fluid were pumped through the column at a flow rate of 35 mL/hr. The effluent exiting the top of the system from the three outlet streams was collected and analyzed using UV-Vis spectrophotometry to determine the concentration of polystyrene in each outlet stream. The results are given in Figure 6-20, which shows that the polystyrene was quite effectively removed from the feed through the central outlet. The overall material balance for the system also closed to within 5% for this experiment, indicating that the analytical techniques used to determine the concentration of the 1 μm polystyrene beads in the feed and fluid samples were accurate, even in the presence of magnetic fluid.

The inlet feed concentration for the experiment was 9.7 ± 0.4 mg PS/mL, the central collection outlet concentration was 29 ± 1 mg PS/mL, and the two side outlets had an average concentration of 0.6 ± 0.1 mg PS/mL. This resulted in a removal of approximately 99% of the polystyrene when compared to the effluent from the two side outlet streams. Less polystyrene was retained in the column for this experiment than for the corresponding experiment with the 2 μm beads. The retention rate at 35 mL/hr for the 1 μm beads was approximately 30%, indicating that 70% of the feed that entered the column exited through the outlets. This decrease in retention was expected, since the change in particle size affects both the magnetic force and the drag force on the non-magnetic particles, with a larger effect on the magnetic force, which scales with the cube of the radius of the particles while the drag force scales simply with the radius. Decreasing the particle size should therefore result in less accumulation in the column for the 1 μm polystyrene beads compared to the 2 μm beads even at lower flow rates, since the axially directed magnetic force is weaker for smaller particles, leading to less accumulation of the polystyrene at the entrance to the magnet assembly, as was observed.

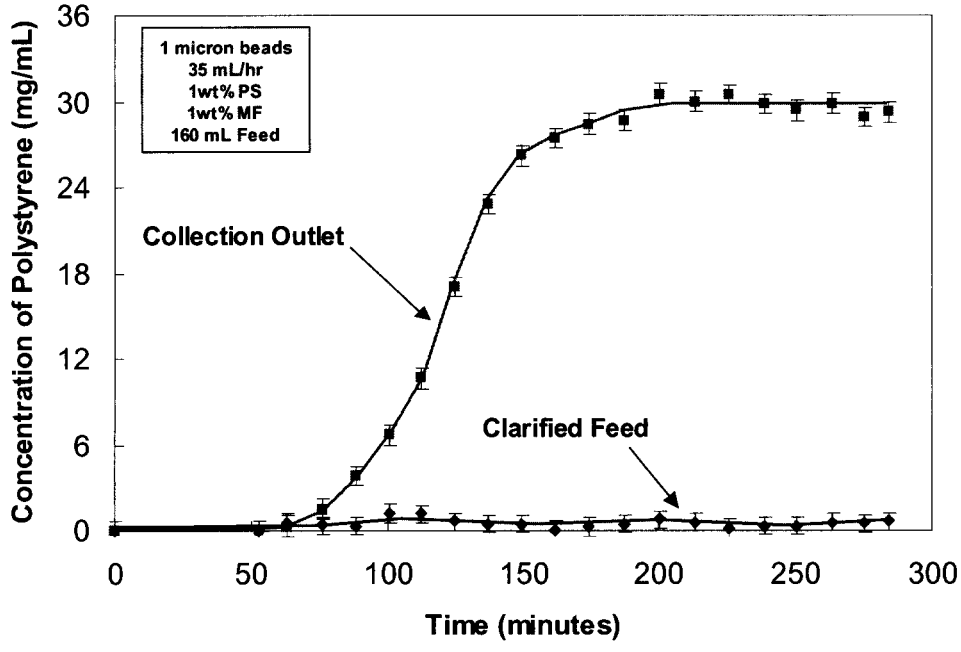

Figure 6-20. Concentration profile of the polystyrene content in the quadrupole outlets for 1.17 micron polystyrene beads using 160 mL of 1 wt% polystyrene and 1 wt% magnetic fluid as the feed with 1 wt% magnetic fluid present in the system. Clarified Feed represents the average concentration of the polystyrene collected at specific time intervals from the two side outlet streams, and Collection Outlet represents the polystyrene concentration collected at specific time intervals from the central outlet stream.

The weaker magnetic force on the 1 μm particles resulted not only in less accumulation of polystyrene in the column, but also in a less intense buildup in polystyrene concentration as the beads traveled through the column, resulting in a breakthrough curve that was less sharp when compared to the corresponding case for the 2 μm particles. At a flow rate of 35 mL/hr, the average residence time of the polystyrene in the system should be approximately 140 minutes, with initial breakthrough expected at 70 minutes for a parabolic velocity profile ($Re << 1$ for the device). This is exactly the behavior shown in Figure 6-20, indicating that the axial magnetic force on the smaller particles is weak enough not to hinder their motion appreciably through the column, even though the force is still strong enough at this flow rate to retain roughly 30% of the particles.

The effect of feed flow rate on the recovery and concentration of 1 and 2 μm polystyrene beads is shown in Figure 6-21 for feeds containing 1 wt% polystyrene in 1 wt% magnetic fluid. The curves for the two sets of beads are similar in that the recovery of polystyrene in the collection outlet exhibited a maximum at some intermediate flow rate, and then declined as the flow rate increased. This decrease in recovery at higher flow rates was anticipated because faster flows translate into a decreased residence time for the polystyrene beads in the column, resulting in fewer beads that are able to migrate to the center of the column under the magnetic force before exiting the device. The results for the lower flow rates, however, were unexpected, as they showed poorer separation even though theoretically the residence times were sufficient for the particles to migrate to the center of the column before exiting the device. These effects were attributed to the accumulation of polystyrene in the column, and hence to the fact that the column had not attained steady state operation, even though the effluent concentrations were unchanging with time for the duration of the experiments. The percent removal of polystyrene beads from the collection outlet was calculated based the amount of polystyrene fed into the device. Thus, if a significant fraction of the polystyrene was retained in the column, the apparent separation capability of the process would decrease, as was observed.

The effect of particle size in the system is as expected, since the smaller particles are less responsive to the applied magnetic field gradients, and hence require longer residence times to effectively migrate to the column centerline for removal from the central outlet. Thus, the entire curve for the 1 μm particles is shifted to lower flow rates relative to the curve for the 2 μm particles. The peak removal efficiency for the 1 μm particles is higher than that for the larger particles, because the smaller particles experience less of a magnetic barrier force, and hence a lower retention rate, upon entering the magnetic portion of the column, and therefore more of the feed from the 1 μm particles is eluted in the outlet channels, even at lower flow rates.

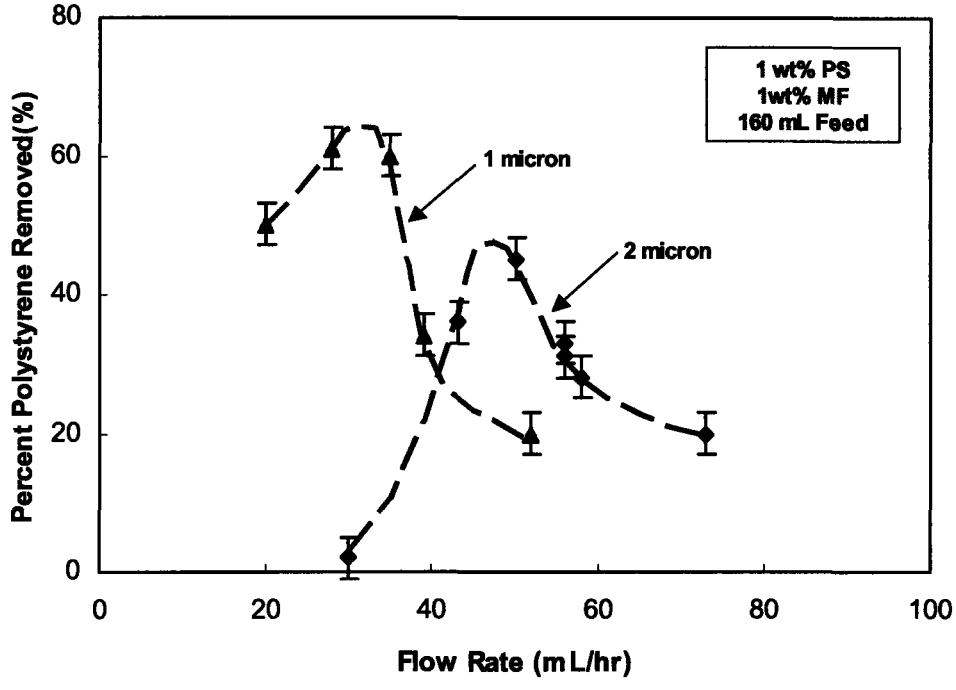

Figure 6-21. Percent of polystyrene beads removed from the feed fluid versus feed flow rate for 1 and 2 micron polystyrene beads, using 1 wt% polystyrene and 1 wt% magnetic fluid for the feed.

These results for the 1 and 2 μm beads also indicate an interesting side-benefit of the retention of non-magnetic particles in the quadrupole system, which can be exploited for fractionation based on size. Since the ideal operational range for 1 μm particles lies below the ideal operational range for 2 μm particles, the quadrupole process could be used for the separation of particles of different sizes, where, for example, the system was operated at a flow rate low enough to retain all of the 2 μm sized particles in a mixture while eluting and concentrating the 1 μm particles, in this case utilizing a flow rate of approximately 30 mL/hr.

Figure 6-21 shows the percent of polystyrene removed through the central collection outlet based on the incoming feed concentration. However, a better measure of the separation capability of the quadrupole process is the amount of polystyrene beads remaining in the clarified feed exiting the system from the two side outlets, since a low concentration of polystyrene in the side outlets represents excellent clarification of the feed, regardless of whether the polystyrene exits through the central outlet or is retained in the system. In addition, if the percent removal of polystyrene is recalculated based on

the ratio of the polystyrene collected in the central outlet to the polystyrene collected in the side outlets, the results yield a pseudo steady state approximation of the separation capability of the device, since all of the polystyrene that makes it past the entrance to the magnetic assembly should no longer be affected by axial magnetic field gradients, and will be eluted at the top of the column.

This pseudo steady state operation can be modeled using the equations developed in Chapter 5 of this work. Neglecting diffusion and gravity, which were shown to be negligible, the governing equation for pseudo steady state operation of the quadrupole process is given by Equation 6-4 (see Chapter 5 for more details):

$$\left(1-\tilde{r}^2\right)\frac{\partial \tilde{C}_p}{\partial \tilde{z}} = \frac{1}{\tilde{r}}\frac{\partial}{\partial \tilde{r}}\tilde{r}\left(\tilde{\Psi}^2\tilde{C}_p\frac{\partial \tilde{C}_p}{\partial \tilde{r}} + \tilde{\beta}\,\tilde{M}\frac{\partial \tilde{H}}{\partial \tilde{r}}\tilde{C}_p\right) \tag{6-4}$$

where $\tilde{\Psi}^2$ and $\tilde{\beta}$ are the dimensionless groups representing the electrostatic repulsive forces and the magnetic forces, respectively. The particle concentration profiles predicted by this model for different values of the parameters $\tilde{\Psi}^2$ and $\tilde{\beta}$ for 2 μm non-magnetic particles are given in Figure 6-22, which shows that both parameters play an important role in particle separation. An increase in the magnetic parameter results in an increase in the effectiveness of the separation of the particles by more strongly forcing them towards the centerline, while an increase in the electrostatic parameter results in a decrease in separation, since the electrostatic term represents a repulsive force between particles that acts to prevent their concentration at the centerline.

The model predictions of the concentration profiles were used to estimate the fraction of the polystyrene beads leaving the column through the central collection outlet. The model results are compared in Figure 6-23 with the experimentally measured values of polystyrene separation, based on the ratio of the polystyrene collected in the central outlet to the polystyrene collected in the side outlets, where the electrostatic group in the model was used as an adjustable parameter to fit the experimental data. A value for the electrostatic group equal to approximately 0.05 provided the best balance between the magnetic and electrostatic forces and the best fit to the experimental data.

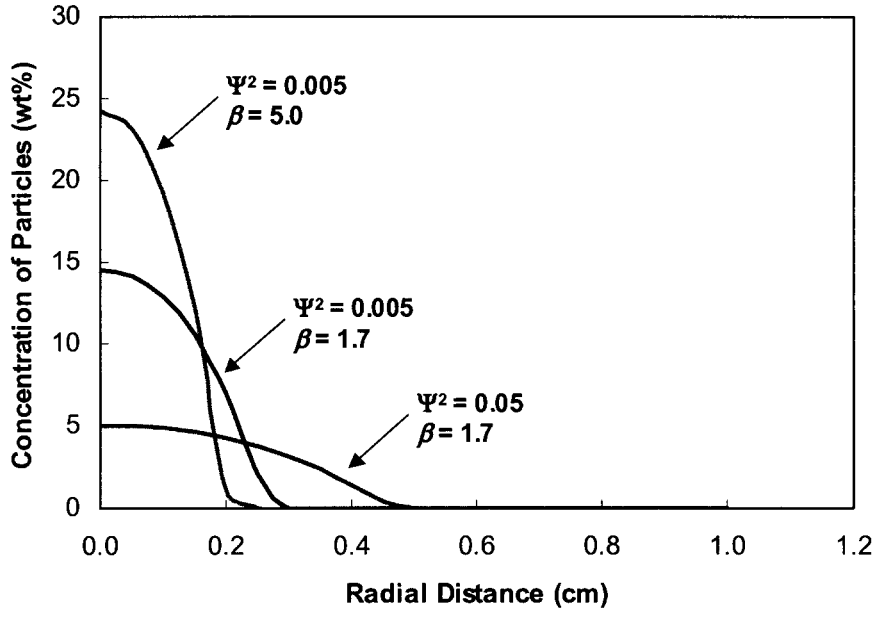

Figure 6-22. Concentration of 2 micron non-magnetic particles as a function of radial distance in the column for different $\tilde{\Psi}^2$ and $\tilde{\beta}$ values, shown at a constant axial distance of 16 cm up the column, just before reaching the central outlet.

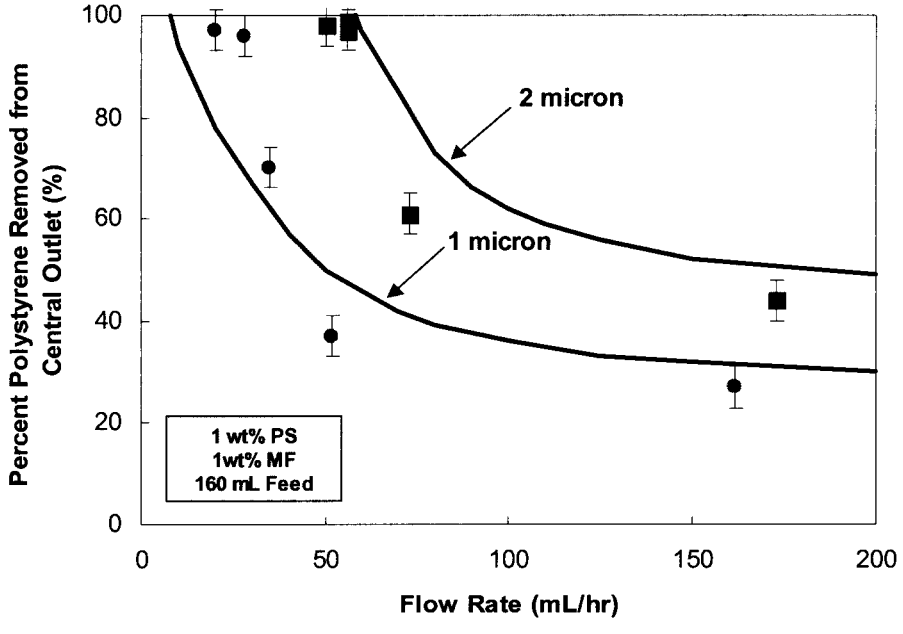

Figure 6-23. Percent of polystyrene beads in the central outlet versus feed flow rate for 1 and 2 micron polystyrene beads using 1 wt% polystyrene and 1 wt% magnetic fluid, with the model predictions present as the dark solid lines. Circles represent 1 micron experimental results, while squares represent the results using 2 micron polystyrene beads.

The fit of the model to the experimental results is good for both the 1 μm and 2 μm beads, and captures the general trend of excellent separation at low flow rates and poorer separation at higher flow rates, where the particles do not have a sufficiently long residence time to achieve good separation. For the 1 μm beads, the model predicts that at high flow rates, the percent recovery of the polystyrene beads should approach roughly 30%, while for the 2 μm beads, the percent recovery should approach roughly 45%, although both eventually asymptote to 20% at extremely high flow rates. Experimentally, the beads both approach 20% recovery at moderately high flow rates, since the central outlet is always operated at 20% of the feed flow rate. Even though the model overpredicts the percent recovery at these moderately high flow rates, it does adequately capture the separation capability of the process at lower flow rates. Indeed, at low flow rates for both particle sizes, separation as high as 99% was achieved experimentally, indicating that the device functions quite well as a clarification system, even with the initial retention of the particles at the magnet assembly entrance.

6.3.3 Experiments with *E. coli* Cells

The separation of *E. coli* cells (wild strain BL21) from raw fermentation broth was explored using the quadrupole process. The cells were cylindrically shaped and measured approximately 2-2.5 μm long by 1-1.5 μm in diameter, as determined by microscopy (see Chapter 3 of this work). The following sections discuss the results of the experiments performed using the cells in the quadrupole system.

6.3.3.1 Analytical Measurements

The concentration of cells in the samples collected during experiments was determined using UV-Vis spectrophotometry (Hewlett Packard UV-Visible Spectrophotometer Model 8463) as described previously for the polystyrene beads. The optical density at 600 nm was measured for both the raw experimental samples and the centrifuged samples, and the difference between the OD_{600} values was used to determine the optical density of just the cells alone. A linear correlation relating optical density to cell concentration was used to determine the concentration of the cells in each sample as

wt% cells on a dry cell basis (see Chapter 3 of this work for more details of the analysis procedure).

6.3.3.2 Control Experiments

A control experiment was performed with the cells in which the feed consisted of 150 mL of 0.47 wt% cells on a dry cell basis in fermentation broth, with no magnetic fluid added, to determine if the cells would be evenly distributed throughout the quadrupole system in the absence of the magnetic force caused by the presence of the magnetic nanoparticles.

The quadrupole column and all tubing were filled with deionized water, after which 150 mL of 0.47 wt% cells in fermentation broth were pumped through the column at a flow rate of 56 mL/hr. The effluent exiting the top of the system from the three outlet streams was collected and analyzed using UV-Vis spectrophotometry to determine the concentration of the cells in the outlet streams. The inlet feed concentration was 4.7 ± 0.2 mg cells/mL, the central collection outlet concentration was 3.8 ± 0.2 mg cells/mL, and the two side outlets had an average concentration of 4.0 ± 0.2 mg cells/mL. This was exactly the result that was expected, as no increase in concentration of the *E. coli* cells was observed at the center of the column. However, the decrease in the effluent concentrations when compared to the feed concentration shows that the cells did experience some settling in the device due to natural cell flocculation, which amounted to approximately 15% of the feed concentration of the cells, and indicates that the system never reached a truly steady state operation despite constant effluent concentrations during the course of the run.

The overall material balance for the system closed to within 5%, demonstrating that the analytical techniques used to determine the concentration of the cells in the feed and fluid samples were accurate. Thus, the quadrupole system was shown to function as expected on a physical level for *E. coli* cells, and the analysis procedures for the cell content in the experimental samples were shown to be accurate.

6.3.3.3 Cells and Magnetic Fluid Experiments

Experiments were performed using a feed mixture of both magnetic fluid and *E. coli* cells to test the full separation capability of the quadrupole system for magnetophoretic cell clarification. Experiments were performed using a constant feed composition of 1 wt% magnetic fluid and 0.5 wt% cells on a dry cell basis using feed flow rates ranging from 47 mL/hr to 67 mL/hr. The results of each of these experiments were identical, and showed that greater than 95% of the cells entering the device were retained in the column, resulting in no real magnetophoretic separation by the system.

Several experiments were performed to investigate the cause of the retention of the cells in the column. Since the cells did not show such a high degree of retention when used in the device without magnetic fluid, the cause of the retention was determined to be related to either the magnetic fluid itself or to the magnetic properties of the system. Experiments performed using the same feed concentrations of cells and magnetic fluid but without the presence of the magnets showed the same high level of retention of the cells. This result indicated that the cell retention was not entirely related to the forces exerted by the magnetized magnetic fluid, but that the magnetic fluid itself was inducing the cells to form aggregates, which were then settling in the column. Further experiments showed that the aggregates were not the result of any lysing of the cells, but were simply loose clumps of cells that were easily dispersed by mechanical agitation of the system. Thus, the magnetic fluid was flocculating the cells and inducing the formation of large cell aggregates.

The large cell aggregates were the cause of the settling behavior observed in the quadrupole device. Theoretically, individual *E. coli* cells should have a settling velocity in fermentation broth of around 0.05 cm/hr. Experimentally, the measured settling velocity of cells in fermentation broth was determined to be 0.07-0.3 cm/hr by tracking the movement of the settling plane in columns filled with different concentrations of the cell suspensions. The settling plane was not sharply defined for the cell suspensions, however, so the measured settling velocity is a rough approximation. When mixed with magnetic fluid, individual *E. coli* cells have a theoretical settling velocity of 0.04 cm/hr. Experimentally, however, cells mixed with magnetic fluid were shown to settle with a velocity of roughly 1.5 cm/hr at all cell concentrations tested, up to 1.1 wt% cells. Based

on the experimentally measured settling velocity, the cells appear to aggregate into loose clumps roughly 12 μm in diameter (assuming spherical aggregates), with an estimated number of cells per aggregate of approximately 151. The settling velocity results would indicate that a linear flow velocity greater than 1.5 cm/hr would be sufficient to overcome the settling of the cell aggregates in the system. Experimentally, however, cells were still retained in the device in the absence of a magnetic field for an average linear velocity as high as 21 cm/hr (59 mL/hr), which would indicate an average cell aggregate size of 46 μm. The mechanism behind the formation of the aggregates in the presence of magnetic fluid is not fully understood, however, and so it is possible that differences in the operation and set up of the experiments could account for the discrepancy in the calculated aggregate sizes. In either case, it is clear that the interactions between the magnetic fluid and the cells result in the formation of cell aggregates in the quadrupole system, which are subsequently responsible for the high rate of accumulation of the cells in the device at the same flow rates used for the polystyrene experiments.

Preliminary testing at higher pH levels was used with the goal of increasing the negative surface charge on the magnetic nanoparticles and *E. coli* cells, thus increasing the electrostatic repulsive forces between them in a effort to reduce the amount of cell flocculation. However, although higher pH levels do correspond with slightly higher surface charge on the magnetic nanoparticles, testing showed that higher pH levels do not show a corresponding increase in the negative surface charge on the *E. coli* cells, and so increasing the working pH level would have little effect on preventing the flocculation of the cells through increased electrostatic repulsion.

Experiments were performed instead to take advantage of the cell flocculation, utilizing much higher flow rates than were used for the polystyrene experiments, thus overcoming the settling of the cell aggregates by simply increasing the drag force on them. The quadrupole column and all tubing were filled with 1 wt% magnetic fluid, after which 160 mL of 0.4 wt% *E. coli* cells on a dry cell basis and 1 wt% magnetic fluid were pumped through the column at a flow rate of 515 mL/hr. The effluent exiting the top of the system from the three outlet streams was collected and analyzed using UV-Vis spectrophotometry to determine the concentration of the cells in each outlet stream. The

results are given in Figure 6-24, which shows that the cells were quite effectively removed from the feed through the central outlet at the high flow rate.

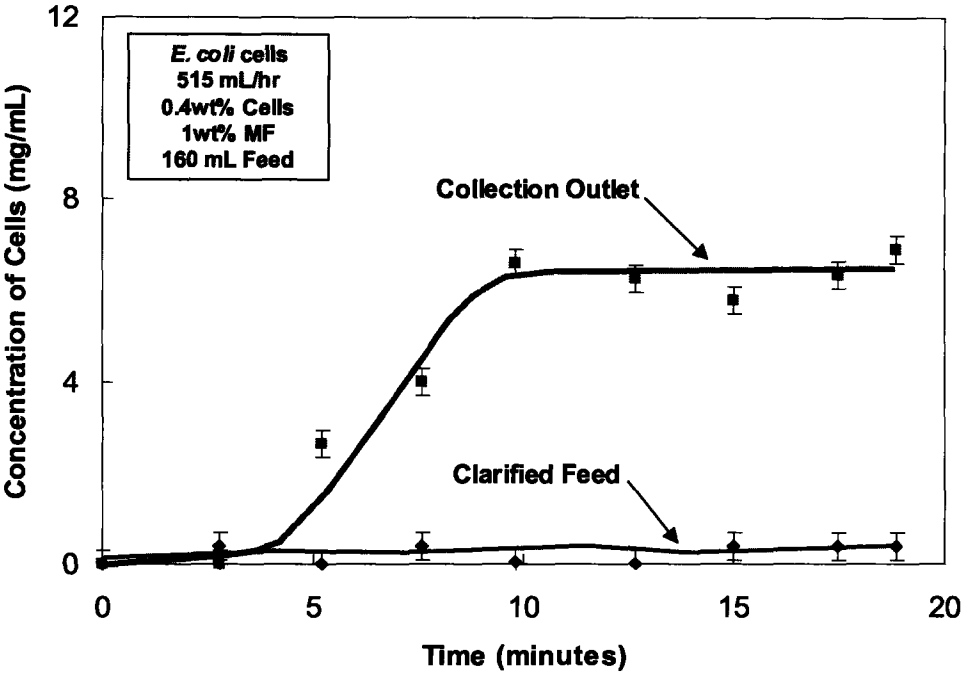

Figure 6-24. Concentration profile of the cell content in the quadrupole outlets for *E. coli* cells using 160 mL of 0.4 wt% cells and 1 wt% magnetic fluid as the feed with 1 wt% magnetic fluid present in the system. Clarified Feed represents the average concentration of the cells collected at specific time intervals from the two side outlet streams, and Collection Outlet represents the cell concentration collected at specific time intervals from the central outlet stream.

The inlet feed concentration for the experiment was 4.0 ± 0.1 mg cells/mL, the central collection outlet concentration was 6.9 ± 0.3 mg cells/mL, and the two side outlets had an average concentration of 0.4 ± 0.1 mg cells/mL. Thus, roughly 95% of the cells were removed, compared to the concentration of cells in the side outlet streams. At a flow rate of 515 mL/hr, the average residence time of the cells in the system should be approximately 9 minutes, with initial breakthrough expected at 4 minutes for a parabolic velocity profile ($Re << 1$ for the device). This is essentially the behavior shown in Figure 6-24, indicating that the axial magnetic force on the cell aggregates was not strong enough to hinder their motion appreciably through the column at the flow rate used in this experiment. Based on these results, calculations involving the balance between the magnetic forces and drag forces on the cells at this flow rate would indicate a cell

aggregate size closer to 12 μm than to 46 μm for this experiment. It is probable that the average size of the cell aggregates is variable depending on the operating conditions of the device, since the mechanism of flocculation is not fully understood, and observations of the cell flocculates show that they are easily dispersed with mechanical agitation of the system.

Even at such a high flow rate, the cells still settled significantly in the column due to the high axial magnetic force on the large flocculated cell aggregates, with approximately 54% of the cells retained in the device. The presence of the cell aggregates also affected the flow through the central outlet valve, which became fouled during the experiment, thereby decreasing the actual amount of exiting cells. A sample of the fluid located directly upstream of the central outlet valve was collected at the conclusion of the experiment, and showed a cell concentration of 9.3 ± 0.5 mg cells/mL. Thus, the quadrupole system was operating with an even better separation capability than the initial concentration profiles would imply, since some of the cells were unable to exit the device due to fouling of the central collection outlet valve, which was not originally designed to accommodate large particulate flows. Samples upstream of the side outlet valves showed no such increase in cell concentration.

The trajectory of the cells in the quadrupole device was calculated for the case of 12 μm cell aggregates, and the results are shown in Figure 6-25 for a flow rate of 500 mL/hr. The general shape of the trajectories are similar to the case for low flow rates with the 1 and 2 μm polystyrene beads, indicating that even though the flow rate is significantly higher for the cell experiments, the magnetic force pushing the cell aggregates to the centerline is enhanced due to the larger volume of the aggregates. Thus, good separation of the cells can be achieved in the quadrupole system even at high flow rates. A flow rate of 515 mL/hr was the highest flow rate tested using the *E. coli* cells. Flow rates lower than 515 mL/hr also showed similarly good separation efficiency, with over 95% of the cells removed when compared to the effluent in the side outlet streams. This is consistent with the pseudo steady state model predictions, which predict a 98% removal of cells for flow rates of 515 mL/hr or less, using an average cell aggregate size of 12 μm. However, lower flow rates also resulted in an increased retention of the cells in the device, with an experimental retention rate of 80% for a flow

rate of approximately 360 mL/hr, further demonstrating that it is a balance between the drag and magnetic forces that determines the extent of cell retention in the quadrupole system. Additionally, no cell lyses was observed during the experiments, indicating that the clarification technique employing the quadrupole system is gentle enough for the removal of whole, undamaged cells from fermentation broth.

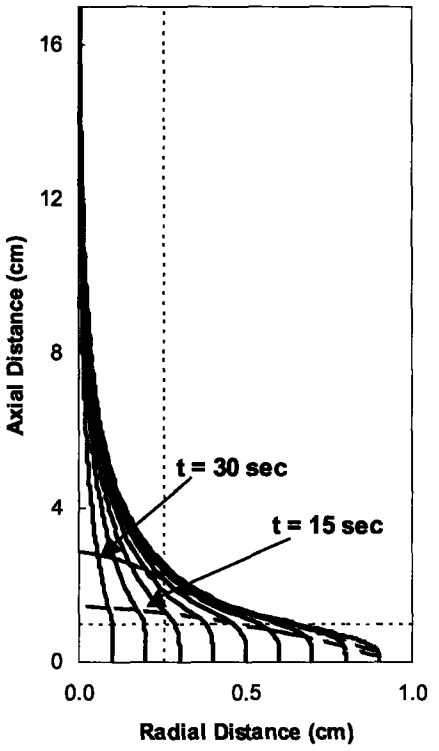

Figure 6-25. Trajectories for 12 micron cell aggregates at different radial locations in the quadrupole column at a flow rate of 500 mL/hr. The thick dashed lines represent position in the column at constant time. The dashed line at an axial distance of 1 cm corresponds to the edges of the magnets, or the entrance into the magnet assembly. The dashed line at a radial position of 0.25 cm corresponds to the position of the coaxial inner cylinder at the top of the column.

6.4 Summary

The quadrupole process represents a new technology for removing non-magnetic particles from a bulk liquid. Using polystyrene beads as a model particle, the quadrupole system was shown to be successful in removing up to 99% of 2 μm sized polystyrene beads from the feed after one pass through the device. At lower flow rates (less than 40 mL/hr), significant accumulation of the 2 μm polystyrene beads was observed in the

column due to the presence of axially directed magnetic field gradients in the entrance region that created a barrier-to-entry force into the magnetic portion of the column. At higher flow rates (greater than 40 mL/hr), the increased drag force from the fluid flow was sufficient to overcome this axial magnetic force, and particle retention in the column was decreased. At much higher flow rates (greater than 55 mL/hr), the recovery of polystyrene from the feed decreased, due to an insufficient residence time in the column to achieve good separation.

Different sized polystyrene beads were also tested in the quadrupole system, and showed results similar to the 2 μm sized beads. For 1 μm sized beads, the quadrupole device was successful in removing up to 99% of the polystyrene beads after one pass through the system. The proportionally smaller magnetic force on the smaller 1 μm particles resulted in a shift of the ideal operating range of the device to slower flow rates when compared to the 2 μm particles, since the smaller magnetic force necessitated an increase in the residence time of the particles in the device to maintain good separation. However, the proportionally smaller magnetic force also resulted in a lower particle retention rate for the 1 μm beads, since the magnetic barrier-to-entry force was reduced for the smaller particles, resulting in fewer retained 1 μm polystyrene beads, even at lower flow rates. This result would allow the quadrupole system to operate as a fractionator for different sized particles, where the device could be operated at a flow rate low enough to retain the larger particles, but high enough to elute and concentrate the smaller particles. In addition, the excellent separation of the 1 and 2 μm polystyrene beads that was achieved at low and moderate flow rates showed a good fit with the separation capability predicted by a pseudo steady state model of the process.

Experiments using *E. coli* cells showed that the magnetic fluid flocculates the cells, resulting in a high degree of cell retention in the quadrupole system at the same feed flow rates used for the polystyrene experiments, due to the increased axial magnetic forces on the larger cell aggregates. However, this increased axial force was overcome by operating the device at flow rates greater than 350 mL/hr, leading to a maximum separation efficiency of approximately 95% when compared to the cell concentration in the clarified side outlets. Cell retention in the device was still significant, even at the highest flow rates used (greater than 500 mL/hr); however, the cells that did enter the

magnetic portion of the device were very efficiently separated, and the cell concentration of the clarified feed was reduced to 7% or less of the incoming feed concentration in all cases.

The quadrupole process was therefore shown to be a successful new technology for the separation of non-magnetic particles from a bulk liquid, and has potential applications in the biotechnological and pharmaceutical industries for the removal of cells from raw fermentation broth. The quadrupole system was also able to successfully process feed volumes that were orders of magnitude larger than was processed using the counter current system, and at significantly higher flow rates. Further modification and scale up of the quadrupole design could allow for future devices capable of fast, efficient processing of even larger volumes of feed.

6.5 References

1. Deen, W.M., *Analysis of Transport Phenomena*. 1998, New York: Oxford University Press, Inc.

Chapter 7

Conclusions

7.1 Summary of Research

Magnetophoretic cell clarification is a novel technique that takes advantage of the properties of magnetic fluids for the separation of cells from raw fermentation broth. Magnetic fluids are stable colloidal dispersions of magnetic nanoparticles that become magnetized in the presence of an applied magnetic field. The magnetization of the fluid under an applied non-uniform magnetic field provides the necessary force for concentrating the cells and removing them from the bulk fermentation liquid, since the cells experience a force in the magnetized fluid that pushes them away from areas of high magnetic field and into areas of low magnetic field. Magnetophoretic cell clarification has several advantages over the current industrial methods for cell clarification – centrifugation and membrane filtration. Unlike centrifugation, magnetophoretic cell clarification has no high speed moving parts and is gentle on cells, so that it can be used to viably capture and concentrate whole cells from bulk fermentation broth. The clarification systems are also completely open to fluid flow, eliminating the problem of fouling and clogging that is prevalent in membrane filtration devices.

The magnetic nanoparticles that made up the magnetic fluid used in this work consisted of a magnetite core approximately 8 nm in diameter surrounded by a polymer shell with a thickness of ~12 nm. The polymer shell was composed of a comb graft copolymer with a polyacrylic acid (PAA) backbone onto which side chains of a polyethylene oxide (PEO)/polypropylene oxide (PPO) random block copolymer were attached. Magnetic fluid was synthesized in aqueous solution in a single batch reaction through chemical coprecipitation of iron(III) and iron(II) chlorides in the presence of the PAA-PEO/PPO graft copolymer, where the carboxylic acid groups on the PAA backbone of the graft copolymer were bound to the iron on the developing magnetite crystals, coating them and preventing further growth. The PEO/PPO side chains on the PAA

backbone provided the stabilizing force that kept the coated magnetic nanoparticles stable in aqueous solution.

Two different magnetophoretic clarification processes were tested in this work, a counter current process and a quadrupole process. The counter current process was shown to be successful in removing up to 95% of *E. coli* cells from the feed after one pass through the system. The importance of the operating parameters on the separation capability of the counter current device was determined, with the separation capability increasing with decreasing flow rate and increasing with increasing magnetic fluid concentration. The concentration of the cells in the feed fluid was shown to have less of an effect on the separation capability of the counter current system than feed flow rate and magnetic fluid concentration.

The overall equation governing magnetophoretic clarification using magnetic fluids was applied to the specific case of a novel quadrupole design. The results of the simulations using this model were used to define the final geometry of the flow column needed for the custom-built quadrupole device, with an estimated recovery rate of 90% of 2 μm sized non-magnetic particles after one pass through the system at a feed flow rate of 50 mL/hr.

Using polystyrene beads as a model particle, the quadrupole system was shown to be successful in removing up to 99% of 2 μm sized polystyrene beads from the feed after one pass through the device, depending on the feed flow rate. At lower flow rates (less than 40 mL/hr), significant accumulation of the 2 μm polystyrene beads was observed in the column due to the presence of axially directed magnetic field gradients in the entrance region that created a barrier-to-entry force into the magnetic portion of the column. At higher flow rates (greater than 40 mL/hr), the increased drag force from the fluid flow was sufficient to overcome this axial magnetic force, and particle retention in the column was decreased. At much higher flow rates (greater than 55 mL/hr), the recovery of polystyrene from the feed decreased, due to an insufficient residence time in the column to achieve good separation. Different sized polystyrene beads were also tested in the quadrupole device, and showed results similar to the 2 μm sized beads, with smaller beads experiencing lower retention rates in the system and requiring slower flow rates for

good separation while larger beads experienced increased retention in the device and required faster flow rates for effective separation.

Experiments using *E. coli* cells showed that the magnetic fluid flocculates the cells, resulting in a high degree of cell retention in the quadrupole system at the same feed flow rates used for the polystyrene experiments, due to the increased axial magnetic forces on the larger cell aggregates. However, this increased axial force was overcome by operating the device at flow rates greater than 350 mL/hr, leading to a maximum separation efficiency of approximately 95% when compared to the cell concentration in the clarified side outlets. Cell retention in the system was still significant, even at the highest flow rates used (greater than 500 mL/hr); however, the cells that did enter the magnetic portion of the device were very efficiently separated, and the cell concentration of the clarified feed was reduced to 7% or less of the incoming feed concentration in all cases.

Both the quadrupole process and the counter current process were therefore shown to be successful new technologies for the separation of non-magnetic particles from a bulk liquid and have potential applications in the biotechnological and pharmaceutical industries for the removal of cells from raw fermentation broth. Further modification and scale up of the designs could allow for second and third generations of devices that are capable of successfully processing large volumes of feed at high flow rates in a optimized manner.

7.2 Process Considerations

For the counter current process, the primary advantage of this design is that the cells can be removed from the fermentation broth without any significant loss of the bulk liquid. This is an important consideration when the biological product of interest in the bulk medium, such as a pharmaceutical compound or protein, is a high value product where all product losses must be minimized. The counter current design could also be optimized such that it produced truly continuous operation, where the concentration of cells in the collection tube of the device could be purged at regular intervals without disrupting the flow of fluid in the flow tube of the device, as is done currently with self-cleaning centrifuges.

The only minor disadvantage of the counter current design is the presence of the moving magnets, which introduces a complexity to the device that is not present for permanently fixed magnetic fields. However, this disadvantage is minor compared to the full potential of the device. A second or third generation counter current device that operates continuously and removes close to 100% of cells from raw fermentation broth without any significant loss of the fluid in the broth itself would have tremendous application in the biotechnological and pharmaceutical industries.

For the quadrupole process, the principle advantage of this design is excellent separation at high throughput volumes. Since the feed is pumped against gravity, large cells or cell aggregates can be processed at a fast rate, since a fast flow rate is required to prevent the particles from settling in the device. Longer flow columns may be needed to increase the residence time of the cells in the system for good separation at very high flow rates, but such modifications are straightforward since the magnetic field is static and moving parts are not an element of the quadrupole design.

In addition, due to the ability of the system to retain larger particles at a certain flow rate while simultaneously eluting smaller particles, the quadrupole system could operate as a fractionator for different sized particles, where the device was operated at a flow rate low enough to retain the larger particles, but high enough to elute and concentrate the smaller particles. This would be a novel application of the quadrupole system, and has potential applications in the biotechnological and pharmaceutical industries for separating different types of cells from a bulk liquid.

The primary disadvantages of the quadrupole design are the costs associated with pumping large volumes of fluid against gravity, as well as the loss of some of the bulk fluid that exits the system with the concentrated cells. However, the operational costs due to the pump are small compared to the operating costs involved in centrifugation and membrane filtration, and the loss of the bulk fluid can be minimized by optimizing the flow rates through the outlets such that the maximum amount of cells is recovered in the minimum volume of fluid. Due to its static magnetic field, the quadrupole device also lends itself well to scale up and parallel processing, as depicted in Figure 7-1, which is an important consideration for the clarification of large volumes of feed fluid at high flow rates.

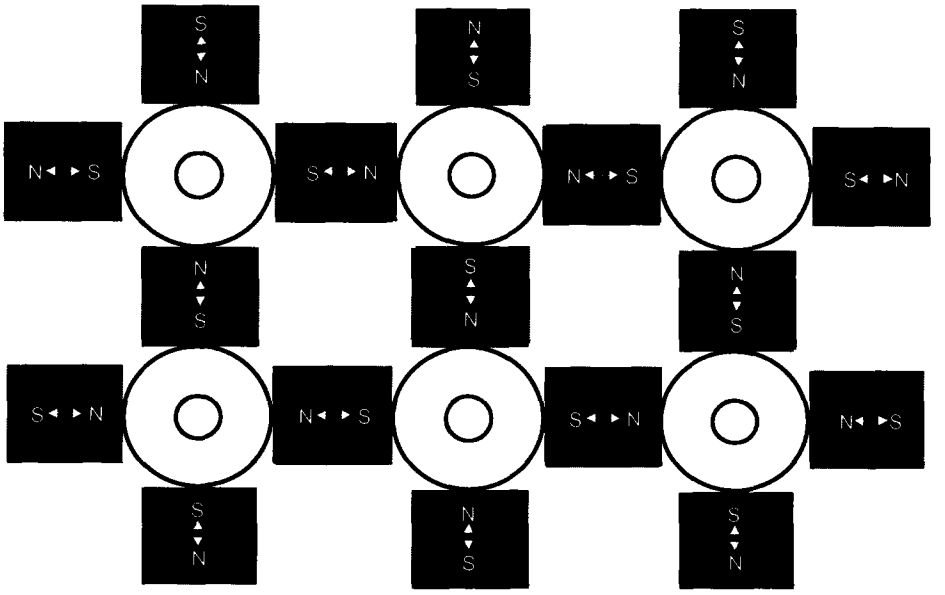

Figure 7-1. Parallel process design for scale up of the quadrupole device.

7.3 Future Research Directions

Future research with magnetophoretic cell clarification could take several directions. Both the counter current process and the quadrupole process could be studied further to optimize the designs and investigate scale up of the devices, as well as to explore the operation of the systems with cell types not studied in this work, such as yeast, fungi, and mammalian cells.

The operation of the quadrupole system could also be enhanced by minimizing the magnetic barrier-to-entry force present in the current design of the device. This can be achieved through the careful design of the magnet shapes and field profiles near the entrance to the column in order to reduce the axial magnetic gradients that impede the entrance of the non-magnetic particles, as illustrated in Figure 7-2a. In addition, the use of premixed feed containing both non-magnetic particles and magnetic fluid could be altered such that mixing occurred within the magnetic portion of the column, as illustrated in Figure 7-2b. The non-magnetic particle suspension without magnetic fluid would flow into the magnetic portion of the device unimpeded by the axial magnetic field gradients, and the magnetic fluid would then be introduced into the column after the

particle suspension had already reached a position where the axial magnetic field gradients had vanished. Thus, the non-magnetic particles would feel no magnetic force due to the magnetized fluid until they were already in the magnetic portion of the column and past the axial magnetic field gradients.

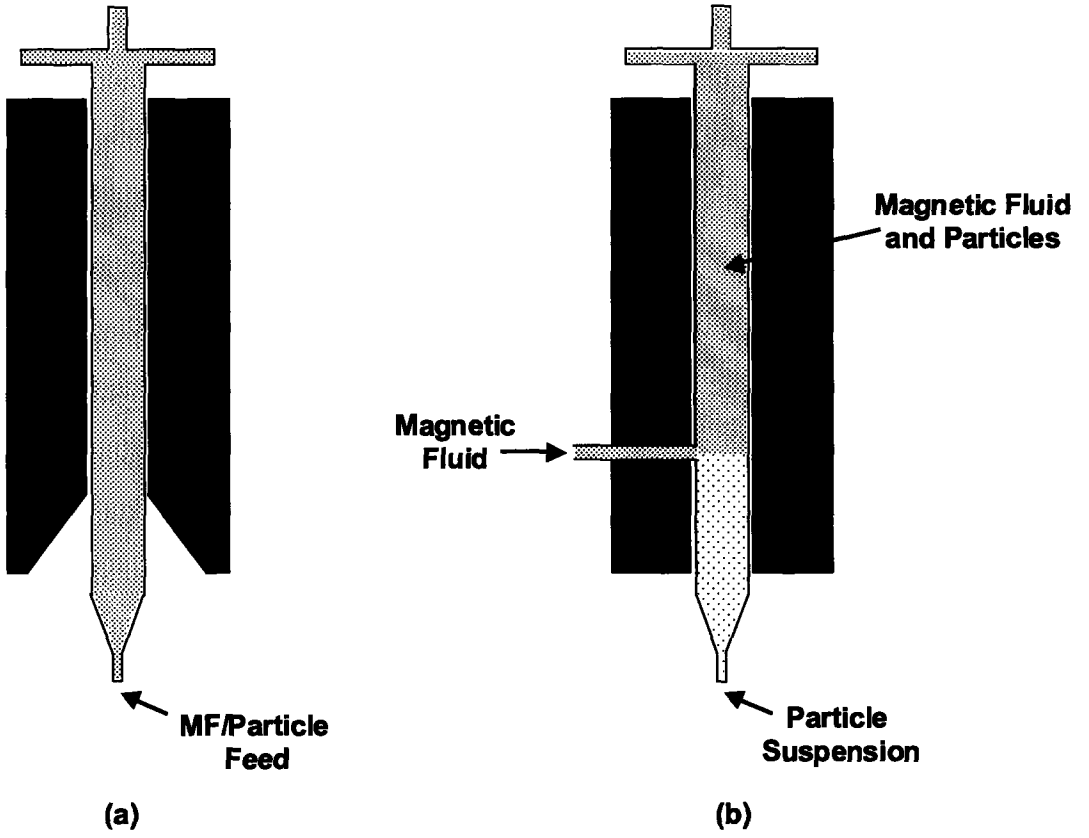

Figure 7-2. Alternate quadrupole system designs for minimizing the barrier-to-entry force, where (a) shows a different design for the permanent magnets and (b) shows a different method of entry into the column for the feed fluid.

The magnetic barrier-to-entry force could also be purposefully exploited to use the quadrupole system as a size fractionator for different sized non-magnetic particles, as mentioned previously. Further research could be performed to optimize the process for size fractionation and to determine the resolution of the system to see how close in size the particles can be while still achieving good separation. A size fractionator that can achieve good separation between particles that differ in size by only a few tenths of a micron would have enormous applications for particle separation in many industries.

Future research should also be directed to the downstream processing of the clarified fluid. Once the magnetic fluid has been mixed with the raw fermentation broth and the cells removed, the magnetic fluid itself must then be recovered from the clarified broth. Different methods currently exist for removing magnetic particles from bulk liquids, such as high gradient magnetic separation (HGMS), but such processes have not been optimized for the removal of magnetic nanoparticles of the size used in this work. An economic analysis of the process should also be performed to determine how competitive magnetophoretic cell clarification can be on an industrial scale. If optimized clarification devices combined with optimized magnetic fluid separation systems can be developed economically, magnetophoretic clarification offers enormous potential wherever small non-magnetic particles need to be removed from a bulk fluid.

Appendix

Appendix A: Calculation of Error

The values measured experimentally in this work all have an error associated with them that provides an indication of the confidence in the numerical value of the stated quantity. The associated error was reported in this work as "numerical value of quantity" ± "associated error". Depending on how the quantity was measured, the error associated with it was calculated in one of three ways.

For quantities measured only once, the associated error was determined by using the error associated with the machine or device used to take the measurement. For example, for measurements of mass, the error associated with the measured mass was equal to the limit of precision of the mass balance, so that a hypothetical measurement of 2.4056 g would have an associated error of ± 0.0005 g, since that is the precision limit of the machine. All machines and devices used in this work were calibrated before use to ensure the highest possible levels of accuracy and precision of the measurements.

For quantities with repeated measurements in which two or more measured values of the quantity exist, the average of all the measurements for that quantity was used for the numerical value. The error associated with this average value, called the standard error, was then calculated using Equation A-1:

$$\text{standard error} = \frac{s}{\sqrt{n}} \tag{A-1}$$

where s is the standard deviation of the average and n is the number of measurements. The standard error represents the difference between the true population mean and the average value that was calculated using the experimental measurements. Thus, for quantities in which a large number of measurements were made, the standard error would be much less than the standard deviation of the average. It was the standard error that was reported in all cases as the error associated with quantities that were calculated using an average of two or more experimentally measured values.

For quantities that were calculated using an equation or formula, the associated error for that quantity was calculated as follows:

a) The associated error resulting from the addition or subtraction of two values was calculated as the sum of the two values' errors.
b) The associated error resulting from the division or multiplication of two values was calculated as the sum of the percent error of the two values.

For example, for the calculation of the quantity A given by the formula in Equation A-2:

$$A = B*(C-D)/E \qquad (A-2)$$

the error associated with A would be calculated as follows:

a) First calculate the error associated with (C-D) as the associated error of C plus the associated error of D.
b) Using the associated error for each of the quantities B, E, and (C-D), calculate the percent error for each quantity.
c) Calculate the percent error in A by adding the percent errors of B, (C-D), and E.
d) Use the percent error of A to calculate the associated error for the value of A.

Since this method of calculating the error sums all the errors associated with every value in the formula, it can overpredict the actual error associated with a calculated quantity, but it does provide an excellent upper limit for the associated error of calculated experimental values.

Appendix B: Matlab Code for the Counter Current Device

The Matlab code used to fit the experimental data to the empirical model for the counter current device is given below. Two different programs were used, one data file containing the experimental data (the same data as listed in Table 4-2) and one function file containing the model itself. These two files were used in conjunction with Matlab's nonlinear equation solver (NLINFIT) to estimate the coefficients of the nonlinear model using a least squares fit of the experimental data.

File name: datacountcur.m

```
% This file loads the experimental data for use with the MFCOUNTCUR function. y is the experimentally
% achieved percent of cells in the outflow (i.e. for a 4% "cells in outflow", 96% of the cells originally in
% the feed were removed by the device and so the amount of cells remaining in the clarified feed is 4%),
```

```
% and each value of y corresponds to a set of operational parameters given by the matrix X. The columns
% in the matrix X are as follows: X1 represents the normalized feed flow rate, X2 represents the
% concentration of magnetic fluid in the feed in weight percent, and X3 represents the concentration of
% E. coli cells in the feed in weight percent. The vector BETA0 contains initial values for the model
% coefficients, which Matlab's nonlinear equation solver, NLINFIT, will use as a starting point for
% calculating the actual model coefficients that best fit the experimental data.

y = [7.1;11.3;6.5;5.1;20.1;9.8;31.0;4.3;7.4;15.9;3.9;37.3;26.4;14.3;13.0;13.0;11.9;7.2;14.8;5.4;2.0;14.0;
20.2;15.0;10.9];

X = [1 1 0.48;0.2 1 0.52;0.2 1 1.44;1 1 0.65;1 1 1.88;1 1.5 0.93;1 0.5 1.1;.2 1.5 1.12;0.2 0.5 0.91;0.6 1.5
1.42;0.6 1.5 0.43;0.6 0.5 1.71;0.6 0.5 0.51;0.6 1 0.73;0.6 1 0.68;0.6 1 0.68;0.3 1 1.47;0.3 1 1.13;0.3 1
1.38;0.3 1 1.02;0.3 1 1.01;1 1 0.88;1 1 1.16;1 1 0.98;0.2 1 0.50];

beta0 = [2;2;2;2;1;1;1;2;2;2];
```

File name: mfcountcur.m

```
function yhat = mfcountcur(beta,X)

% This function file defines the non-linear model used to fit the experimental data from the counter current
% magnetophoretic cell clarification device. The function YHAT = MFCOUNTCUR(BETA,X) gives the
% predicted value of the percent of cells in the outflow for a single pass of feed mixture through the
% counter current device (i.e. for a 4% predicted "cells in outflow", 96% of the cells originally in the feed
% were removed by the device and so the amount of cells remaining in the clarified feed should be 4%).
% YHAT is a function of the vector of fitted coefficients for the model, BETA, and the matrix of
% experimental data, X, where X1 represents the normalized feed flow rate, X2 represents the
% concentration of magnetic particles in the feed in weight percent, and X3 represents the concentration of
% E. coli cells in the feed in weight percent. BETA must have ten elements and X must have three
% columns. The MFCOUNTCUR function is passed to Matlab's non-linear equation solver, NLINFIT,
% which takes the experimental data and the desired model form and estimates the coefficients of the
% model (BETA) using a least squares fit of the experimental data.
%
%  The model form is:
%  y = b1 + b2x1 + b3x2 + b4x3 + b5x1^2 + b6x2^2 + b7x3^2 + b8x1x2 +  b9x2x3 + b10x1x3

b1 = beta(1);
b2 = beta(2);
b3 = beta(3);
b4 = beta(4);
b5 = beta(5);
b6 = beta(6);
b7 = beta(7);
b8 = beta(8);
b9 = beta(9);
b10 = beta(10);
x1 = X(:,1);
x2 = X(:,2);
x3 = X(:,3);
yhat = b1+b2*x1+b3*x2+b4*x3+b5*x1.^2+b6*x2.^2+b7*x3.^2+b8*x1.*x2+b9*x2.*x3+b10*x1.*x3
```

Using these two programs, Matlab's non-linear equation solver, NLINFIT, was used to estimate the coefficients (b_1 through b_{10}) for the model. The syntax used in Matlab's command window was as follows:

```
>> load datacountcur.m
```

(Note: the LOAD function in Matlab is often finicky and sometimes does not work. When that happens, the data located in the datacountcur.m file were just copied and pasted into Matlab's command window.)

```
>> beta = nlinfit(X,y,@mfcountcur,beta0)
```

The Matlab function NLINFIT takes the experimental data (given in the matrix X and the corresponding vector y) and the functional form of the model (given in the function program MFCOUNTCUR) and uses a least squares fit to return the coefficients for the model (BETA) using initial values of the coefficients (BETA0) as a starting point for the calculations. For the counter current model, the calculated coefficients were as follows, in numerical order from b_1 to b_{10}:

```
beta =

   19.6174
   57.9649
  -35.9251
   -4.1463
  -35.6476
   16.2578
    0.9976
  -19.8267
   -0.5548
   15.3564
```

These coefficients were then used in the model to determine which of the three parameters was most important (flow rate, magnetic fluid concentration, cell concentration) and to determine how accurately the model predicted the separation capability of the device given an initial set of the three operating parameters, as discussed in more detail in Chapter 4.

Appendix C: Matlab Code for the Quadrupole Device

The Matlab code used to solve the governing equation for magnetophoretic separation in the quadrupole system is given below. The code makes use of Matlab's partial differential equation solver, PDEPE, to solve the equation. Numerical values and equations for estimating other parameters in the equation are given in the code, as are the axial and radial boundary conditions. The equation solved by Matlab corresponds to Equation 5-19.

File name: mfquadrupole.m

```
function out = mfquadrupole(w1o)

% mfquadrupole file

rho = 1.017e3;  % density of entire fluid (water+MF+particles) at 21C, kg/m^3
rhop = 1.05e3;  % density of particles, kg/m^3
RT = 8.314*294;  % kg*m^2/mol*s^2
NA = 6.022e23;  % Avogadro's number, 1/mol
eps = 78.5*8.854e-12;  % dielectric constant of MF+water (electric permittivity of MF+water) =
      eps(water)*eps(free space), A*s/V*m
kappa = 1040000;  % inverse Debye length, 1/m (assumes no salt, with a maximum ionic
      strength of 1e-7 M, equal to a pH of 7)
d = 2.01e-6;  % particle diameter, m (all particles assumed to be spherical)
muo = pi*4e-7;  % permeability of free space, Tesla*m/A
visc = 0.995e-3;  % viscosity of the entire fluid at 21C, kg/m*s
D = RT/(3*pi*visc*d)/NA;  % diffusivity of the particles, m^2/s (Stokes Eq)
MWf = 0.020;  % MW of the fluid, assumed to be roughly the same as water at 20 g/mol, kg/mol
MWp = (pi/6)*d*d*d*rhop*NA;  % MW of the particles, calculated as
      Vol(part)*density(part)*NA, kg/mol
Vp = (pi/6)*d*d*d*NA;  % partial molar volume of the particles (m^3/mol)
%w1o = 0.01;  % initial mass fraction of the particles
Cpo = w1o*rho/MWp;  % initial concentration of the particles in the feed, mol/m^3
C = rho/MWf;  % concentration of water+particles+MF, mol/m^3
Ms = 614;  % saturation magnetization of MF extrapolated from SQUID data, A/m
Ht = 43500;  % H at which M = Ms/2, A/m
Ho = 0.6282/muo;  % maximum H in the system, A/m
R = 0.0095;  % radius of the column, m
L = 0.18;  % length of column that lies within the magnets, m
Vo = 0.0676;  % zeta potential of the particles, V (V = kg*m^2/A*s^3)
Q = 50;  % feed flow rate, mL/hr
Q = Q/100^3/3600;  % feed flow rate, m^3/s
vmax = 2*Q/pi/R^2;  % maximum linear velocity of the fluid, m/s
Re = 2*vmax*R/visc;  % Reynolds number for fluid flow
```

```
EntranceL = R*(1.18+0.112*Re);     % distance required for the velocity profile to approach
        within 1% of its final shape, m
Pe = R^2*vmax*rho/D/L/MWf/C;  % dimensionless Peclet number
diff = 1/Pe;  % dimensionless diffusion group
phisquiggle  =  (16*pi^2*eps*Vo*Vo*d*d/4/kappa/kappa*(1+kappa*d)*NA*NA*Cpo/RT)/Pe;
        % dimensionless electrostatic group (the 4 turns the diameter into radius)
beta = (muo*Vp*Ms*Ho/RT)/Pe;  % dimensionless magnetic group
grav = 9.80665*rho*Vp*R^2/RT/L*(1-rhop/rho)/Pe;  % dimensionless gravity group
m = 1;  % number of r dimensions (Cartesian = 0, cylindrical = 1, spherical = 2)
X = [linspace(0,1,21)];  % radial distance in the column, nondimensionalized as r/R
t = linspace(0,1,101);  % axial distance in the column (length of column), nondimensionalized as
        z/L


% parameters to be transferred to the PDE solver

va(1)= diff;
va(2)= phisquiggle;
va(3)= beta;
va(4)= grav;

sol = pdepe(m,@pdex1pde,@pdex1ic,@pdex1bc,X,t,[],va);

% m = a parameter corresponding to the symmetry of the problem, m = 1 for
%  cylindrical coordinates
% @pdexlpde = name of the function (below) that defines the components of
%  the PDE
% @pdexlic = name of the function (below) that defines the initial
%  conditions
% @pdexlbc = name of the function (below) that defines the boundary
%  conditions
% X = a vector [xo,x1,...,xn] specifying the points at which a solution is
%  requested for every value in the time span (t), which equals the length
%  span (L) in this case
% t = a vector [to,t1,...,tn] specifying the points at which a solution is
%  requested for every value in the X span, which equals the radial
%  distance in this case
% [] = uses default set of "options"
% va = additional, optional parameters to be passed to pdexlpde

% sol is the multidimensional solution returned by pdepe.  It has the form
%  sol(t,X,u), where u is the dependent variable (particle concentration here).
%  Thus, sol(1,:,1) yields the values of normalized particle concentration
%  at each X value (each radial position) for z=1 (corresponding to the top of the column).

ui=sol;  % normalized particle concentration
out1 = ui(1,:,1);    % the : means for all dimensions
out2 = ui(20,:,1);
out3 = ui(40,:,1);    % The algebra here picks out different places
out4 = ui(60,:,1);    % along the full length of the column (the total column length is equal
out5 = ui(1+0.9*(length(t)-1),:,1);    % to the quantity (length(t)-1) in this case).
```

```
wt1 = out1*Cpo*MWp*100/rho;     % transforms normalized particle concentration to particle
        weight percent
wt2 = out2*Cpo*MWp*100/rho;
wt3 = out3*Cpo*MWp*100/rho;
wt4 = out4*Cpo*MWp*100/rho;
wt5 = out5*Cpo*MWp*100/rho;

Cp1 = out1*Cpo*MWp*1000*1000/100^3;    % transforms normalized particle concentration to
        regular particle concentration, from mol/m^3 to mg/mL
Cp2 = out2*Cpo*MWp*1000*1000/100^3;
Cp3 = out3*Cpo*MWp*1000*1000/100^3;
Cp4 = out4*Cpo*MWp*1000*1000/100^3;
Cp5 = out5*Cpo*MWp*1000*1000/100^3;

G = [0 : 1/(length(X)-1) : 1]';   % G here is just the normalized radial positions in the column (the
        "r" values)
G = G*R*100;   % transforms the normalized radial positions to radial positions in cm
O1 = wt1';
O2 = wt2';
O3 = wt3';
O4 = wt4';
O5 = wt5';
F = [G O1 O2 O3 O4 O5];
dlmwrite('results1',F);   % saves the results of the simulation to a delimited file

% plot (x, y, symbol on graph, x, y, symbol, etc.)
% plot (x axis from 0 to 1 with a step size length of 1/(length (X)-1) - this is G)
figure
plot(G, Cp1, '-', G, Cp2, '*', G, Cp3, '^', G, Cp4, 'o', G, Cp5, '.')
title('Particle Concentration vs. Radial Distance at Different Lengths Along the Column')
xlabel('Radial Distance in the Column (cm)')
ylabel('Particle Concentration (mg/mL)')

figure
plot(G, wt1, '-', G, wt2, '*', G, wt3, '^', G, wt4, 'o', G, wt5, '.')
title('Particle Concentration vs. Radial Distance at Different Lengths Along the Column')
xlabel('Radial Distance in the Column (cm)')
ylabel('Weight Percent Particles (wt%)')

figure
plot(G, H(X), '*')
title('Magnetic Field vs. Radial Distance in the Column')
xlabel('Radial Distance in the Column (cm)')
ylabel('Magnetic Field, H (A/m)')

figure
vel = V(X)*vmax;
plot(G, vel, '*')
title('Linear Fluid Velocity vs. Radial Distance in the Column')
xlabel('Radial Distance in the Column (cm)')
```

```
ylabel('Linear Fluid Velocity (m/s)')


% --------------------------------------------------------------------

function [c,f,s] = pdex1pde(X,t,u,DuDx,va)

% convection term, nondimensionalized
c(1) = V(X) - va(4);

% flux term, nondimensionalized
f(1) = va(1)*DuDx(1) + va(2)*u(1)*DuDx(1) + va(3)*u(1)*M(X)*dH(X);

% source term
s = [0];


% --------------------------------------------------------------------

function u0 = pdex1ic(X,va)
u0 = [1];  % defines the initial normalized particle concentration everywhere as 1 (normalized
        particle concentration = Cp/Cpo)


% --------------------------------------------------------------------

function [pl,ql,pr,qr] = pdex1bc(xl,ul,xr,ur,t,va)
pl = [0];  % flux equals 0 at left boundary
ql = [1];  % flux equals 0 at left boundary
pr = [0];  % flux equals 0 at right boundary
qr = [1];  % flux equals 0 at right boundary

% total equation has form of p + (q)(f) = 0


% --------------------------------------------------------------------

function dh = dH(X)

% this function calculates the magnetic field gradient for different radial positions
% the magnetic flux density values were fit to a parabola for the magnetic field gradient
% calculations

muo=pi*4e-7;   % permeability of free space, Tesla*m/A
Ho = 0.6282/muo;  % maximum H in the system, A/m
x=X;

 b1=[0.5633 0.1146];
 dh=2*b1(1)*x;  % dh here is acutally dB, the gradient of the magnetic flux density, in Tesla
 dh=dh/muo;  % convert to dH (dB = muo*dH for assumption of M << H, which is valid for our
        system), A/m^2
```

```
 dh=dh/Ho;  % make dimensionless (grad term is already dimensionless)


% ------------------------------------------------------------------------

function mag = M(X)

% this function calculates the magnetization of the fluid for different radial positions

Ht = 43500;   % H at which M = Ms/2, A/m
x=X;

 mag = H(X)/(Ht+H(X));

% ------------------------------------------------------------------------

function h = H(X);

% this function calculates the magnetic field for different radial positions
% the magnetic flux density values were fit to a second order polynomial

muo=pi*4e-7;   % permeability of free space, Tesla*m/A
x=X;

   b=[0.2212 0.3662 0.0436];   % parameters that fit the magnetic field profile to a second order
        polynomial
   h=b(1)*x.^2+b(2)*x+b(3);   % h here is actually B, the magnetic flux density, in Tesla
   h=h/muo;   % convert to H (B = muo*H for assumption of M << H, which is valid for our
        system), A/m

% ------------------------------------------------------------------------

function v = V(X);

% this function calculates the velocity profile, which was assumed to be parabolic

x=X;

   v=(1-x.^2);   % velocity profile, nondimensionalized after dividing by vmax, m/s

% ------------------------------------------------------------------------
```